JSCSEN 73(3)259–384(2008)

Journal of the Serbian Chemical Society

VOLUME 73
NO 3
BELGRADE 2008

Available on line at
СХД 1897
www.shd.org.yu/JSCS/

Journal of
the Serbian
Chemical Society
version electronic
JSCS@tmf.bg.ac.yu • www.shd.org.yu/JSCS

J. Serb. Chem. Soc. Vol. 73, No. 3 (2008)

CONTENTS

Editor's note

Organic Chemistry and Biochemistry

Theoretical Chemistry

Physical Chemistry

Electrochemistry

Materials

Metallurgy

Published by the Serbian Chemical Society
Karnegijeva 4/III, 11120 Belgrade, Serbia
Printed by the Faculty of Technology and Metallurgy
Karnegijeva 4, P.O. Box 35-03, 11120 Belgrade, Serbia

EDITOR'S NOTE

In memoriam: Academician Dragutin M. Dražić

Dragutin M. Dražić, Member of the Serbian Academy of Science and Art, Professor of Physical Chemistry and Electrochemistry at the Faculty of Technology and Metallurgy, University of Belgrade, Honorary President of the Serbian Chemical Society, Honorary Editor of the *Journal of the Serbian Chemical Society*, died on February 6, 2008. To maintain the memory of Dragutin Dražić's colossal contribution to science, particularly to physical chemistry and electrochemistry (see *J. Serb. Chem. Soc.* **66** (2001) 731), and to the activities of the Serbian Chemical Society, is not necessary to dwell long on nearly 45 years of teaching at the Faculty of Technology and Metallurgy, supervising tens of PhD, MS and Diploma thesis and publishing hundreds of scientific papers, chapters and books. His huge contribution to the *Journal of the Serbian Chemical Society* during more than two decades in the capacity of Editor-in-Chief (see *J. Serb. Chem. Soc.* **72** (2007) 1 and *J. Serb. Chem. Soc.* **72** (2007) 1171) will remain always deeply acknowledged. All of us active in the Serbian Chemical Society will attempt to continue his efforts in maintaining and improving the level of the *Journal*, always bearing in mind the memory of Professor Dražić.

Journal of the Serbian Chemical Society
JSCS@tmf.bg.ac.yu • www.shd.org.yu/JSCS

J. Serb. Chem. Soc. 73 (3) 261–270 (2008)
JSCS–3708

UDC 547.631.6.001+547.384
Original scientific paper

A convenient preparation of novel benzophenone derivatives

BELGUR S. SUDHA[1]*, RAVINDRA R. KAMBLE[1] and SHEENA SHASHIKANTH[2]

[1]*Department of Chemistry and Food Science, Yuvaraja's College, University of Mysore, Mysore – 570 005 and* [2]*Department of Studies in Chemistry, Manasagangotri, Mysore – 570 006, India*

(Received 21 June, revised 18 September 2007)

Abstract: A simple and high yielding method for the synthesis of novel benzophenone derivatives has been developed starting from ethyl(4-aroylaroxy)acetates. Confirmation for the structures of the newly synthesized compounds was proved by their physical, analytical and spectral data (IR, ^{1}H-NMR, ^{13}C-NMR and MS).

Keywords: aroylaryloxy esters; 2-oxazolines; *N*-arylacetamides; HIV reverse transcriptase (RT); antihaemostatic activity.

INTRODUCTION

In continuation of our ongoing project on synthetic studies of benzophenones,[1–3] the synthesis and spectral characterization of some benzophenone derivatives, *viz*., 2-(4-aroylaroxy)acetic acids (**2a**–**c**)[4–15], 2-[(4-aroylaroxy)methyl]-2-oxazolines (**3a**–**c**), 2-(4-aroylaroxy)acetyl chlorides (**4a**–**c**)[14,16,17] and 2-(4-aroylaroxy)-*N*-arylacetamides (**6d**–**i**),[18] is now reported. Benzophenone is an ultraviolet light (UV) absorbing agent that has been used in industry and medicine for more than 40 years.[19] The British India Biological Research Association (BIBRA) has published a toxicity profile of benzophenone on the basis of local effects (skin, eye and respiratory tract irritation), sensitization, intolerance, general systemic effects, reproductive toxicity, carcinogenicity and other genotoxicity.[20] Broitman[21] studied the toxicity of benzophenone derivatives on rabbits, rats and guinea pigs. These can penetrate intact skin and cause changes in the activity of the nervous system, along with changes in the kidneys and mucosa of the small intestine. Benzophenone derivatives have a local anesthetic effect and 2-hydroxy-4-propoxybenzophenone was found to be the least toxic. Benzophenone derivatives including garcinol and isogarcinol extracted from *Garcinia* plants are claimed to be inhibitors for Epstein–Barr virus early antigen induction and anti-tumor agents.[22]

---

* Corrsponding author. E-mail: sudha2k2@rediffmail.com

doi: 10.2298/JSC0803261S

Wyatt *et al.*[23] synthesized some benzophenone derivatives, *i.e.*, (2-benzoylphenoxy)acetic acid and 2-(2-benzoylphenoxy)-*N*-[4-(2-diethylamino)ethoxy]phenylacetamide, to study their structure activity relationship. Benzophenone derivatives were initially tested for their ability to inhibit the poly(rA)-oligo(dT)[24–28] directed RT activity of HIV-I. Replacement of the methoxy group of ring A with fluorine resulted in a change in the activity, whereas removal of the substitution resulted in a modest increase in the inhibition of RT. Introduction of a methoxy group at the 4-position of ring B resulted in a slight loss of RT inhibition; however, introduction of a chlorine atom at the 5 position gave a 10-fold increase in activity in the RT assay but resulted in a compound toxic in the whole cell assay. SAR suggests that the major interaction is through the amide carbonyl.

Oxazolines have been known for many years[29–31] but only in recent years has the chemical literature shown considerable activity in this field.[32–35] Excellent review articles were published in 1949 and in 1971 covering the preparation, reactions and applications of oxazoline.[30,31] Substituted 2-oxazolines have been widely investigated for pharmaceutical uses. Substituted arylamino-2-oxazolines are useful in raising blood sugar levels and exhibit local anesthetic, sedative, vasoconstrictor, blood pressure depressant and gastric fluid secretion inhibitory effects.[36–38]

A survey of the literature on the structure–activity relationship among benzophenone derivatives revealed that no effort has been directed towards the study of the effect on antimicrobial activity of incorporation of the oxazoline ring system and amide group into the side chain of the benzophenone moiety and hence 2-oxazolines (**3a**–**c**) (Scheme 1) and the amide analogs (**6d**–**i**) were synthesized and their pharmacological activities studied.

Normally the haemostatic process maintains a delicate balance between keeping blood in the fluid state to maintain flow and rapidly forming an occluding plug following vessel injury. Thrombosis occurs because of an alteration in this balance. Recent advances in understanding the haemostatic process have led to the design of novel antihaemostatic drugs. In the light of this observation, the title compounds were subjected to a preliminary determination of their antihaemostatic activity.

RESULTS AND DISCUSSION

The reaction scheme for the preparation of the title compounds is given in Scheme 1.

The analytic and spectral data for the acids **2a**–**c** are given below.

*Compound **2a***. Yield: 75 %; m.p. 130–132 °C. Anal. Calcd. for $C_{15}H_{12}O_4$: C, 70.31; H, 4.69. Found: C, 70.40; H, 4.60 %. IR (KBr, cm^{-1}): 3350 (−OH stretching of −COOH group), 1730 (−C=O stretching of −COOH group), 1645 (−C=O stretching of keto group); ^{1}H-NMR (300 MHz, $CDCl_3$, δ, ppm): 4.6 (2H, *s*, $-OCH_2$), 6.75 (2H, *d*, J = 7.3 Hz, aromatic), 6.8–7.8 (5H, *bm*, aromatic), 7.75 (2H, *d*, J = 7.3 Hz, aromatic), 9.2 (1H, *s*, COOH); MS (*m*/*z*, (relative abundance, %)): 226 (M^+, 55), 212 (BP, 100), 197 (70), 175 (46), 151 (21), 105 (9), 77 (14).

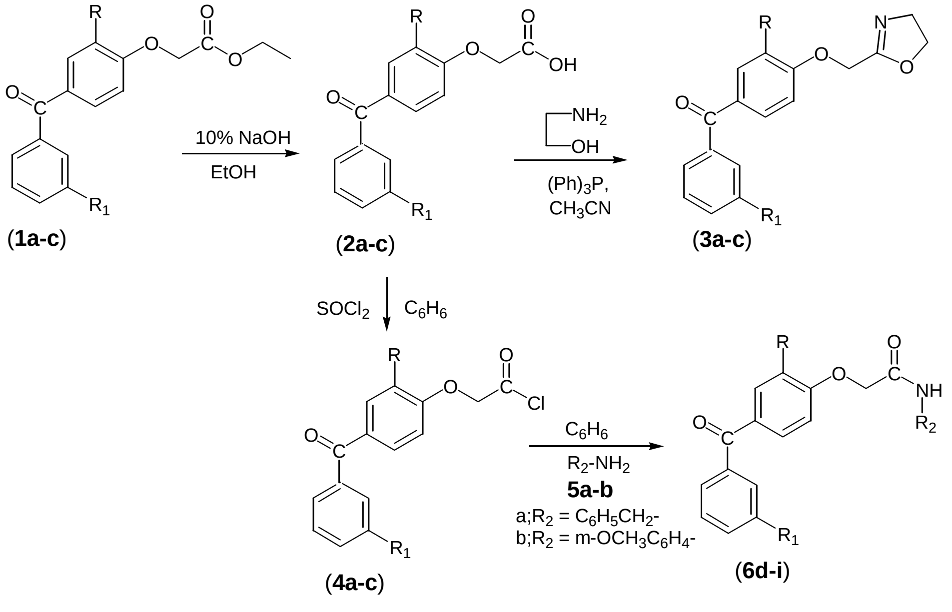

a: $R=R_1=H$, b: $R=CH_3$, $R_1=H$, c: $R=H$ $R_1=Cl$, d: $R=R_1=H$, $R_2=C_6H_5CH_2$-, e: $R=CH_3$, $R_1=H$, $R_2=C_6H_5CH_2$-
f: $R=H$, $R_1=Cl$, $R_2=C_6H_5CH_2$-, g: $R=R_1=H$, $R_2=$ m-$OCH_3C_6H_4$-, h:$R=CH_3$, $R_1=H$, $R_2=$m-$OCH_3C_6H_4$-,
i: $R=H$, $R_1=Cl$, $R_2=$ m-$OCH_3C_6H_4$-

Scheme 1. The starting compounds (**1a**–**c**) and the products 2-(4-aroylaroxy)acetic acids (**2a**–**c**), 2-[(4-aroylaroxy)methyl]-2-oxazolines (**3a**–**c**), 2-(4-aroylaroxy)acetyl chlorides (**4a**–**c**) and 2-(4-aroylaroxy)-*N*-benzyl/*m*-methoxyphenyl/acetamides (**6d**–**i**).

*Compound **2b***. Yield: 78 %; m. p. 140–142 °C. Anal. Calcd. for $C_{16}H_{14}O_4$: C, 71.11; H, 5.19. Found: C, 71.22; H, 5.15 %. IR (KBr, cm^{-1}): 3400 (−OH stretching of −COOH group), 1725 (−C=O stretching of −COOH group), 1638 (−C=O stretching of keto group); ^{1}H-NMR (300 MHz, $CDCl_3$, δ, ppm): 2.2 (3H, *s*, $-CH_3$), 4.5 (2H, *s*, $-OCH_2$), 6.9–8.0 (8H, *bm*, aromatic), 9.5 (1H, *s*, −COOH); MS (*m*/*z*, (relative abundance, %)): 270 (M^+, 54), 226 (BP, 100), 211 (70), 193 (48), 165 (43), 105 (9), 77 (14).

*Compound **2c***. Yield: 80 %, m. p. 128–130°C. Anal. Calcd. for $C_{15}H_{11}ClO_4$: C, 61.96; H, 3.79; Cl, 12.22. Found: C, 61.88; H, 3.70; Cl, 12.18 %. IR (KBr, cm^{-1}): 3400 (−OH stretching of −COOH group), 1732 (−C=O stretching of −COOH group), 1642 (−C=O stretching of keto group); ^{1}H-NMR (300 MHz, $CDCl_3$, δ, ppm): 4.5 (2H, *s*, $-OCH_2$), 6.95 (2H, *d*, $J = 7.4$ Hz, aromatic), 7.0–7.8 (4H, *bm*, aromatic), 7.95 (2H, *d*, $J = 7.4$ Hz, aromatic), 9.25 (1H, *s*, −COOH); MS (*m*/*z*, (relative abundance, %)): 290 (M^+, 56), 246 (BP, 100), 231 (72), 175 (42), 151 (20), 139 (9), 111(15).

The acid **2a** showed two strong IR absorptions at 1645 cm^{-1} and 1730 cm^{-1} due to aromatic carbonyl and acid carbonyl groups, respectively. The strong broad absorption at 3350 cm^{-1} is assigned to −OH groups. The ^{1}H-NMR spectrum of **2a** showed a singlet at δ 4.6, assigned to methylene protons, two doublets in the region δ 6.75 and δ 7.75, assigned to four aromatic protons, a broad multiplet at δ 6.8–7.8, assigned to the remaining five aromatic protons, and a singlet at δ 9.2, due to one proton of the acid hydroxyl group. All the compounds **2a**–**c** showed mass spectra with the molecular ion peaks at their respective mass numbers *m*/*z* 226, 270 and 290.

The analytic and spectral data for compounds **3a**–**c** are given below.

Compound ***3a***. Yield: 50 %; m. p. 117–118 °C. Anal. Calcd. for $C_{17}H_{15}NO_3$: C, 72.60; H, 5.34; N, 4.98. Found: C, 72.56; H, 5.40; N, 4.90 %. IR (KBr, cm^{-1}): 1638 (−C=O stretching of keto group), 1600 (−C=N stretching of oxazoline ring); ^{1}H-NMR (300 MHz, $CDCl_3$, δ, ppm): 3.35 (2H, *t*, J = 6 Hz, N–CH_2), 4.2 (2H, *t*, J = 6 Hz, ring OCH_2), 4.65 (2H, *s*, −OCH_2), 6.8 (2H, *d*, J = 7.3 Hz, aromatic), 6.9–7.8 (5H, *bm*, aromatic), 7.85 (2H, *d*, J = 7.3 Hz, aromatic); MS (*m*/*z*, (relative abundance, %)): 281 (M^+, 58), 253 (54), 237 (42), 105 (BP, 100), 77 (16).

Compound ***3b***. Yield: 52 %; m. p. 115−116 °C. Anal. Calcd. for $C_{18}H_{17}NO_3$: C, 73.22; H, 5.76; N, 4.75. Found: C, 73.28; H, 5.80; N, 4.82 %. IR (KBr, cm^{-1}): 1640 (−C=O stretching of keto group), 1605 (−C=N stretching of oxazoline ring); ^{1}H-NMR (300 MHz, $CDCl_3$, δ, ppm): 2.1 (3H, *s*, Ph−CH_3), 3.45 (2H, *t*, J = = 6 Hz, N−CH_2), 4.25 (2H, *t*, J = 6 Hz, ring OCH_2), 4.55 (2H, *s*, −OCH_2), 6.9–−7.8 (8H, *bm*, aromatic); MS (*m*/*z*, (relative abundance, %)): 295 (M^+, 59), 267 (52), 251 (40), 105 (100), 77 (17).

Compound ***3c***. Yield: 50 %; m. p. 109–110 °C. Anal. Calcd. for $C_{17}H_{14}ClNO_3$: C, 64.66; H, 4.44; N, 4.44; Cl, 11.25. Found: C, 64.70; H, 4.52; N, 4.48; Cl, 11.20 %. IR (KBr, cm^{-1}): 1641 (−C=O stretching of keto group), 1603 (−C=N stretching of oxazoline ring); ^{1}H-NMR (300 MHz, $CDCl_3$, δ, ppm): 3.4 (2H, *t*, J = = 6 Hz, N−CH_2), 4.2 (2H, *t*, J = 6 Hz, ring OCH_2), 4.54 (2H, *s*, −OCH_2), 6.85 (2H, *d*, J = 7.4 Hz, aromatic), 6.9–7.75 (4H, *bm*, aromatic), 7.85 (2H, *d*, J = 7.4 Hz, aromatic); MS (*m*/*z*, (relative abundance, %)):315 (M^+, 55), 287 (53), 271 (40), 139 (BP, 100), 111 (15).

The IR spectrum of **3a** showed absorption peaks at 1600 and 1638 cm^{-1}, assigned to −C=N and aromatic carbonyl groups. The ^{1}H-NMR spectrum showed a triplet centered at δ 3.35, assigned to the two protons of −N−CH_2, with coupling constant J = 6 Hz, a triplet centered at δ 4.2, assigned to the two protons of the ring −OCH_2 group, a singlet at δ 4.65, assigned to the two protons of the −OCH_2 group, two doublets, one in the upfield region at δ 6.8 and the other in the downfield region at δ 7.85 with a coupling constant J = 7.3 Hz, due to four aromatic protons and a broad multiplet at δ 6.9–7.8, due to the remaining five aromatic protons. The mass spectra of **3a**–**c** showed molecular ion peaks at their respective mass numbers.

The analytic and spectral data for compounds **4a**–**c** are given below.

*Compound **4a***. Yield: 92 %. Anal. Calcd. for $C_{15}H_{11}ClO_3$: C, 65.58; H, 4.04; found C, 65.60; H, 4.05 %. IR (KBr, cm^{-1}): 1800 (−C=O stretching of −COCl group), 1642 (−C=O stretching of keto group); ^{1}H-NMR (300 MHz, $CDCl_3$, δ, ppm): 4.5 (2H, *s*, OCH_2), 6.95 (2H, *d*, J = 7.3 Hz, aromatic), 7.0–7.4 (5H, *bm*, aromatic), 7.5 (2H, *d*, J = 7.3 Hz, aromatic); MS 274 (M^+, 32), 243 (30), 227 (25), 95 (BP, 100).

*Compound **4b***. Yield: 80%. Anal. Calcd. for $C_{16}H_{13}ClO_3$: C, 66.56; H, 4.54. Found: C, 66.50; H, 4.50. IR (KBr, cm^{-1}): 1805 (−C=O stretching of −COCl group), 1638 (−C=O stretching of keto group); ^{1}H-NMR (300 MHz, $CDCl_3$, δ, ppm): 2.30 (3H, *s*, $-CH_3$), 4.3 (2H, *s*, $-OCH_2$), 7.0 (2H, *d*, J = 7.0 Hz, aromatic), 7.0–7.5 (4H, *bm*, aromatic), 7.6 (2H, *d*, J = 7.0 Hz, aromatic); MS (*m*/*z*, (relative abundance, %)): 288 (M^+, 45), 257 (43), 241 (20), 109 (100).

*Compound **4c***. Yield: 75 %. Anal. Calcd. for $C_{15}H_{10}Cl_2O_3$: C, 58.28; H, 3.26. Found: C, 58.29; H, 3.25. IR (KBr, cm^{-1}): 1799 (−C=O stretching of −COCl group), 1630 (−C=O stretching of keto group); ^{1}H-NMR (300 MHz, $CDCl_3$, δ, ppm): 4.70 (2H, *s*, $-OCH_2$), 6.87 (2H, *d*, aromatic), 7.30–7.58 (4H, *m*, aromatic), 7.60 (2H, *d*, aromatic). MS (*m*/*z*, (relative abundance, %)): 312 (M+4, 5), 310 (M+2, 25), 308 (M^+, 28), 278 (45), 262 (11), 130 (BP, 98).

The IR spectrum of **4a** showed peaks in the region 1642 cm^{-1}, assigned to aromatic carbonyls, and in the region 1800 cm^{-1}, assigned to the acid chloride carbonyl group. The ^{1}H-NMR spectrum of **4a** showed a singlet at δ 4.5 due to two protons of OCH_2 group and two doublets at δ 6.95 and δ 7.5 with a coupling constant J = 7.3 Hz, assigned to four aromatic protons and a broad multiplet in the range δ 7.0–7.4, assigned to the remaining four aromatic protons. The IR and ^{1}H-NMR spectrum of **4b** was similar to that of **4a**, except for a singlet at δ 2.2 of the aromatic methyl group and all the aromatic protons appeared as a broad multiplet.

The analytic and spectral data of compounds **6d**–**i** are given below.

*Compound **6d***. Yield: 80 %, m. p. 115–116 °C. Anal. Calcd. for $C_{22}H_{19}NO_3$: C, 76.52; H, 5.50; N, 4.05. Found: C, 76.42; H, 5.40; N, 3.96. IR (KBr, cm^{-1}): 3275 (−NH stretching of $-CONH_2$ group), 1710 (−C=O stretching of $-CONH_2$ group), 1638 (−C=O stretching of keto group); ^{1}H-NMR (300 MHz, $CDCl_3$, δ, ppm): 4.25 (3H, *s*, CH_2), 4.6 (2H, *s*, $-OCH_2$), 6.8 (2H, *d*, J = 8.0 Hz, aromatic), 6.9–7.8 (10H, *bm*, aromatic), 7.9 (2H, *d*, J = 8.0 Hz, aromatic), 9.55 (1H, *bs*, NH, D_2O exchangeable); MS (*m*/*z*, (relative abundance, %)): 345 (M^+, 9), 328 (10), 294 (16), 252 (2), 157 (21), 129 (25), 101 (BP, 100).

*Compound **6e***. Yield: 85 %, m. p. 120–122 °C. Anal. Calcd. for $C_{23}H_{21}NO_3$: C, 76.86; H, 5.89; N, 3.90. Found: C, 76.82; H, 5.85; N, 3.92. IR (KBr, cm^{-1}): 3260 (−NH stretching of $-CONH_2$ group), 1720 (−C=O stretching of $-CONH_2$ group), 1641 (−C=O stretching of keto group); ^{1}H-NMR (300 MHz, $CDCl_3$, δ, ppm): 2.2 (3H, *s*, CH_3), 4.3 (2H, *s*, CH_2) 4.5 (2H, *s*, $-OCH_2$), 6.7–7.9 (13H, *bm*, aromatic), 9.6 (1H, *bs*, NH, D_2O exchangeable); MS (*m*/*z*, (relative abundance, %)): 359 (M^+, 8), 342 (10), 308 (16), 266 (16), 177 (14), 149 (2), 121 (BP, 100).

Compound ***6f***. Yield: 82 %; m. p. 155–156 °C. Anal. Calcd. for $C_{22}H_{18}ClNO_3$: C, 69.57; H, 4.78; N, 3.69; Cl, 9.33. Found: C, 69.50; H, 4.72; N, 3.65; Cl, 9.30. IR (KBr, cm^{-1}): 3300 (−NH stretching of $-CONH_2$ group), 1700 (−C=O stretching of $-CONH_2$ group), 1630 (−C=O stretching of keto group); ^{1}H-NMR (300 MHz, $CDCl_3$, δ, ppm): 4.0 (2H, *s,* CH_2), 4.5 (2H, s, $-OCH_2$), 6.8 (2H, *d*, J = 8.2 Hz, aromatic), 6.85–7.8 (9H, *bm*, aromatic), 7.85 (2H, *d*, aromatic, J = 8.2 Hz), 9.55 (1H, *bs,* NH, D_2O exchangeable); MS (*m*/*z*, (relative abundance, %)): 381 (M+2, 10), 379 (M^+, 32), 362 (10), 268 (5), 215 (18), 148 (BP, 100), 123 (24).

Compound ***6g***. Yield: 76 %, m. p. 132–133 °C. Anal. Calcd. for $C_{22}H_{19}NO_4$: C, 73.12; H, 5.30; N, 3.88. Found: C, 73.08; H, 5.25; N, 3.85. IR (KBr, cm^{-1}): 3425 (−NH stretching of $-CONH_2$ group), 1714 (−C=O stretching of $-CONH_2$ group), 1619 (−C=O stretching of keto group); ^{1}H-NMR (300 MHz, $CDCl_3$, δ, ppm): 3.73 (3H, *s*, $-OCH_3$), 4.88 (2H, *s*, $-OCH_2$), 6.75 (2H, *d*, J = 8.0 Hz, aromatic), 6.87 (2H, *d*, J = 8.0 Hz, aromatic), 7.0–7.59 (9H, *bm*, aromatic), 10.05 (1H, *bs,* NH, D_2O exchangeable); MS (*m*/*z*, (relative abundance, %)): 361 (M^+, 9), 344 (7), 310 (15), 268 (100).

Compound ***6h***. Yield: 88 %, m. p. 176–178 °C. Anal. Calcd. for $C_{23}H_{21}NO_4$: C, 73.58; H, 5.64; N, 3.73. Found: C, 73.52; H, 5.65; N, 3.72. IR (KBr, cm^{-1}): 3410 (−NH stretching of $-CONH_2$ group), 1720 (−C=O stretching of $-CONH_2$ group), 1625 (−C=O stretching of keto group); ^{1}H-NMR (300 MHz, $CDCl_3$, δ, ppm): 2.2 (3H, *s*, $-CH_3$), 3.80 (3H, *s*, $-OCH_3$), 4.80 (2H, *s*, $-OCH_2$), 6.75 (2H, *d*, J = 6.0 Hz, aromatic), 6.82 (2H, *d*, J = 6.0 Hz, aromatic), 7.36–7.82 (8H, *bm*, aromatic), 9.70 (1H, *bs*, NH, D_2O exchangeable); MS (*m*/*z*, (relative abundance, %)): 375 (M^+, 11), 358 (9), 322 (17), 269 (BP, 100).

Compound ***6i***. Yield: 82 %, m. p. 167–168 °C. Anal. Calcd. for $C_{22}H_{18}ClNO_4$: C, 66.75; H, 4.55; N, 3.54; Cl, 8.98. Found: C, 66.82; H, 4.60; N, 3.62; Cl, 8.90. IR (KBr, cm^{-1}): 3290 (−NH stretching of $-CONH_2$ group), 1710 (−C=O stretching of $-CONH_2$ group), 1640 (−C=O stretching of keto group); ^{1}H-NMR (300 MHz, $CDCl_3$, δ, ppm): 4.12 (3H, *s*, $-OCH_3$), 4.63 (2H, *s*, $-OCH_2$), 6.8 (2H, *d*, J = = 8.2 Hz, aromatic), 6.85–7.8 (78H, *bm*, aromatic), 7.85 (2H, *d*, J = 8.2 Hz, aromatic), 9.86 (1H, *bs*, NH, D_2O exchangeable); MS (*m*/*z*, (relative abundance, %)): 395 (M^+, 10), 378 (10), 284 (3), 231 (16), 164 (BP, 100), 139 (21), 111 (25), 107 (24).

The IR and ^{1}H-NMR spectra of **6d**–**i** showed almost similar type of absorptions except for the substituents. The IR absorption of **6d** in the region 1638 cm^{-1} was assigned to aromatic carbonyl, the absorption at 1710 cm^{-1} to amide carbonyl stretching and the absorption at 3275cm^{-1} due to −NH stretching. The ^{1}H-NMR spectrum of **6d** exhibits a singlet at δ 4.25 due to two benzylic protons, a singlet at δ 4.6 due to the $-OCH_2$ group, two doublets in the region δ 6.8 and 7.9, with a coupling constant J = 8.0 Hz, assigned to four aromatic protons and a broad multiplet at δ 6.9–7.8 due to the remaining ten aromatic protons and a broad singlet at δ 9.55, assigned to the −NH proton. For the compound **6e**, a singlet appeared at δ 2.2 from the aromatic $-CH_3$ group and a broad multiplet appeared in the region δ 6.7–7.9 due to all the aromatic protons. The IR and ^{1}H-NMR spectra of **6e**–**f** are similar to that of **6d**. The IR absorptions in the region 1630–1640 cm^{-1}, 1700–1710 cm^{-1} and 3290–3300 cm^{-1} were assigned to aromatic carbonyl, amide carbonyl and −NH stretching, respectively. The ^{1}H-NMR spectral signals of **6g**–**i** were the same as those of **6d**–**f**, except for the absence of benzylic protons. A singlet appeared at δ 3.7–4.1 due to the three protons of the methoxy group and the aromatic protons appeared as a broad multiplet. The mass spectra of **6d**–**i** showed molecular ion peaks at their respective mass numbers *m*/*z*.

The antihaemostasis results (Fig. 1) revealed that the compounds **3a**–**c**, containing the 2-oxazoline ring exhibited considerable antihaemostatic activity. The compound **3c**, containing an electronegative chlorine atom, had an activity (487) almost equal to that of the standard indomethacin. However, the remaining compounds **4a**–**c** and **6d**–**i** exhibited poor antihaemostatic activities. The compound **6g** did not show the significant activity.

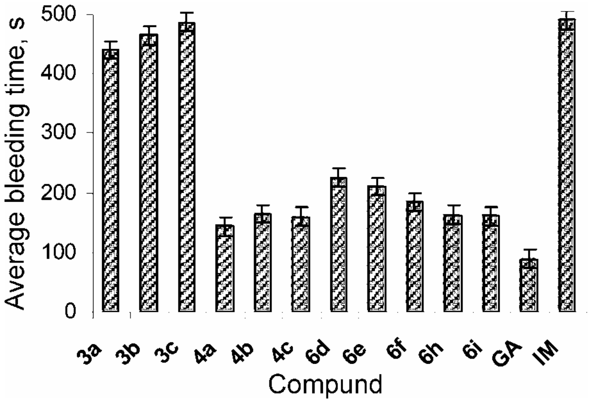

Fig. 1. The average bleeding time exhibited by the compounds **3a**–**c**, **4a**–**c** and **6d**–**i**. (GA – gum acacia, IM – indomethacin). Dose 100 mg/kg for all.

EXPERIMENTAL

Materials

TLC was run on silica gel G plates using acetone-benzene (1:3) as the mobile phase. Melting points were determined in open capillaries and are uncorrected. IR (KBr) spectra were recorded on a Nicolet Impact-410 FTIR spectrometer and the NMR spectra in $CDCl_3$ (δ, ppm downfield from TMS) were recorded on a Bruker Varian-300 MHz FT-NMR spectrometer. Elemental analyses were performed on a CEST 1106 elemental analyzer. Mass spectra were recorded on EI-70 eV and FR ver. 1on UIC 002002 spectrometers. The ethyl(4-aroylaroxy)acetates (**1a**–**c**) were prepared according to the reported literature.[39]

Methods

*General preparation procedure for 2-(4-aroylaroxy)acetic acids (**2a**–**c**)*: Ethyl(2-(4-benzoylphenoxy)acetate) (**1a**) (8.0 g, 0.028 mol) was dissolved in ethanol (25 ml) and sodium hydroxide (2.256 g, 0.056 mol) in water (20 ml) was added and the mixture refluxed for 1 h. The reaction mixture was cooled and acidified with hydrochloric acid (4M). The precipitate was extracted with dichloromethane (25×3 ml), washed with water (15×3 ml). For further purification, the product was extracted into 10 % sodium bicarbonate solution (25×3 ml) and acidified with hydrochloric acid (4M). The white solid which separated was filtered, dried and on recrystallization from hexane gave pure crystals of **2a**.

*General preparation procedure for 2-[(4-aroylaroxy)methyl]-2-oxazolines (**3a–c**)*: A mixture of 2-(4-benzoylphenoxy)acetic acid (**2a**) (1 g, 4 mmol), acetonitrile (27 ml), ethanolamine (1.16 g, 19 mmol) and carbon tetrachloride (2.44 g, 0.02 mol) was stirred at 2 °C for 2 h. Triethylamine (2.02 g, 0.02 mol) in 25 ml acetonitrile was added slowly followed by the addition of triphenylphosphine (2.62 g, 0.01 mol) at 2–3 °C. Then the temperature was raised to 29 °C and the stirring continued for 1 h. The precipitate of $Et_3N{\cdot}HCl$ was removed by filtration and the filtrate was concentrated to 50 ml and cooled to 0 °C. The contents were filtered to remove the precipitated triphenylphosphine oxide and washed with acetonitrile. The filtrate was extracted with hexane (25×3 ml). The hexane layer was cooled to obtain solid oxazoline **3a**.

*General procedure for 2-(4-aroylaroxy)acetyl chlorides (**4a–c**)*: A mixture of 2-(4-benzoylphenoxy)acetic acid (**2a**) (4 g, 0.014 mmol), thionyl chloride (28 g, 0.235 mol) and benzene (28 ml) was heated at reflux for 30 min and then evaporated. The residue was dissolved in benzene (8 ml) and on re-evaporation gave **4a** as a pale yellow oily liquid.

*General procedure for 2-(4-(aroylaroxy)-*N*-benzyl/*m*-methoxyphenyl/acetamides (**6d–i**)*: A mixture of 2-(4-benzoylphenoxy)acetyl chloride (**4a**) (1 g, 3.24 mmol) in benzene (20 ml) was stirred at room temperature for 30 min and then benzylamine (**5a**) (0.466 g, 4.35 mmol) in benzene (10 ml) was added dropwise. The mixture was stirred at room temperature for 3 h and then water (20 ml) was added, extracted with diethyl ether (3×10 ml). The ether layer was washed with dilute aqueous sodium hydroxide (3×5 ml), dried over anhydrous sodium sulfate and evaporated to give **6d** as colorless crystals.

Antihaemostatic screening

All protocols of animal experiments were approved by the Institutional Animal Ethics Committee (IAEC). The tail bleeding time in conscious mice was used to determine the antihaemostatic activity of the title compounds.[40] Mice of either sex weighing 20–25 g were divided into 13 groups each being comprised of five mice. The control group received 0.4 ml of 2 % gum acacia. The test compounds were administered in 2 % gum acacia to the remaining 12 groups. Thirty minutes after administration of the test compounds, the tail bleeding time was measured.

CONCLUSIONS

In the present study, a highly efficient and simple procedure for the synthesis of novel benzophenone derivatives was developed. The method is simple, inexpensive, gave good yields and could be useful in for the construction of pharmacologically important molecules. Antihaemostatic analysis of the newly synthesized compounds showed that the compounds having the 2-oxazoline moiety, *viz*., **3a**–**c**, exhibited promising activity.

Acknowledgments. The authors would like to express their appreciation and thanks to RSIC, Punjab University, Chandigarh and Mass spectroscopic Division IICT, Hyderabad for the ^{1}H-NMR and mass spectral analyses.

ИЗВОД

ПОГОДНА СИНТЕЗА НОВИХ БЕНЗОФЕНОНСКИХ ДЕРИВАТА

BELGUR S.SUDHA[1], RAVINDRA R. KAMBLE[1] и SHEENA SHASHIKANTH[2]

[1]Department of Chemistry and Food Science, Yuvaraja's College, University of Mysore, Mysore – 570 005 и
[2]Department of Studies in Chemistry, Manasagangotri, Mysore – 570 006, India

Развијен је једноставан поступак синтезе нових бензофенонских деривата у високом приносу полазећи од етил-(4-ароиларокси)ацетата. Структуре новосинтетисаних једињења потврђене су физичким, аналитичким и спектралним (ИЦ, ^{1}H-NMR, ^{13}C-NMR и MS) подацима.

(Примљено 21. јуна, ревидирано 18. септембра 2007)

REFERENCES

1. B. S. Sudha, S. Shashikanth, S. A. Khanum, *Indian J. Chem.* **42B** (2003) 2652
2. B. S. Sudha, S. Shashikanth, S. A. Khanum, *Heterocycl. Commun.* **10** (2004) 85
3. S. Shashikanth, B. S. Sudha, S. A. Khanum, *Heteroat. Chem.* **16** (2005) 212
4. L. Vanmaele, J. Loccufier, Y. Chen, H. Frey, European patent, EP 1616899 AI (2006)
5. L. P. Coleman, S. L. Crooks, G. W. Griesgraber, K. J. Landstrom, B. A. Merrill, J. M. Rice, U. S. Patent, US, 6,45,1810 (2003)
6. R. E. Burrows, R. S. Davidson, S. L. Helihy, PCT Int. Appl, WO 2003033452 AI (2003)
7. L. P. Coleman, S. L. Crooks, G. W. Griesgraber, K. J. Landstrom, B. A. Merrill, J. M. Rice, PCT Int. Appl, WO 2000076505 AI (2000)
8. S. Rajgopalan, G. Radke, J. Tomich, *Synth. Commun.* **27** (1997) 187
9. G. Massolini, M. L. Carmellino, P. Borgna, *Farmaco* **45** (1990) 263
10. D. Yamashiro, C. H. Li, *Int. J. Pept. Protein Res.* **31** (1988) 322
11. N. Buckley, T. L. Burkoth, *Clin. Chim. Acta* **62** (1975) 73
12. P. De Cointet, V. Loppinet, R. Somay, J. L. Morinere, A. Boucherle, F. J. Renson, H. Voegelin, C. Dumount, *Chim. Ther.* **8** (1973) 574
13. M. Oki, M. Hirota, *Bull. Chem. Soc. Jpn.* **33** (1960) 119
14. S. H. Merrill, C. Unruch, C. Cornelius, E. M. Robertson, U. S. Patent, 2831768 (1958)
15. R. L. Weintraub, J. W. Brown, J. A. Throne, *J. Agric. Food Chem.* **2** (1954) 996
16. M. Hashimoto, K. Hemmi, T. Kamiya, T. Komori, O. Nakaguti, Y. Satio, Y. Shiokawa, H. Tkasugi, T. Takaya, T. Teraji, U. S. Patent, 694, 891 (1980)
17. W. Leuders, Ger. Offen, DE 2400418 (1975)
18. T. Fex, A. Stamvik, J. Carlsson, B. Asp, B. Anita, PCT Int. Appl. WO 9529155 AI (1995)
19. Y. Nakagawa, T. Suzuki, S. Tayama, *Toxicology* **27** (2000) 156
20. Anon, (BIBRA, UK) Report (1995), [CA 125/(1996) 240286r]
21. A.Y. Broitman, G. Truda, *Zabolevaniya,* **6** (1962) 20 [CA **57** (1962) 11486a]
22. Chugai Pharmaceutical Co., Ltd., Jpn. Kokai Tokkyo Koho JP 57, 185, 219 [82, 185, 219] (Cl. A61K31/135), 15 Nov 1982, Appl. 81/70,226, 12 May 1981 [CA **98** (1983) 78152u]
23. P. G. Wyatt, R. C. Bethell, N. Cammack, D. Charon, N. Dodic, B. Dumaitre, D. N. Evans, D. V. S. Green, L. Hopewell, D. C. Humber, R. B. Lamont, D. C. Orr, S. J. Plested, D. M. Pyan, S. . Solli, R. Storer, G. G. Weingarten, *J. Med. Chem.* **38** (1995) 1657
24. D. Evans, M. E. Cracknell, J. C. Saunders, C. E. Smith, W. R. N. Williamson, W. Dawson, W. J. F. Sweatman, *J. Med. Chem.* **30** (1987) 1321
25. G. R. Pettit, G. M. Cragg, S. B. Singh, *J. Nat. Prod.* **50** (1987) 386

26. G. R. Pettit, B. Toki, D. L. Herald, P. Verdier-Pinard, M. R. Boyd, E. Hamel, R. K. Pettit, *J. Med. Chem.* **41** (1998) 1688
27. H. P. Hsieh, J. P. Liou, Y. T. Lin, N. Mahindroo, J. Y. Chang, Y. N. Yang, S. S. Chen, U. K. Tan, C. W. Chang, T. W. Chen, C. H. Lin, Y. Y. Chang, C. C. Wang, *Bioorg. Med. Chem. Lett.* **13** (2003) 101
28. J. P. Liou, C. W. Chang, J. S. Sang, Y. N. Yang, C. F. Yeh, H. Y. Tseng, Y. K. Lo, Y. L. Chang, C. M. Chang, H. P. Hsieh, *J. Med. Chem.* **45** (2002) 2556
29. R. Andreasch, *Monatsh. Chem*. **5** (1984) 33
30. R. H. Wiley, L. L. Bennett Jr., *Chem. Rev*. **44** (1949) 447
31. J. A. Frump, *Chem. Rev*. **71** (1971) 483
32. X. Chenet, *J. Am. Chem. Soc.* **118** (2006) 78
33. A. R. Katritzky, C. Cai, K. Suzuki, S. K. Singh, *J. Org. Chem.* **69** (2004) 811
34. B. P. Bandgar, S. S. Pandit, *Tetrahedron Lett*. **44** (2003) 2331
35. S. Rajaram, M. S. Sigman, *Org. Lett*. **4** (2002) 3399
36. H. Wollweber, R. Hiltmann, K. Stoepel, W. Puls, British Patent, **132** (1968) 409 [CA **70** (1969) 47428]
37. H. Wollweber, R. Hiltmann, K. Stoepel, W. Puls, British Patent, **139** (1969) 458 [CA **70** (1969) 77936]
38. R. Hiltmann, H. Wollweber, K. Stoepel, W. S. Puls, African Patent 6705 (1958) 645 [CA **71** (1969) 101842]
39. B. S. Sudha, *Ph.D. Thesis*, University of Mysore, Mysore, 2004, p. 38
40. G. Hornstra, H. E. Chrisr, E. Haddeman, H. F. Ten, D. H. Nagsteren, *Prostaglandins* **21** (1981) 727.

Journal of the Serbian Chemical Society

JSCS@tmf.bg.ac.yu • www.shd.org.yu/JSCS

J. Serb. Chem. Soc. 73 (3) 271–282 (2008)
JSCS–3709

UDC 547.979.7+52–74:547.284.3+547.216
Original scientific paper

Bleaching of chlorophylls by UV irradiation *in vitro*: the effects on chlorophyll organization in acetone and *n*-hexane

JELENA ZVEZDANOVIĆ[#] and DEJAN MARKOVIĆ*[#]

Faculty of Technology, 16000 Leskovac, Serbia

(Received 17 May, revised 8 August 2007)

Abstract: The stability of chlorophylls toward UV irradiation was studied by Vis spectrophotometry in extracts containing mixtures of photosynthetic pigments in acetone and *n*-hexane. The chlorophylls underwent destruction (bleaching) obeying first-order kinetics. The bleaching was governed by three major factors: the energy input of the UV photons, the concentration of the chlorophylls and the polarity of the solvent, implying different molecular organizations of the chlorophylls in the two solvents.

Keywords: chlorophyll; UV-irradiation; kinetics; acetone; hexane.

INTRODUCTION

Beyond being the ultimate driving force of photosynthesis and its important regulatory factor, solar light is also a major source of stress to photosynthetic organisms. Depletion of stratospheric ozone has led to an increase of biologically damaging UV light at ambient levels (mainly UV-B light, 280–320 nm). Though photosynthetic pigments, such as chlorophylls and carotenoids, primarily absorb in the Vis region, their composure is significantly altered when exposed to UV light *in vivo* and *in vitro.*[1] This may cause an impairment of their photosynthetic function.[2] Plants generally respond to UV-B irradiation through very different mechanisms, including the synthesis of protective pigments and degradation of chlorophyll.[3]

Chlorophyll (Chl) is a major photosynthesis pigment. Its major function in photosynthesis is related to light collection and light conversion processes,[4] since chlorophylls perform a light-harvesting function in the antennas of the photosynthetic apparatus or act as exciton traps and electron-carriers in reaction centers (RC).[5] Chlorophyll is a chlorin, porphyrin derivative, a cyclic tetrapyrrole with an isocyclic cyclopentanone ring fused at the edge of the right-bottom pyrrole ring; the central Mg-atom plays a coordinating role[6] (Fig. 1). Significant progress has been made in the understanding of the *in vitro* properties of Chl and

---

[#] Serbian Chemical Society member.

* Corresponding author. E-mail: markovic57@info-net.co.yu; dejan_markovic57@yahoo.com

doi: 10.2298/JSC0803271Z

this has contributed to a better understanding of the role of Chl on the molecular level in photosynthesis.[7]

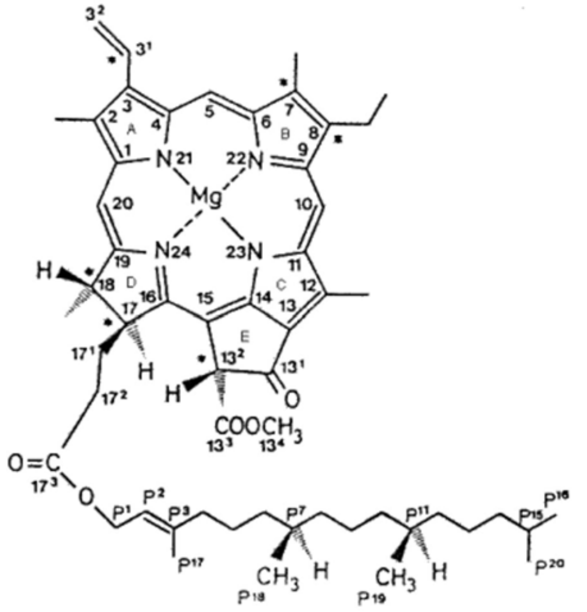

Fig. 1. Structure of chlorophyll *a*, with numerated atom positions.

Chlorophylls are not efficient UV-absorbers but are still able to absorb UV radiation, especially around 350 nm. The irradiation of chlorophyll solutions with UV and visible light results in the irreversible breakdown of chlorophyll, accompanied by the appearance of a number of intermediate and final products.[8] The chemical structure of these products is largely unknown because of the diversity of the pathways involved and the lability of the primary photoproducts.[9] Photobleaching of chlorophyll in solution may proceed without pheophytinization and could involve the opening of the porphyrin ring,[10] although small amounts of allomers have also been detected.[11]

The stability of chlorophylls in extracts of photosynthetic pigments (extracted chlorophylls), extracted from spinach leaves, against UV irradiation of three different ranges (UV-A, UV-B and UV-C) and for three different concentrations of Chl ($c(\mathrm{Chl}a + \mathrm{Chl}b) \approx 10^{-6}$, 10^{-5} and 10^{-4} mol dm^{-3}) was studied in this work. The irradiation was performed in acetone and *n*-hexane solutions for different irradiation periods, providing for the possibilities of kinetics analysis.

EXPERIMENTAL

All experiments were performed under dim light as much as possible and inside vessels and equipment covered with aluminum foil or black cloth to prevent possible chlorophyll photo-oxidation with visible light.

Extraction of plant pigments

The plant pigments were extracted from spinach leaves (*Spinacia oleracea* L.) using a previously reported method.[12,13] The extraction and re-extraction mixtures were methanol and 40–75 °C petroleum ether in a 2:1 ratio, and 40–75 °C petroleum ether and diethyl ether in a 1:1 ratio, respectively. The methanol removes water from the plant material and the petroleum ether picks up the pigments before they undergo secondary reactions. The diethyl ether increases pigments solubility in the organic phase. The final extract was a mixture of pigments containing large amounts of various Chl-forms (with a predominant contribution of chlorophyll *a* – Chl*a*), as well as accessory pigments, carotenoids (carotenes and xanthophylls). For Chl*a* identification, HPLC chromatography was used with a Chl*a* standard ($C_{55}H_{72}MgN_4O_5$, M_r = 893.5 g mol^{-1}, Sigma-Aldrich) in acetone. The pigment extracts were evaporated and diluted in acetone or *n*-hexane and then subjected to HPLC, which showed a large content of Chl*a* in each of them with a significant contribution of Chl*b*.

The Chl*a* + Chl*b* content in the extracts was calculated as reported[14,15] in acetone and adjusted to give three ranges of concentration: *c*(Chl*a* + Chl*b*) ≈ 1.2×10^{-6}, 1.2×10^{-5} and 1.4×10^{-4} mol dm^{-3} (*c*(Chl*a*) ≈ 8.5×10^{-7}, 8.5×10^{-6} and 1.0×10^{-4} mol dm^{-3} and *c*(Chl*b*) ≈ 3.4×10^{-7}, 3.4×10^{-6} and 3.5×10^{-5} mol dm^{-3}, respectively). The content of carotenoids (xanthophylls + carotenes – (x + c)) in the extracts was calculated as reported[14] and the *c*(Chl*a* + Chl*b*)/*c*(x + c) ratio was found to be about 3:1. The molar extinction coefficient (ε) for Chl*a* in 100 % acetone at 661.6 nm is 8.260×10^4 dm^3 mol^{-1} cm^{-1} and for Chl*b* at 644.8 nm is 4.686×10^4 dm^3 mol^{-1} cm^{-1}.[16] The molar extinction coefficient (ε) for Chl*a* in *n*-hexane at 663 nm is 9.01×10^4 dm^3 mol^{-1} cm^{-1}.[17] Chlorophyll bleaching values (%) were calculated using Eq. (1), in which the chlorophyll concentration before UV-irradiation (c_0) represents 100 % of chlorophyll, the chlorophyll concentration after one of the UV-irradiation treatments (c_1) represents X % of chlorophyll and (100 – X) % represents the percentage of UV-induced chlorophyll bleaching.[18]

$$\text{Bleaching of chlorophyll (\%)} = 100(c_0 - c_1)/c_0 \qquad (1)$$

*Chl*a *standard in acetone*

To compare the kinetics of the Chl*a* bleaching processes in the pigment extract and in pure solution (in the same concentration range), a Chl*a* standard dissolved in acetone and irradiated at all three UV-irradiation ranges was employed. The concentration of the standard was ≈ 8.26×10^{-6} mol dm^{-3}.

UV treatment

Continuous irradiation of the chlorophylls in acetone and in *n*-hexane was performed in a cylindrical photochemical reactor "Rayonnet", with 8 symmetrically placed lamps having emission maxima at: 350 nm (UV-A), 300 nm (UV-B) and 254 nm (UV-C). The samples were irradiated in quartz cells (1×1×4.5 cm^3) placed on the rotating circular holder. The total measured energy flux (hitting the samples) was about 10.3 W m^{-2} for 350 nm, 12.0 W m^{-2} for 300 nm and 14.3 W m^{-2} for 254 nm radiation.

Vis spectroscopy

The spectrophotometric measurements were made on a Varian Cary-100 spectrophotometer equipped with 1.0 cm quartz cells. All spectra before and after irradiation were recorded from 300 to 800 nm with 1.0 bandwidth.

HPLC analysis

HPLC analysis of the extracted chlorophylls and Chl*a* standard solutions was performed under isocratic conditions; apparatus: Agilent 1100 Series, Waldborn, Germany; column: Zorbax Eclipse XDB-C18; mobile phase: acetonitrile/methanol/ethyl acetate, 60:20:20; flow rate: 0.5 cm^3 min^{-1} at 25 °C. The monitoring wavelength was 430 nm.

RESULTS AND DISCUSSION

Chlorophylls have two major absorption regions in the visible range, due to their extended π-delocalization at the edge of cyclic tetrapyrrole (porphyrin) skeleton: a "red" (Q) band and a "blue" (Soret or B) band.[19] The Q-band absorption maxima ($A_{\max}$) for Chl*a* and Chl*b* in acetone are located at 662.1 nm and 645.5 nm, respectively.[20] The UV-induced changes of the chlorophylls were detected in the mixtures of pigments using the Q-bands as sensitive indicators, since they are exhibited by only the chlorophylls and not by carotenoids.[21]

The absorption spectra of the Chl*a*-standard sample measured after its bleaching in acetone by UV-C radiation are shown in Fig. 2A. The irradiation induces a gradual decrease in the intensity of the Q-band, *i.e.*, a hypochromic effect was clearly observed for irradiated Chl*a* relative to irradiation time, t_{irr}. Apparently, bleaching of Chl*a* resulted in a progressive flattening of the absorption spectra in the "red" region and a slower absorption decrease in the "blue" region. An increase in the absorbance was observed between 450 and 560 nm for all three UV ranges. The absorbance ratio A_{430}/A_{411} (where A_{430} and A_{411} correspond to the absorbance intensity measured at 430 and 411 nm, respectively) decreased during UV-C irradiation and was proportional to the extent of bleaching of the chlorophylls – Fig. 2B (plot 1). The ratio behavior indirectly suggests the formation of UV-induced bleaching products which absorb above 410 nm.[18] Also, the ratios of the Q-band maximum at 661 nm to the intersection points of the absorption maxima at 450 and 560 nm (A_Q/A_i, *i.e.*, A_{661}/A_{450} and A_{661}/A_{560}, respectively) markedly decreased during irradiation, and is linearly proportional to the extent of chlorophylls bleaching (Fig. 2B, plots 2 and 3, respectively, with an average correlation coefficient, $R \approx 0.99$). A similar behavior was observed for UV-B and UV-A induced bleaching of the Chl*a* standard in acetone (not shown).

The absorption spectra of the chlorophylls from the extracted chlorophylls in acetone and *n*-hexane showed very similar behavior during the corresponding regime of irradiation with UV-A, UV-B and UV-C light, for all three concentration ranges. The absorption spectra of the pigments extract during its bleaching in *n*-hexane by UV-B light, with a calculated concentration of chlorophylls of 1.2×10^{-5} mol dm^{-3}, are shown in Fig. 3A.

In this case, the absorption spectra have intersection points at 490 and 570 nm. The first intersection point is "red shifted" compared to the Chl*a* standard solution (Fig. 2). The probable reason for this is the absorption of accessory pigments in the spectral region about 450 nm.[21] The absorbance ratios A_{665}/A_{488} and A_{665}/A_{570}, as well as A_{430}/A_{410} plotted *versus* the bleaching of the chlorophylls are shown in Fig. 3B (plots 2 and 3 and plot 1, respectively, the average correlation coefficient is $R \approx 0.99$). A clear linear decrease was found. These results indicate the possible formation of UV-induced bleaching products of the chlorophylls in spectral regions above 410 and 480–570 nm.[18] Moreover, Merzlyak found that irradiation of solutions containing purified carotenoids resulted in a uniform bleaching of these pigments without any appreciable formation of products absorbing between 350 and 500 nm.[18] Similar Vis spectral behavior (to that shown in Figs. 2 and 3) was observed in flash photolysis experiments of chlorophylls. The bleaching of chlorophylls was claimed to be related to the absorption by the triplet state of Chl (^{3}Chl) in organic solvents.[22]

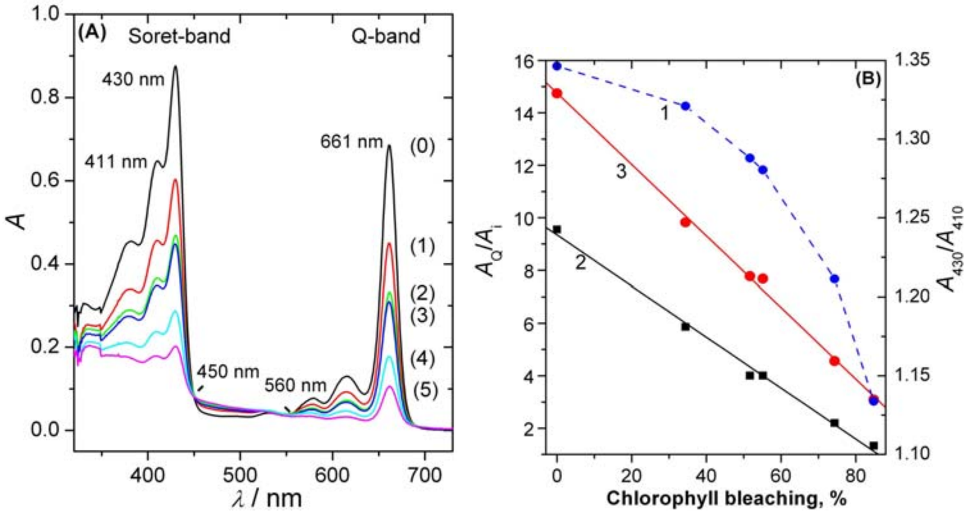

Fig. 2. (A) Changes in the Chl*a* standard absorption spectra following its exposure to UV-C radiation in acetone. The exposure time periods were: (0) 0, (1) 2, (2) 3, (3) 4, (4) 5 and (5) 7 min. (B) Dependence of the absorbance ratios of the red (Q) peak to the pseudo-isosbestic points, A_Q/A_i (plots 2 and 3 refer to the left ordinate) and of the ratio of the Soret bands, A_{430}/A_{410} (plot 1 refers to the right ordinate) on the extent of chlorophyll bleaching. (1) Soret band maximums are at 430 and 410 nm; (2) λ_{Qmax} = 661 nm, λ_{imax} = 450 nm; (3) λ_{Qmax} = 661 nm, λ_{imax} = 560 nm. The % chlorophyll bleaching was calculated according to Eq. (1). The absorption spectra showed very similar responses during irradiation with UV-A and UV-B light.

In chlorophyll, the central magnesium coordinates four nitrogen atoms of the pyrrole rings, providing for one or both Mg axial positions to be occupied by a molecule possessing a lone electron pair capable of acting as an electron donor. When Chl is dissolved in a nucleophilic polar solvent, such as acetone, the solvent acts as an electron donor to Mg and the chlorophyll then appears as “monomer”, with five- and/or six-coordinated Mg.[23] On the other hand, Chls may also act as electron donors, due to presence of a few keto groups, mostly belonging to the peripheric ester groups (C=O group in position C−13^1 in the Chl*a* molecule, an additional C=O group in the Chl*b* molecule in position C−7 and two ester groups in positions C−13^3 and C−17^3, Fig. 1).

Hence, one chlorophyll may act as an electron donor (*via* its ring E, keto group, C−13^1 position, Fig. 1) and the other Chl molecule can act as an electron acceptor *via* its central Mg atom.[24] Thus, in nonpolar solvents, such as *n*-hexane, chlorophyll predominantly appears in aggregated forms ("dimers" and "oligomers") at higher concentrations (over 10^{-5} mol dm^{-3})[23,25] and as a "monomer" at low concentrations. The Q-band $A_{\max}$ of "monomeric" Chl in *n*-hexane lies at ≈ 660 nm at c(Chl*a* + Chl*b*) = 1.2×10^{-6} mol dm^{-3}. In the concentration range about 10^{-5} to 10^{-4} mol dm^{-3}, the Q-band $A_{\max}$ is "red" shifted due to Chl–Chl interaction in the "dimeric" chlorophyll form (≈ 665 nm).[23]

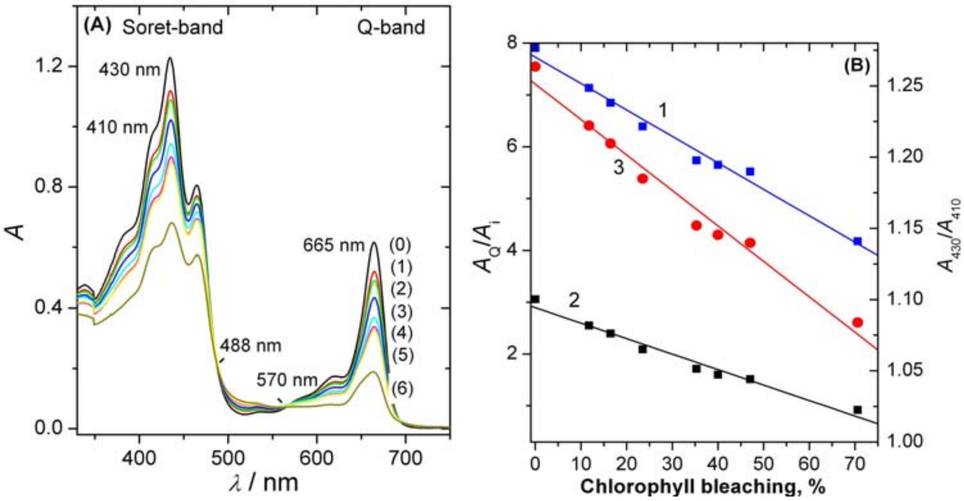

Fig. 3. UV-B induced bleaching of the extracted chlorophylls (Chl*a* + Chl*b*) in *n*-hexane. (A) Changes in the pigments absorption spectra following their exposure to UV-B radiation. The exposure time periods were: (0) 0, (1) 5, (2) 7, (3) 10, (4) 15, (5) 20 and (6) 30 min. (B) Dependence of the absorbance ratios of the red (Q) peak to the pseudo-isosbestic points A_Q/A_i (plots 2 and 3 refer to the left ordinate) and of the maximum of the Soret bands, A_{430}/A_{410} (plot 1 refers to the right ordinate) on the extent of chlorophyll bleaching. (1) Soret band maximums are 430 and 410 nm; (2) λ_{Qmax} = 665 nm, λ_{imax} = 488 nm; (3) λ_{Qmax} = 665 nm, λ_{imax} = 570 nm. The % chlorophyll bleaching was calculated according to Eq. (1). The absorption spectra showed very similar responses during irradiation with UV-A and UV-C light.

Bearing this in mind, chlorophylls *in vitro* should show a different behavior toward UV-irradiation in solvents with different polarities and in different concentration ranges.

Ultraviolet radiation can induce the generation of free radicals in organic compounds, especially those containing C=C bonds. In chlorophylls these bonds appear in great numbers (see Fig. 1).[26] Once created, free radicals can initiate chain reactions, which, in some cases, may be linked particularly to the presence of C=C and C=O bonds.[27] Absorption of electromagnetic radiation resulting in the generation of free radicals may occur through two competing mechanisms:

(*i*) Excitation by energy absorption and subsequent decomposition into radicals;

(*ii*) photosensitized energy transfer.[28]

To assess the possibility of direct UV absorption by photosynthetic pigments, Johnson and Day measured the absorbance of extracted chlorophylls and noticed that Chl*a* had absorbance peaks at 340 and 389 nm, which were 49 and 72 % of the Soret peak absorbance, and Chl*b* had absorbance peaks at 315 and 346 nm, which were both 35 % of the Soret peak value.[29] The excited chlorophylls can be oxidized photochemically to their π-cation radicals (*i*).[30,31] On the other hand, both the proposed mechanisms (*i*) and (*ii*) may lead to Chl bleaching in more complicated ways, which include the relatively stable excited triplet state (^{3}Chl, lifetime of 10^{-5}–10^{-3} s) and the presence of reactive oxygen species (ROS), by three most probable pathways:[32]

(1) formation of an active complex between ^{3}Chl and the ground state of oxygen ($^3O_2$), which can then oxidize HO^- to the extremely powerful oxidizing agent $HO^\bullet$;

(2) energy transfer from ^{3}Chl to $^3O_2$, leading to very reactive singlet oxygen ($^1O_2$);

(3) electron transfer from ^{3}Chl to $^3O_2$ resulting in formation of superoxide radical anion ($O_2^{\bullet-}$) which can then generate $HOO^\bullet$, H_2O_2, $HO^\bullet$ and $^1O_2$. This type of reactions deals with a mechanism in which the initial attack of oxygen is directed toward position C-5 (Fig. 1).[33] These mechanisms may be called Chl self-destruction mechanisms due to their pronounced photosensitizing capability.

Exposure of Chls to UV-A and UV-B radiation *in vivo* is believed to enhance the amount of ROS.[34–36] Singlet oxygen also attacks the double bonds of the phytyl chain leading to the formation of numerous isoprenoid photoproducts.[37]

A report about ROS production *in vitro* under photosynthetically active radiation (PAR) in hexane solutions of chlorophylls[38] is relevant for this work, because chlorophyll absorbs UV-A and UV-B[29] and oxygen was certainly present, due to oxygen diffusion in acetone and hexane.[22,39] In addition, acetone and *n*-hexane have similar viscosities (the viscosity of acetone is $\eta = 0.303\times10^{-3}$ Pa s and of *n*-hexane 0.29×10^{-3} Pa s),[22,40] which should imply that the concentrations of oxygen in these solvents is similar. The authors[38] concluded that in disorganized organic solutions (such as those studied in the present work), UV-induced bleaching of chlorophyll seems to be related to the photochemical generation of $^1O_2$ by mechanism (*ii*); no role of $O_2^{\bullet-}$ or H_2O_2 was proposed.

The kinetics of the bleaching of chlorophylls seems to obey a first-order law, as already reported.[41–43] The corresponding kinetic logarithmic plots as a result of increasing time of irradiation for the extracted chlorophylls in *n*-hexane, for all three UV-ranges, are shown in Fig. 4. The corresponding kinetic ln plots for all three concentrations of chlorophylls in both solvents are of very similar shape to the presented ones (not shown).

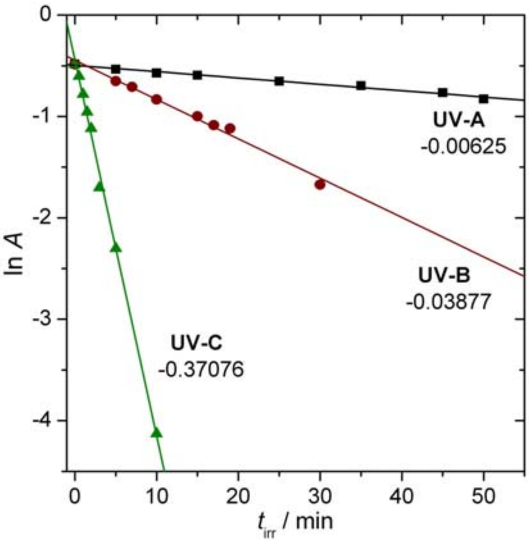

Fig. 4. The kinetic plots of the bleaching of the extracted chlorophylls (Chl*a* + + Chl*b*) in *n*-hexane with increasing irradiation time of UV-A, UV-B and UV-C radiation. The absorbance of Chl*a* was followed at A_{max} of the Q-band (≈ 665 nm). The chlorophyll concentration was 1.2×10^{-5} mol dm^{-3}. The corresponding slopes (in min^{-1}) are displayed for all three UV irradiation ranges (UV-A, UV-B and UV-C).

The bleaching rate constants, *k*, for the Chl*a* standard and the extracted chlorophylls, for all three UV-ranges and the same Chl*a* concentration, calculated from the slopes given in Fig. 4,

$$y = -kx + n \tag{2}$$

where *y* is log of the extract absorbance in acetone or *n*-hexane at 662 nm and 660—665 nm, respectively, *x* is the UV-irradiation time and *k* is the rate constant for the bleaching of chlorophyll, are shown in Table I.

TABLE I. Kinetics of chlorophylls bleaching in acetone (Chl*a*-standard and the pigments extract) with increasing UV irradiation time for the three different UV-ranges: UV-A, UV-B and UV-C. Chlorophylls absorbencies were followed at A_{max} of the Q-band (661 nm for the Chl*a* standard and 662 nm for the Chls in the pigments extract)

λ_{UV} / nm	Chl*a*-standard solution	Chls in pigment extract	
	c_{Chla} and c / 10^{-6} mol dm^{-3}		
	8.26	8.02 (~c_{Chla})	8.54 (~c_{Chla})
	k / min^{-1}		
350 (UV-A)	0.10616	0.12797	0.08587
300 (UV-B)	0.32170	0.29548	0.23985
254 (UV-C)	0.26800	0.26788	0.22602

The bleaching rate constants of the chlorophylls in the extract were very similar to those of the standard for the same concentration range (Table I, 0.26800, 0.26788 and 0.22602 min^{-1} for UV-C irradiated Chl*a*-standard and the extracted chlorophylls of the concentration of 8.02×10^{-6} and 8.54×10^{-6} mol dm^{-3}, respectively). This proves that bleaching rate of Chls in solution does not depend significantly on the presence of the accessory pigments in the environment. The very similar *k* values for the Chl*a* standard and the extracted Chls also indicates that Chl*b* is possibly also very sensitive to UV irradiation; consequently, Chl*a* is the major contributor to the bleaching of the extracted Chls.[41]

The calculated bleaching rate constants for the extracted chlorophylls, for all three UV-ranges in the two solvents and for all three concentrations (1.2×10^{-6}, 1.2×10^{-5} and 1.4×10^{-4} mol dm^{-3}) are shown in Table II.

TABLE II. Bleaching kinetics of the extracted chlorophylls in acetone and *n*-hexane with increasing UV-irradiation time for the three different UV-ranges: UV-A, UV-B and UV-C at three different concentration ranges (≈ 10^{-6}, 10^{-5} and 10^{-4} mol dm^{-3}). Chlorophylls absorbances were followed at $A_{\max}$ of the Q-band (662 nm in acetone, 660 nm in *n*-hexane at 1.2×10^{-6} mol dm^{-3} and at 665 nm in *n*-hexane in the 10^{-5}–10^{-4} mol dm^{-3} concentration range).

c(Chl*a*+Chl*b*) / 10^{-5} mol dm^{-3}		UV-A (350 nm)	UV-B (300 nm)	UV-C (254 nm)
			k / min^{-1}	
0.12	In acetone	0.41480	0.70000	0.42526
	In *n*-hexane	0.03265	0.21101	1.43295
1.2	In acetone	0.08587	0.23985	0.22602
	In *n*-hexane	0.00625	0.03877	0.37076
14	In acetone	0.01246	0.03961	0.10130
	In *n*-hexane	0.00180	0.00364	0.01716

The presented data (Tables I and II) suggest that the bleaching rate of chlorophylls *in vitro* depends on the UV irradiation range (*i.e.*, the energy of the photons), the chlorophylls concentration and the solvent polarity.

n-Hexane is transparent in the UV range down to 201 nm and the UV radiations used in this work should have no influence on the solvent molecules in terms of their excitation, ionization and formation of *n*-hexyl cation-radicals, which could then participate in the bleaching of the extracted chlorophylls. The influence of energy on photobleaching rate constants in non-polar *n*-hexane progressively increased from UV-A to UV-C for all three studied concentrations (Table II). The ratios of bleaching rate constants obtained for the concentration when Chl is "monomeric" and the two concentrations when Chl is "aggregated" (10^{-6}, 10^{-5} and 10^{-4} mol dm^{-3}, respectively) are: for UV-A, $k_{10^{-6}}/k_{10^{-5}}$ ($k_{\text{mon}}/k_{\text{agg}}$) = 5, $k_{10^{-5}}/k_{10^{-4}}$ (k_{agg}) = 3; for UV-B, $k_{10^{-6}}/k_{10^{-5}}$ ($k_{\text{mon}}/k_{\text{agg}}$) = 5, $k_{10^{-5}}/k_{10^{-4}}$ (k_{agg}) = 11; for UV-C, $k_{10^{-6}}/k_{10^{-5}}$ ($k_{\text{mon}}/k_{\text{agg}}$) = 4, $k_{10^{-5}}/k_{10^{-4}}$ (k_{agg}) = 22. Increasing the chlorophyll concentration by about one order of magnitude distinctly decreases the ratios of the bleaching rates of the extracted chlorophylls (Table II). It would be expected that aggregated extracted chlorophylls should be much more stable against UV-A radiation (as was found for UV-B and UV-C induced bleaching). However, the data from Table II suggest that chlorophylls aggregation probable does not play a major stability role against UV-A bleaching of the extracted chlorophylls in *n*-hexane (decreases of the bleaching rates ratios of 5 and 3, respectively, Table II). On the other hand, aggregation of Chl molecules plays a significant stability role against UV-B and, especially, UV-C irradiation (Table II). Chlorophylls aggregates are reportedly excellent quenchers, showing an extreme shortening of the lifetime of the chlorophyll triplet excited state.[23,44] The possibility of the existence of a free radical "dimeric" form[45] (*i.e.*, *in vitro* UV-induced formation of "dimeric" chlorophyll cation radicals $(\mathrm{Chl}_2)^+$) was not considered because no available information was provided.

Acetone absorbs in the UV range below 350 nm (two absorption maximums at 280 and 190 nm, related to the forbidden n–π^* transition and the highly intensive π–π^* transition, respectively).[46] Considering the influence of the energy of the photon input on the stability of the extracted chlorophylls in acetone, it is evident that the bleaching rates decline by a factor of 1.7–3.2 when going from UV-A to UV-C radiation for all three studied concentrations: for $\approx 10^{-6}$ mol dm^{-3}, $k_{\text{UV-B}}/k_{\text{UV-A}} = 1.7$; for $\approx 10^{-5}$ mol dm^{-3}, $k_{\text{UV-B}}/k_{\text{UV-A}} = 2.8$; for $\approx 10^{-4}$ mol dm^{-3}, $k_{\text{UV-B}}/k_{\text{UV-A}} = 3.2$. The only exception was noted in the case of UV-C radiation, for irradiated extracted chlorophylls in the concentrations ranges of $\approx 10^{-6}$ and 10^{-5} mol dm^{-3} (Table II). In the former case, the observed bleaching rate constant for UV-C irradiation was slightly higher than the one obtained for UV-A irradiation ($k_{\text{UV-C}}/k_{\text{UV-A}} = 1.02$), while in the latter case the observed bleaching rate constant for UV-C irradiation was slightly lower than the one for UV-B irradiation ($k_{\text{UV-C}}/k_{\text{UV-B}} = 0.94$). However, the $k_{\text{UV-C}}/k_{\text{UV-B}}$ ratios progressively increased with increasing concentration of chlorophylls (for 1.2×10^{-6} mol dm^{-3}, $k_{\text{UV-C}}/k_{\text{UV-B}} = 0.61$, while for 1.4×10^{-4} mol dm^{-3}, $k_{\text{UV-C}}/k_{\text{UV-B}} = 2.56$).

When acetone molecules interact with "monomeric" extracted chlorophylls *via* acetone carbonyl "bridges", the electron density of the chlorin ring is not arranged between the two chlorophyll molecules (as in the Chl "dimer" formed at higher Chl concentrations in *n*-hexane) but is distributed between one chlorophyll molecule and one or two acetone molecules.[23] Since acetone absorbs over the whole UV range (which overlaps with the UV-ranges used in this study),[46] this may lead to a decreased stability of the extracted chlorophylls against UV radiation, compared to the extracted chlorophylls in *n*-hexane. If one compares the photobleaching rate constants for the three chlorophyll concentration ranges obtained in the two solvents, then it is obvious that the photobleaching rate constants obtained with UV-A radiation in acetone were about 12, 13 and 7 times higher than the corresponding values obtained in *n*-hexane, while the corresponding relations obtained for UV-B radiation were about 3, 6 and 11 higher. In fact, going from UV-A to UV-C, and for increasing Chls concentrations ($10^{-6} \rightarrow \rightarrow 10^{-5} \rightarrow 10^{-4}$ mol dm^{-3}), the extracted "aggregated" chlorophylls appear more stable in *n*-hexane than in acetone, probably due to "dimer" formation. On the other hand, the "monomeric" extracted chlorophylls (1.2×10^{-6} mol dm^{-3}) expressed lower stability against UV-C irradiation in *n*-hexane than in acetone (by a factor of 3).

CONCLUSIONS

1. The UV-induced bleaching of chlorophylls in the pigment extract fits the first-order kinetic model.

2. The bleaching rate of the extracted Chls *in vitro* did not significantly depend on the presence of accessory pigments (carotenoids) in the pigment extract.

3. UV-induced bleaching of the extracted chlorophylls is probably followed by the formation of chlorophyll bleaching products which absorb in spectral regions above 410 nm and 480–570 nm.

4. The bleaching rate of Chls *in vitro* depended on the energy input of the UV-photons, the concentration of chlorophylls and the molecular organization of the chlorophylls in n-hexane and acetone. The Chls aggregates in *n*-hexane protect best against UV-C and UV-B radiation and to a less extent against UV-A irradiation.

Acknowledgements. This work was supported under the project Development of Technology and Products of Pharmaceutical and Cosmetic Industry, number TR-6708B, by the Ministry of Science of the Republic of Serbia.

ИЗВОД

ОБЕЗБОЈАВАЊЕ ХЛОРОФИЛА UV ЗРАЧЕЊЕМ *IN VITRO*: ЕФЕКТИ НА ОРГАНИЗАЦИЈУ ХЛОРОФИЛА У АЦЕТОНУ И ХЕКСАНУ

ЈЕЛЕНА ЗВЕЗДАНОВИЋ и ДЕЈАН МАРКОВИЋ

Технолошки факултет, 16000 Лесковац

Стабилност хлорофила према UV зрачењу проучавана je Vis спектрофотометријом у екстрактима који садрже смеше фотосинтетских пигмената у ацетону и хексану. Хлорофили подлежу деструкцији (обезбојавању) покоравајући се кинетици првог реда. На кинетику обезбојавања утичу три главна фактора: енергија UV фотона, концентрација хлорофила и поларност растварача, која подразумева различите молекуларне организације хлорофила у њима.

(Примљено 17. маја, ревидирано 8. августа 2007)

REFERENCES

1. A. H. Teramura, L. H. Ziska, in *Photosynthesis and the Environment*, N. Baker, Ed., Kluwer, Dordrecht, 1996, p. 435
2. J. Grzymski, C. Orrico, O. Schofield, *Photosynth. Res*. **68** (2001) 181
3. A. Stird, R. J. Porra, *Plant Cell Physiol*. **33** (1992) 1015
4. H. Scheer, in *CRC Handbook of organic photochemistry and photobiology*, W. Horspool, S. Song, Eds., CRC Press, Boca Raton, 1994, p. 1402
5. H. Scheer, in *CRC Handbook of Organic Photochemistry and Photobiology*, W. Horspool, F. Lenci, Eds., CRC Press, Boca Raton, 2003, p. 117
6. H. Scheer, in *Chlorophylls*, H. Scheer, Ed., CRC Press, Boca Raton, 1991, p. 1
7. H. Scheer, in *Chlorophylls and Bacteriochlorophylls: Biochemistry, Biophysics, Functions and Applications*, B. Grimm, R. J. Porra, W. Rüdier, H. Scheer, Eds., Springer, Amsterdam, 2006, p. 397
8. P. H. Hynninen, in *Chlorophylls*, H. Scheer, Ed., CRC Press, Boca Raton, 1991, p. 145
9. G. A. F. Hendry, J. D. Houghton, S. B. Brown, *New Phytol*. **107** (1987) 255

10. J. J. Jen, G. MacKiney, *Photochem. Photobiol.* **11** (1970) 303
11. C. A. Llewellyn, R. F. G. Mantoura, R. G. Brereton, *Photochem. Photobiol.* **52** (1990) 1043
12. W. A. Svec, in *Chlorophylls*, H. Scheer, Ed., CRC Press, Boca Raton, 1991, p. 89
13. J. Petrović, G. Nikolić, D. Marković, *J. Serb. Chem. Soc.* **71** (2006) 501
14. H. K. Lichtenthaler, *Methods Enzymol.* **148** (1987) 350
15. R. J. Porra, in *Chlorophylls*, H. Scheer, Ed., CRC Press, Boca Raton, 1991, p. 31
16. R. J. Ritchie, *Photosynth. Res.* **89** (2006) 27
17. V. Rassadina, V. Domanski, N. G. Averina, S. Schochb, W. Rüdiger, *Physiol. Plant.* **121** **(**2004) 556
18. M. N. Merzlyak, S. I. Pogosyan, L. Lekhimena, T. V. Zhigalova, I. F. Khozina, Z. Cohen, S. S. Khrushchev, *Russ. J. Plant Physiol.* **43** (1996) 160
19. A. J. Hoff, J. Amesz, in *Chlorophylls*, H. Scheer, Ed., CRC Press, Boca Raton, 1991, p. 723
20. *Phytoplankton Pigments in Oceanography: Guidelines to Modern Methods*, S. W. Jeffrey, R. F. C. Mantoura, S. W. Wright, Eds., UNESCO Publishing, 1996
21. H. Scheer, in *Advances in Photosynthesis*, B. R. Green, W. W. Parson, Eds., Kluwer, Dordrecht, 2003, p. 29
22. A. Drzewiecka-Matuszek, A. Skalna, A. Karocki, G. Stochel, L. Fiedor, *J. Biol. Inorg. Chem.* **10** (2005) 453
23. J. J. Katz, L. L. Shipman, T. M. Cotton, T. R. Janson, in *The Porphyrins*, D. Dolphin, Ed., Academic Press, New York, 1978, p. 401
24. A. D. Trifunac, J. J. Katz, *J. Am. Chem. Soc.* **96** (1974) 5233
25. T. Oba, M. Mimuro, Z. Y. Wang, T. Nozawa, S. Yoshida, T. Watanabe, *J. Phys. Chem. B* **101** (1997) 3261
26. J. Ramirez-Niño, D. Mendoza, V. M. Castaño, *Radiat. Meas.* **29** (1998) 195
27. W. L. Hawkins, *Polymer stabilization*, Wiley, New York, 1972, p. 17
28. G. Odian, *Principle of polymerization*, Wiley, New York, 1993, p. 179
29. G. A. Johnson, T. A. Day, *Physiol. Plant.* **116** (2002) 554
30. N. Ohta, L. Kevan, *J. Phys. Chem.* **89** (1985) 3070
31. P. Faller, T. Maly, A. W. Rutherford, F. Macmillan, *Biochem.* **40** (2001) 320
32. A. N. Melkozernov, R. E. Blankenship, in *Chlorophylls and Bacteriochlorophylls: Biochemistry, Biophysics, Functions and Applications*, B. Grimm, R. J. Porra, W. Rüdier, H. Scheer, Eds., Springer, Amsterdam, 2006, p. 397
33. W. Mühlecker, B. Kräutler, S. Ginsberg, P. Matle, *Helv. Chim. Acta* **76** (1993) 2976
34. P. K. Sharma, P. Anand, S. Sankhalkar, *Curr. Sci.* **75** (1998) 359
35. C. Barta, T. Kalai, K. Hideg, I. Vass, E. Hideg, *Funct. Plant Biol.* **31** (2004) 23
36. P. Zhang, J. Yu, X. Tang, *J. Integr. Plant Biol.* **47** (2005) 683
37. J.-F. Rontani, G. Baillet, C. Aubert, *J. Photochem. Photobiol., A* **59** (1991) 369
38. V. Caspi, S. Malkin, J. B. Marder, *Photochem. Photobiol.* **71** (2000) 441
39. I. Cibulka, A. Heintz, *Fluid Phase Equilib.* **107** (1995) 235
40. J. H. Dymond, M. A. Awan, *Int. J. Thermophys.* **10** (1989) 941
41. S. Santabarbara, *Arch. Biochem. Biophys.***455** (2006) 77
42. P. Cuny, J.-C. Romano, B. Beker, J.-F. Rontani, *J. Exp. Mar. Biol. Ecol.* **237** (1999) 271
43. N. Mircin, A. Peled, *Appl. Surf. Sci.* **248** (2005) 91
44. A. Scherz, V. Rosenach-Belkin, T. J. Michalski, D. L. Worcester, in *Chlorophylls*, H. Scheer, Ed., CRC Press, Boca Raton, 1991, p. 237
45. J. R. Norris, R. A. Uphaus, H. L. Crespi, J. J. Katz, *Proc. Natl. Acad. Sci. U.S.A.* **68** (1971) 625
46. M. Yujing, A. Mellouki, *J. Photochem. Photobiol. A* **134** (2000) 31.

www.shd.org.yu

Journal of the Serbian Chemical Society

JSCS@tmf.bg.ac.yu • www.shd.org.yu/JSCS

J. Serb. Chem. Soc. 73 (3) 283–297 (2008)
JSCS–3710

UDC **Stevia rebaudiana*+581.45:633.879+
547.384:665.52/.54(497.113)
Original scientific paper

Chemical composition of leaf extracts of *Stevia rebaudiana* Bertoni grown experimentally in Vojvodina

IVANA S. MARKOVIĆ[1#], ZOLTAN A. ĐARMATI[2#] and BILJANA F. ABRAMOVIĆ[3#*]

[1]College of Technology, Đorđa Stratimirovića 23, 23000 Zrenjanin, [2]Bioecological Center, Petra Drapšina 1, 23000 Zrenjanin and [3]Faculty of Science, Department of Chemistry, Trg D. Obradovića 3, 21000 Novi Sad, Serbia

(Received 8 June, revised 9 August 2007)

Abstract: The chemical composition of leaf extracts of *Stevia rebaudiana* Bertoni, grown for the first time on an experimental field near Zrenjanin, was examined by GC–MS. The tested plant material was harvested in September of 2002. To analyze the chemical composition of the lipophilic components of the plant leaves, essential oils and ethyl acetate extract were isolated. Qualitative analysis of the essential oil obtained by hydrodistillation showed that among the identified 88 compounds, the majority were mono- and sesquiterpenes (50 types identified). By analysing the ethyl acetate extract, the presence of fatty acids (present as free and as esters), *n*-alkanes, *n*-alkenes, cyclic alkanes, alcohols, aldehydes, ketones, *etc*. was ascertained. Sesquiterpenes prevailed among the terpenes (50 types identified). Further constituents identified in ethyl acetate extract included sterols. Nerol, β-cyclocitral, safranal, aromadendrene, α-amorphene and T-muurolol were identified for the first time in this species, with match values over 90 %. Taking into consideration that these terpenes were identified for the first time in this species, it is obvious that *Stevia rebaudiana* grown in this area possesses certain specific characteristics that can be ascribed to cultivation on a domestic plantation.

Keywords: *Stevia rebaudiana* Bertoni; essential oil; ethyl acetate extract; GC–MS; composition.

INTRODUCTION

Stevia rebaudiana Bertoni belongs to the family Compositae (Asteraceae)[1,2] and is one of only two of the 154 members of the genus *Stevia* producing sweet steviol glycosides.[1] *Stevia rebaudiana* is a small bush that originates from Paraguay.[2] The intensive sweet taste of its leaves has been well known to local Guarani Indians for centuries. In the first place, *Stevia rebaudiana* is known as *yerba*

[#] Serbian Chemical Society member.

[*] Corresponding author. E-mail: abramovic@ih.ns.ac.yu

doi: 10.2298/JSC0803283M

dulce in South America, since native Latin American nations called it by many different names: *caá-êhê*, *azuca-caá, kaá-hê-E* and *ca-a-yupe*.[3,4] Most of these names in different ways point to the sweet taste of the leaves of *Stevia rebaudiana*, a property which has been the subject of numerous botanical, physiological and chemical investigations.

Today, exceeding South American continent, all over the world *Stevia rebaudiana* represents a new crop from which natural high-potency non-caloric sweeteners can be obtained. The two main glycosides are stevioside and rebaudioside A, the latter being even 150–320 times sweeter than sucrose.[1] Since numerous studies have established certain effects of *Stevia rebaudiana* and its extracts on the human organism, it has become interesting for the pharmaceutical industry. Among the therapeutic activities attributed to it, hypotensive regulation, hypoglycemic, antimicrobial and contraceptive activities can be listed.[4–8] As a result, *Stevia rebaudiana* has become rather widespread over a wide range of climatic locations around the world and can apparently be successfully grown under different cultivation conditions. Since the chemical composition of extracts of the leaves of *Stevia rebaudiana* is dependent on the applied conditions of plant cultivation, they have become the subject of many research projects.

The increasing importance of the essential oils in various domains of human life (pharmacy, cosmetics, as well as food and drinks industries) has made this field very interesting for chemical investigations.[9–13] Considering the current research of *Stevia rebaudiana* essential oil, it may be observed that it has been insufficiently investigated. Namely, to the best of our knowledge, there have only been a few studies concerning the composition of *Stevia rebaudiana* essential oil. Fujita *et al.*[9] examined the essential oil of *Stevia rebaudiana* plants collected in several zones of Japan and found that they mainly contained the sesquiterpenes: β-caryophyllene, *trans*-β-farnesene, α-humulene, δ-cadinene, caryophyllene oxide, nerolidol and an unidentified alcohol and the monoterpenes: linalool, terpinen-4-ol and α-terpineol. Martelli *et al.*[10] identified 54 components of a steam distillate of dried plant leaves from Brazil. The main components were caryophyllene oxide and spathulenol, making up 43 % of the overall content. Cioni *et al.*[11] examined the composition of the essential oil of the aerial parts of five different *Stevia rebaudiana* genotypes from Brazil and Paraguay cultivated in the coastal area of Tuscany (Italy). Forty different components were identified and the main constituents in all the samples were spathulenol, caryophyllene oxide, β-caryophyllene and β-pinene.

In order to determine the lipophilic constituents of *Stevia rebaudiana* leaves provided by the Steviafarma Industry (Maringá, RP, Brazil), Yoda *et al.*[12] used supercritical fluid extraction with carbon dioxide. They identified six classes of compounds, *i.e.*, sesquiterpenes, alcohols, labdanic diterpenes, aliphatic hydrocarbons, sterols and triterpenes. In the investigated extract, the main compounds were diterpenes, of which the most abundant was austroinulin. The other labdanic diterpene represented in a higher level was jhanol. Significant portions of the contents of non-polar components belonged to the hydrocarbons *n*-tetracosane and *n*-pentacosane.

A survey of the pertinent literature showed that no *Stevia rebaudiana* plant material grown in our region has hitherto been examined, except for a material obtained by an *in vitro* procedure of propagation.[14]

In view of the above, the objective of this work was to study the chemical composition of the essential oil and ethyl acetate extract of leaves of *Stevia rebaudiana* Bertoni from Brazil grown on a domestic plantation.

EXPERIMENTAL

Plant material

Stevia rebaudiana leaves (seeds originating from Brazil) were harvested from a domestic plantation near Zrenjanin, Vojvodina. The experimental cultivation of *Stevia rebaudiana* in Vojvodina commenced in 2001, by propagating from seeds. In accordance with the local climate conditions, the seedlings were grown in a glasshouse prior to the growth season. The seedlings were transplanted to the field in the middle of May and harvested in September of 2002.

Extraction

The essential oil of *Stevia rebaudiana* leaves was obtained by hydrodistillation. An amount of 100 g of dried (at 105 °C to constant mass) ground leaves was heated with 1.0 l of water. The distillation was run for 150 min and the essential oil collected in 2.0 ml of *n*-hexane. Subsequently, 1.0 ml of fresh *n*-hexane was added and after separation, the *n*-hexane layer was dried with anhydrous sodium sulphate; the dried filtrate was refrigerated until examination.

The ethyl acetate extract was prepared by heating 500 g of dried and ground plant leaves with 5.0 l of ethyl acetate at the boiling temperature. The treated material and the solvent were left over night and then, after the filtration and vaporization to dryness, the extraction process was repeated with a further 5.0 l of the same solvent. The dry residues after the first (31.30 g) and second (5.56 g) extraction were mixed to make a pooled ethyl acetate extract.

The analytical scheme for the isolation and analysis of the lipophilic constituents of *Stevia rebaudiana* leaves is presented in Fig. 1.

Column chromatography

Dry ethyl acetate extract (30 g) was after the appropriate preparation applied to a silica gel column (Merck, 0.05–0.2 mm). A gradient elution was performed by increasing the concentration of ethyl acetate in benzene from 0 to 25 % (Table I). A constant flow of 1.5 l/24 h was used. The elution was performed continually and 1.5 l volume fractions were collected daily. Each fraction was evaporated to dryness under vacuum.

Thin layer chromatography

Thin layer chromatography (TLC) was used to monitor the qualitative composition of the fractions of the ethyl acetate extract obtained by column chromatography. TLC was performed on 20 cm×20 cm glass plates precoated in our laboratory with silica gel. Silica gel (20 g) was suspended in distilled water (50 ml) and the suspension was applied onto the glass plates using Desaga equipment. The coated plates were dried in the air at room temperature for 24 h, followed by activation of the plates by drying at 100 °C for 1 h. Small portions of each collected fraction were dissolved in a small volume of ethyl acetate and then applied onto silica gel plates and examined by TLC using benzene as the mobile phase. The chromatograms were observed after spraying with vanillin spray and drying at 130 °C for 10 min.

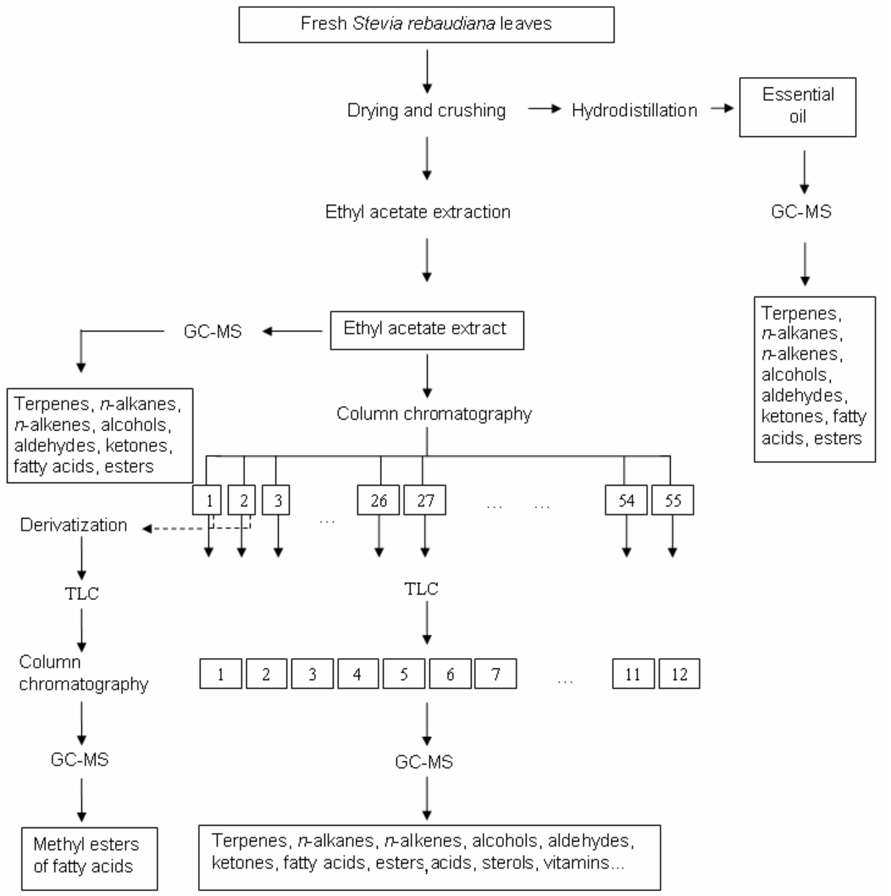

Fig. 1. Analytical scheme for the isolation and analysis of the lipophilic constituents of *Stevia rebaudiana* leaves.

TABLE I. Fractions of ethyl acetate extract eluted by varying polarity of the mobile phase

Composition of mobile phase ethyl acetate–benzene (v/v)	Fraction eluted
0:100	1–28
5:95	29–34
10:90	35–41
15:85	42–47
20:80	48–52
25:75	53–55

Derivatization

The first two ethyl acetate fractions obtained by column chromatography (Fig. 1) were derivatized. To two vessels with 100 mg of elementary sodium dissolved in 100 ml of absolute methanol, 1.00 g of each of the first two ethyl acetate fractions were added under stirring. As the TLC analysis showed their composition to be similar, the two solutions were combined and the resulting solution was filtered and treated with a cationic exchange resin (Purolite C 100E) under constant stirring. After attaining a pH 4–5, the solution was filtered and evaporated to dryness. The mass of the dry residue was 0.45 g. The dry residue was dissolved in 4.0 ml of benzene, of which 3.5 ml were fractionated on a small silica gel column, and the remaining 0.50 ml was kept for TLC observation of fractionation. The elution of methyl esters of fatty acids was realized by passing 200 ml of benzene through silica gel column, followed by the same volume of 25 % ethyl acetate in benzene, for elution of alcohols. Both the collected fractions were evaporated to dryness and the first one was dissolved in benzene, and the second in 25 % ethyl acetate in benzene, the undissolved residues being discarded. After repeating the evaporation to dryness, first fraction, containing methyl esters of fatty acids, was dissolved in 2.0 ml of *n*-hexane, and second containing alcohols, in 2.0 ml of ethyl acetate, to be used for GC–MS analysis.

Gas chromatography–mass spectrometry

The analyses were performed on an Agilent Technologies 6890N gas chromatograph, equipped with a 19091S-433 HP-5MS capillary column (30 m×0.25 mm, 0.25 μm film thickness); the carrier gas was He (43.2 ml min^{-1}). In the analysis of essential oil, the operating conditions were: column temperature 50 °C (1.0 min), 5.0 °C min^{-1} to 100 °C, 9.0 °C min^{-1} to 200 °C (2.89 min), run time 25 min; 5.0 μl of the essential oil solution were injected in the splitless mode at a temperature of 250 °C. The temperature regime in the analysis of ethyl acetate extracts was the following: column temperature 50 °C, 22 °C min^{-1} to 130 °C (1.0 min), 12 °C min^{-1} to 280 °C (12.86 min), run time 30 min, with an injector temperature of 250 °C. A volume of 5.0 μl of ethyl acetate extract solution in *n*-hexane (5.0 mg extract/ml *n*-hexane) was injected onto the column, also in the splitless mode. The Agilent 5973N mass selective detector was equipped with an Agilent 7683 autoinjector; the carrier gas was helium at a constant flow of 1.1 ml min^{-1}. The detector temperature was 230 °C. Ionization was performed by electrons at 70 eV; the scan range was 50–550 *m*/*z*.

Identification procedure

The data was collected with GCD ChemStation (G1074A HP, Version A.00.00) software, which enabled comparison of their mass spectra with those from the Wiley 275.1 MS library. An all-mass range of *m*/*z* 50–550 was used in the matching equation for identification.

RESULTS AND DISCUSSION

Essential oil

The GC–MS total ion current (TIC) chromatograms of the essential oil are shown in Fig. 2. After software processing of the mass fragmentation data and their comparison with the mass spectra from the library, 88 different components were identified in the essential oil of *Stevia rebaudiana* leaves. The identified components are presented in Table II, from which it can be seen that the composition of the essential oil is complex and rich in mono- and sesquiterpenes. Namely, of the 88 identified components, 52 were terpenes. The essential oil was characterized by a high content of sesquiterpenes, a smaller amount of monoterpenes, and a few diterpenes, namely, 18 monoterpene, 32 sesquiterpene compounds and only two diterpene compounds – alcohol phytol and neophytadiene.

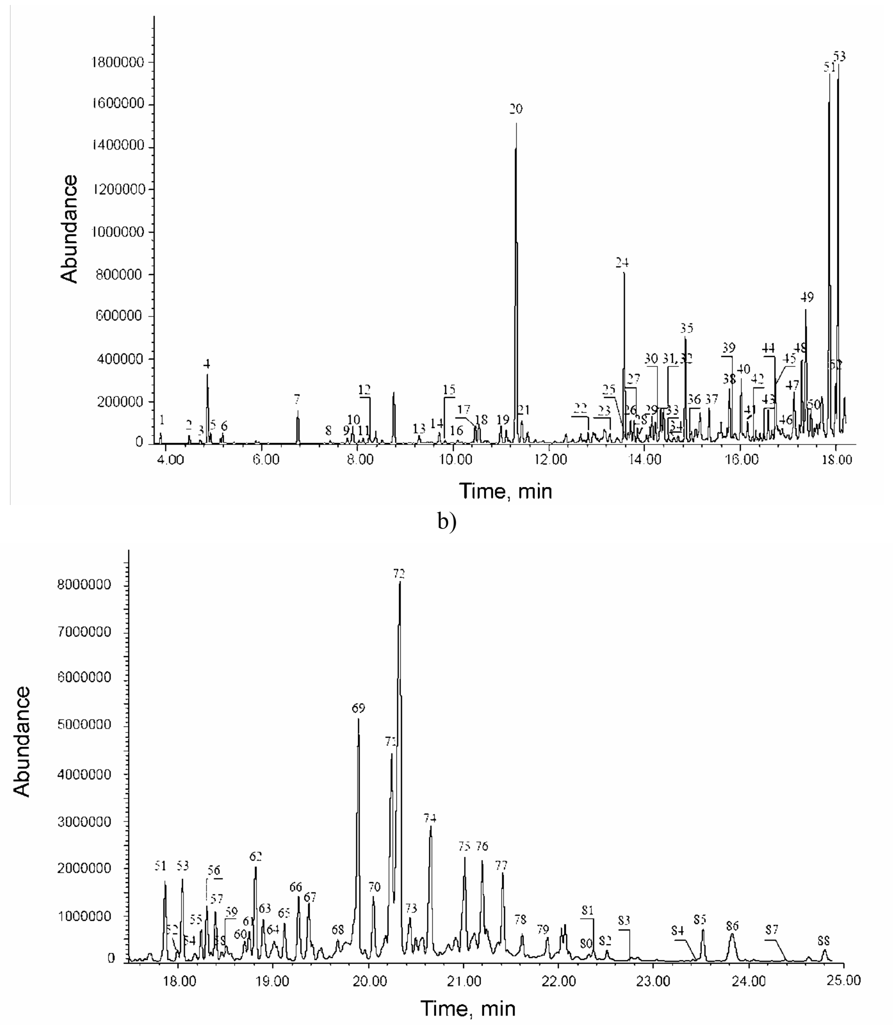
a)
b)

Fig. 2. GC–MS TIC chromatogram of the essential oil of *Stevia rebaudiana* leaves: a) 3.5–18 min; b) 17.5–25 min. Identification of the peaks is given in Table II.

In the group of monoterpenes, three compounds were present that had not previously been reported as constituents of *Stevia rebaudiana*. They are monoterpene nerol and monoterpene aldehydes β-cyclocitral and safranal. Safranal, a biologically very active substance, is the main component of the essential oil of saffron (*Crocus sativus* L.).[15,16]

TABLE II. Identification of peaks from Figs. 2a and 2b

Symbol	Compound	Match value %	Symbol	Compound	Match value %
1	*n*-Hexanal	83	45	1,1,6-Trimethyl-1,2-dihydronaphthalene	90
2	Furfural	90	46	Decanoic acid	97
3	5-*tert*-Butyl-1,3-cyclopentadiene	91	47	*α*-Copaene$^{\mathrm{s}}$	99
4	*trans*-2-Hexenal	97	48	*tans*-*β*-Damascenone$^{\mathrm{s}}$	90
5	*cis*-3-Hexenal	96	49	*β*-Bourbonene$^{\mathrm{s}}$	98
6	1-Hexanol	83	50	15-Methyltricyclo[6.5.2(13,14).0(7,15)]-pentadeca-1,3,5,7,9,11,13-heptaene	83
7	*α*-Pinene$^{\mathrm{m}}$	97	51	β-Caryophyllene$^{\mathrm{s}}$	99
8	Benzaldehyde	91	52	Germacrene D$^{\mathrm{s}}$	92
9	Sabinene$^{\mathrm{m}}$	97	53	(–)-*endo*-2,6-Dimethyl-6-(4-methyl-3-pentenyl)bicyclo[3.1.1]hept-2-ene	93
10	1-Octen-3-ol	80	54	Aromadendrene$^{\mathrm{s}}$	91
11	6-Methyl-5-hepten-2-one	96	55	Geranylacetone$^{\mathrm{s}}$	86
12	2,4-Heptadienal	94	56	*β*-Farnesene$^{\mathrm{s}}$	97
13	Limonene$^{\mathrm{m}}$	98	57	*α*-Humulene$^{\mathrm{s}}$	99
14	Benzeneacetaldehyde	90	58	3,4,4a,7,8,8a-Hexahydro-1,1,3,6-tetramethyl-3-vinyl-1*H*-2-benzopyran	80
15	*trans*-*β*-Ocimene$^{\mathrm{m}}$	97	59	*allo*-Aromadendrene$^{\mathrm{s}}$	99
16	2-Octenal	83	60	*α*-Elemene$^{\mathrm{s}}$	93
17	3,5-Octadiene-2-one	91	61	*α*-Curcumene$^{\mathrm{s}}$	97
18	*cis*-Linalool oxide$^{\mathrm{m}}$	91	62	*β*-Ionone$^{\mathrm{s}}$	96
19	*trans*-Linalool oxide$^{\mathrm{m}}$	83	63	*β*-Selinene$^{\mathrm{s}}$	99
20	Linalool$^{\mathrm{m}}$	97	64	*α*-Selinene$^{\mathrm{s}}$	98
21	2-Methyl-4-propylimidazol	83	65	*β*-Bisabolene$^{\mathrm{s}}$	98
22	*trans*-2-Nonenal	86	66	*α*-Amorphene$^{\mathrm{s}}$	97
23	Terpinen-4-ol$^{\mathrm{m}}$	98	67	*δ*-Cadinene$^{\mathrm{s}}$	98
24	*α*-Terpineol$^{\mathrm{m}}$	91	68	Calacorene$^{\mathrm{s}}$	72
25	Methyl salicylate	96	69	Nerolidol$^{\mathrm{s}}$	95
26	Myrtenol$^{\mathrm{m}}$	94	70	2,6,10-Trimethyl-7,10-epoxy-2,11-dodecadien-6-ol	87
27	Safranal$^{\mathrm{m}}$	98	71	Spathulenol$^{\mathrm{s}}$	99
28	*n*-Decanal	91	72	Caryophyllene oxide$^{\mathrm{s}}$	95
29	1-*p*-Menthen-9-al$^{\mathrm{m}}$	94	73	Ledene$^{\mathrm{s}}$	89
30	*β*-Cyclocitral$^{\mathrm{m}}$	94	74	Humulene epoxide$^{\mathrm{s}}$	83
31	Nerol$^{\mathrm{m}}$	94	75	*α*-Cadinol$^{\mathrm{s}}$	91

TABLE II. Continued

Symbol	Compound	Match value %	Symbol	Compound	Match value %
32	*m*-Mentha-1,8-diene[m]	90	76	T-Muurolol[s]	94
33	2-Bornene[m]	93	77	Caryophyllenol II[s]	90
34	2-Hexylbutyrate	78	78, 79	Isomers: 2-(1-cyclohexen-1-yl)-3--hydroxy-5,5-dimethylcyclohex--2-enone	90
35	Geraniol[m]	91		2-(1-cyclohexen-1-yl)-3-hydroxy--5,5-dimethylcyclohex--3-enone	90
36	2,6,6-Trimethyl-cyclohexene-1-acetaldehyde	99	80	Tetradecanoic acid (Myristic acid)	98
37	*trans*,*trans*,*trans*-Nona--2,4,6-trienal	87	81	Oplopenone[s]	81
38	Carvacrol[m]	94	82	Caryophylle-3,8(13)-dien-5α-ol[s]	96
39	1,1,6-trimmethyl-1,2,3,4--tetrahydronaphthalene	86	83	Cyclohexadecane	95
40	*trans,trans*-2,4--Decadienal	95	84	Neophytadiene[d]	99
41	*cis*-3-Hexenyl tiglate	90	85	Hexahydrofarnesylacetone[s]	95
42	*n*-Octyl-2-methyl-butyrate	72	86	Phytol[d]	91
43	Methyl anthranilate	83	87	Nonadecane	86
44	*α*-Cubebene[s]	99	88	Farnesylacetone[s]	90

m – monoterpene; s – sesquiterpene; d – diterpene

Sesquiterpenes prevailed in the investigated essential oil as the most numerous group of identified compounds. The most abundant component was caryophyllene oxide, followed by nerolidol and spathulenol. Studies on *Satureja parnassica* oil, which is rich in caryophyllene oxide, has shown antibacterial activity against *Helicobacter pylori*.[17] Furthermore, spathulenol and caryophyllene oxide, identified in *Salvia sclarea* oil, are active against *Staphylococcus aureus*.[18] Nardi[19] showed that the high content of sesquiterpenes and, particularly, the presence of *β*-caryophyllene, spathulenol and caryophyllene oxide could partially account for the antimicrobial activity of aqueous extracts of *Stevia rebaudiana*.

On comparing the present results, obtained by analyzing domestic *Stevia rebaudiana* essential oil, with those of other authors, it can be concluded that there are certain unique properties of the examined oil concerning the composition of sesquiterpenes and monoterpenes.[9–13] One such characteristic is the fact that the sesquiterpenes *α*- and *β*-selinene have been detected in plants from other geographic locations (Japan and Paraguay) but not in the essential oil of leaf. As well as domestically grown *Stevia rebaudiana*, the other *Stevia rebaudiana* lines with

European origins contain sesquiterpene selinene in their leaves. In addition to many sesquiterpenes that have been identified in *Stevia rebaudiana* essential oil, three more were shown as specific constituents of domestic *Stevia rebaudiana*. These compounds are aromadendrene, α-amorphene and T-muurolol. Concerning the biological activity of the identified sesquiterpenes, aromadendrene and its isomer ledene (also identified in domestic *Stevia rebaudiana*) have been used as a starting material for the synthesis of fragrances and pheromones.[20] In general, cadinene-type sesquiterpenes have a wide spectrum of biological activity and T-muurolol, which belongs to this group of sesquiterpenes, exhibits significant antifungal activity.[21]

Apart from terpenes in the extracted *Stevia rebaudiana* essential oil (Fig. 2, Table II), numerous organic compounds were identified which contribute to the complex composition of the essential oil, *i.e.*, *n*-alkanes, *n*-alkenes, alcohols, aldehydes, ketones, acids, esters, *etc*.

Ethyl acetate extract

The other investigated extract was the ethyl acetate extract of *Stevia rebaudiana* leaves, which does not include the sweet steviol glycosides.[22–25] Since chloroform and ethyl acetate have been successfully applied as purifying solvents in the extraction of the sweet components from *Stevia rebaudiana* leaves, this procedure enabled the isolation of the other types of components.

The GC–MS analysis of the ethyl acetate extract of *Stevia rebaudiana* leaves showed the presence of *n*-alkanes, *n*-alkenes, fatty acids and many terpenes (Fig. 3).

In order to characterize the components of the ethyl acetate extract more specifically, it was fractionated by column chromatography. 55 fractions were collected, which were preliminarily examined by thin layer chromatography. Similar TLC chromatogram fractions were pooled into separate groups, so that the final number of samples to be analyzed by GC–MS was 12 (Table III). As can be seen, the first 28 fractions, which were eluted with benzene in the column chromatographic separation (Table I), corresponding to the first 7 samples (Table III), made up about 80 % of the total content, which suggests these compounds were of a non-polar character.

A comparison of the TLC chromatograms of the first two fractions of ethyl acetate extract with TLC chromatograms of refined sunflower oil and *Maclura pomifera* extract showed the presence of fatty acids,[26] as a result of which, it was decided to determine the fatty acids in these fractions. In order to release fatty acid, the first two collected fractions were derivatized after a treatment which led to the alkaline hydrolysis of the fatty acid esters. Separation of the methyl esters of the fatty acids from their alcoholic components was achieved by column chromatography. The fraction containing the methyl esters of the fatty acids was also examined by GC–MS (Fig. 4). As can be seen, the GC–MS analysis enabled the identification of methyl esters of both saturated and polyunsaturated fatty acids.

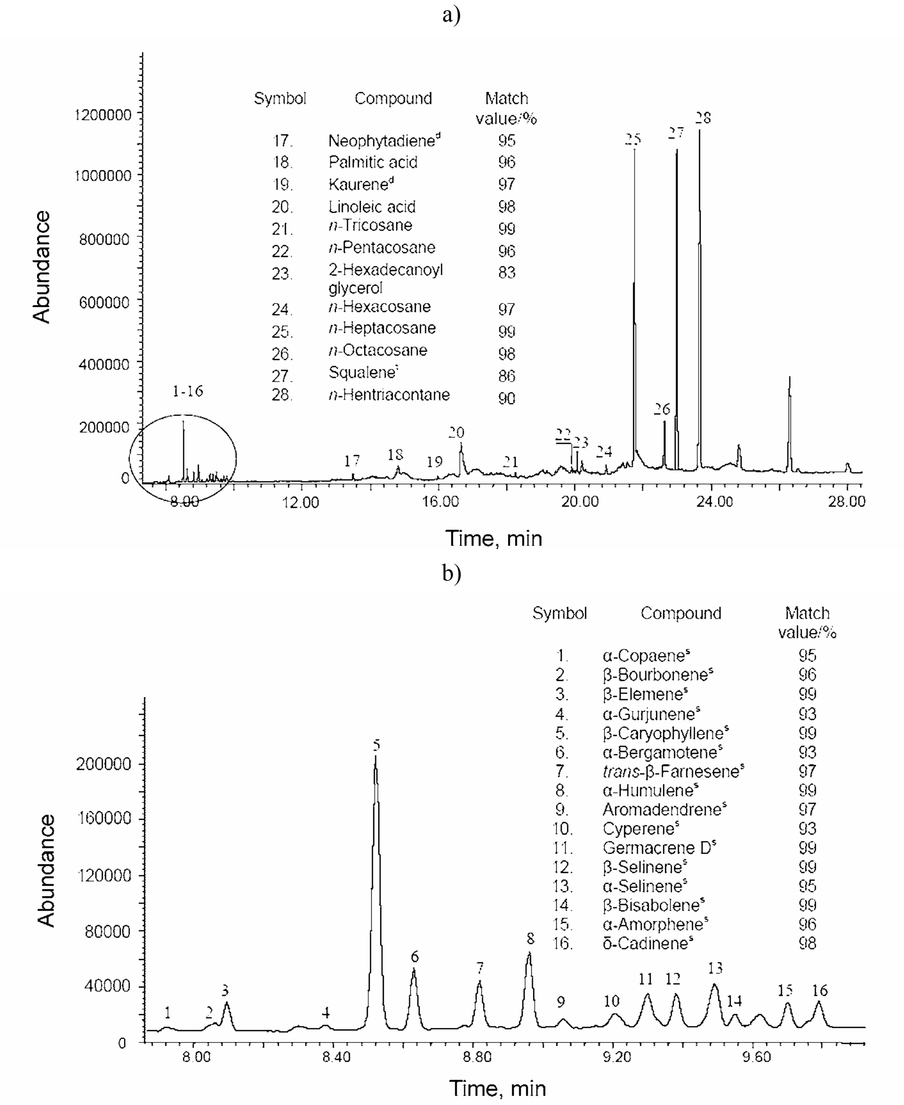

Symbol	Compound	Match value/%
17.	Neophytadiene^{d}	95
18.	Palmitic acid	96
19.	Kaurene^{d}	97
20.	Linoleic acid	98
21.	*n*-Tricosane	99
22.	*n*-Pentacosane	96
23.	2-Hexadecanoyl glycerol	83
24.	*n*-Hexacosane	97
25.	*n*-Heptacosane	99
26.	*n*-Octacosane	98
27.	Squalene^{t}	86
28.	*n*-Hentriacontane	90

Symbol	Compound	Match value/%
1.	α-Copaene^{s}	95
2.	β-Bourbonene^{s}	96
3.	β-Elemene^{s}	99
4.	α-Gurjunene^{s}	93
5.	β-Caryophyllene^{s}	99
6.	α-Bergamotene^{s}	93
7.	*trans*-β-Farnesene^{s}	97
8.	α-Humulene^{s}	99
9.	Aromadendrene^{s}	97
10.	Cyperene^{s}	93
11.	Germacrene D^{s}	99
12.	β-Selinene^{s}	99
13.	α-Selinene^{s}	95
14.	β-Bisabolene^{s}	99
15.	α-Amorphene^{s}	96
16.	δ-Cadinene^{s}	98

Fig. 3. a) GC–MS TIC chromatogram of the ethyl acetate extract of *Stevia rebaudiana* leaves; b) enlarged encircled segment of A (s – sesquiterpene; d – diterpene; t – triterpene).

Further investigation of the fractions of ethyl acetate extract gave a more complete picture about the rest of lipophilic components present in *Stevia rebaudiana* leaves. Namely, in the GC–MS TIC chromatogram of the ethyl acetate extract recorded before separation by column chromatography, only 28 compounds (Fig. 3) were identified, while after separation 161 compounds were identified.

This is certainly a consequence of the significantly larger concentrations of analyte in the latter case.

TABLE III. Distribution of the fractions collected in 12 samples and their masses

Sample	Fraction collected	Mass, g
1	1	4.81
2	2	6.93
3	3	2.92
4	4–9	3.90
5	10–15	0.96
6	16–21	2.61
7	22–32	3.26
8	33–37	0.52
9	38–39	0.31
10	40–46	1.81
11	47–50	0.81
12	51–55	0.72

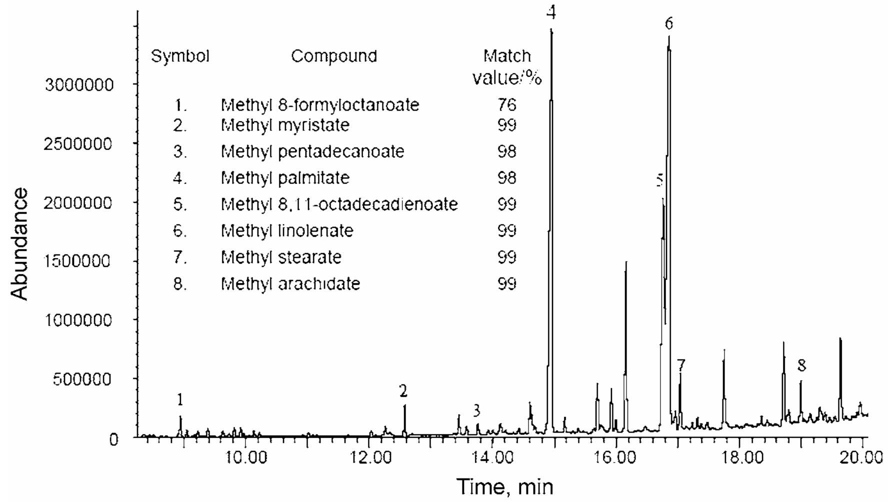

Fig. 4. GC–MS TIC chromatogram of the methyl esters of fatty acids from *Stevia rebaudiana* leaves.

A comparison of the terpene composition of *Stevia rebaudiana* essential oil and its ethyl acetate extract showed the absence of monoterpenes in the ethyl acetate extract, whereas 35 sesquiterpenes were identified. Most of them were already determined in *Stevia rebaudiana* essential oil, whereas the rest were specific for the ethyl acetate extract. Those newly identified in the ethyl acetate extract were cyperene, γ-gurjunene, globulol, ledol, α-isocedren-15-al and oxygen and methyl derivatives of ionone. Sesquiterpenes were the most abundant group of compounds in the ethyl acetate extract prior to fractionation and in the first two fractions collected during column chromatography. In these fractions, sesquiterpenes were accompanied mostly with fatty acid esters, *n*-alkanes, *n*-alkenes and ketones. It is interesting to note that the sesquiterpenes *β*-caryophyllene, *α*-humulene and *β*-farnesene, which were identified in both the essential oil and the ethyl acetate extract of *Stevia rebaudiana*, were also found in the essential oil of hop. Namely, they are 3 of the 4 most common compounds of hop aroma, their ratios being distinctive for the variety.[27]

Nine diterpenes were identified in the ethyl acetate extract. This group of compounds were also more numerous than the diterpenes identified in the essential oil of *Stevia rebaudiana*. Identification of diterpene kaur-16-ene indicates the presence of kaurene-type diterpenes. This group of diterpenes represents a skeleton for forming steviol glycosides, the main sweet components in *Stevia rebaudiana* leaves. Apart from this, a manoyl oxide-type of diterpenes was also determined. Manoyl oxide, along with *epi*-13-manoyl oxide, has been biologically investigated as a natural product of different plant species, since it shows certain anti-inflammatory activity and also exhibits an important activity against specific parasites.[28] The labdane diterpene sclareol, which was also present, is also a biologically active compound. Some recent investigations were concerned with the cytotoxic and antitumor activity of liposome-incorporated sclareol against cancer cell lines and human colon cancer xenografts.[29] It was found that liposomes incorporate sclareol at a drug to lipid mole ratio of 0.43, suggesting an incorporation efficiency of almost 80 %, and induced a reduced growth rate of human colon cancer tumours (HCT116) developed in SCID mice, without any significant side effects.

In view of the low polarity of first collected fractions, the total content of triterpenes in stevia leaves was eluted by benzene. Squalene, amyrin and lupenon, together with triterpene alcohols, constitute this group of compounds.

With the same non-polar solvent, almost the total content of *n*-alkanes, *n*-alkenes, alcohols, aldehydes and ketones was eluted. Only a few of them were collected straight after the mobile phase was made more polar by the addition of ethyl acetate to benzene. The *n*-alkanes identified in the investigated extract were mostly long-chain *n*-alkanes C_{13}–C_{31}, with only two cycloalkanes, *i.e.*, cyclotetracosane and cyclooctacosane. The two most common *n*-alkanes were *n*-heptacosane and *n*-hentriacontane. Similar results were also obtained in a study of the *n*-alkanes from plants of the genus *Achillea*.[30] Unsaturated hydrocarbons, apart from the mentioned terpenes, are represented by a group of C_{14}–C_{23} *n*-alkenes, whereas alcohols are a dominant group among oxygen derivatives in the ethyl acetate extract.

A white crystalline substance was isolated from the eighth ethyl acetate fraction. GC–MS analysis of the very light white crystal showed that it consisted mainly of a long-chain aliphatic alcohol, *n*-eicosanol.

Among the 14 identified acids, saturated and unsaturated fatty acids, *i.e.*, palmitic, oleic, stearic, linoleic, *etc*., were the most abundant.

The non-polar fractions of the ethyl acetate extract, obtained using column chromatographic separation with benzene as the eluent (Tables I and III), contained most of the identified esters. Prior to the application of column chromatography, one monoglyceride, 2-monopalmitate, was identified in this extract, whereas after fractionation it was possible to identify esters of formic and adipic acid, followed by fatty acid esters and unsaturated monoglycerides (1-monolinolenin and 1-monolinolein). These fractions were also richer in aromatic compounds, mostly alkyl derivatives of naphthalene, and vitamin E was identified in some of them.

All the sterols and stanols identified in the wax of *Stevia rebaudiana* leaves were also present as constituents of the fractions of the extract eluted with benzene. The compounds identified were sitosterol and a derivative of stigmastanol. This type of phytosterols plays an important role in human biology. By lowering the level of low-density lipoprotein cholesterol, these phytosterols protect the cardiovascular system of humans.[31]

The polarity of the eluting solvent was gradually changed by adding ethyl acetate to benzene. A smaller number of compounds were identified in the more polar fractions of ethyl acetate extract due to the nature of the rather complex mixture. During column chromatography, oxygen derivatives of sesquiterpenes and diterpenes were eluted with a polar mixture of solvents. Only a few *n*-alkanes, *n*-alkenes, alcohols and ketones, together with several acids, were identified in the more polar fractions of the investigated extract.

A group of lactones was specific for the more polar solvent fractions. Loliolide and dihydroactinidiolide represent degradation products of carotenoides.[32,33] Moreover, the identified imide of maleic acid, 2-ethyl-3-methylmaleimide, might be present as a by-product of the photo-oxidation of chlorophyll,[34] since this pigment is evidentially present in *Stevia rebaudiana* leaves.

CONCLUSIONS

A qualitative analysis of the essential oil from leaves of domestic *Stevia rebaudiana* Bertoni showed that mono- and sesquiterpenes prevailed (50 types identified) among the 88 identified compounds. By analyzing the ethyl acetate extract, the presence of terpenes, fatty acids (present as free and esters), *n*-alkanes, *n*-alkenes, cyclic alkanes, alcohols, aldehydes, ketones, *etc*., was ascertained. Among the terpenes (50 types identified), sesquiterpenes prevailed. Further constituents identified in the ethyl acetate extract include sterols. Taking into account that some of the compounds were identified for the first time in this species (nerol, β-cyclocitral, safranal, aromadendrene, α-amorphene and T-muurolol), it is obvious that *Stevia rebaudiana* grown in this area possesses certain specific characteristics, which can be ascribed to the cultivation conditions on the domestic plantation, *i.e.*, location, climate, soil and plant growing conditions.

This examination is a contribution to a better understanding of all the aspects and potential uses of *Stevia rebaudiana* leaves and their extracts. It becomes even more important in view of the development and improvement of plant cultivation in Serbia. The results also support the necessity of research and use of *Stevia rebaudiana* extract as the source of natural products different from steviol glycosides, since it is rich in terpenes, alcohols and fatty acids.

Acknowledgments. The authors would like to express their special gratitude to the people of the Bio-Ecological Centre in Zrenjanin, the Republic of Serbia, for their precious support, valuable discussions and kind help during this work. This work was financially supported by the Ministry of Science of the Republic of Serbia (Project No.: ON142029).

ИЗВОД

ХЕМИЈСКИ САСТАВ ЕКСТРАКАТА ЛИСТА *Stevia rebaudiana* BERTONI ЕКСПЕРИМЕНТАЛНО ГАЈЕНЕ У ВОЈВОДИНИ

ИВАНА С. МАРКОВИЋ[1], ЗОЛТАН А. ЂАРМАТИ[2] и БИЉАНА Ф. АБРАМОВИЋ[3]

[1]*Виша техничка школа, Технолошки одсек, Ђорђа Стратимировића 23, 23000 Зрењанин,* [2]*Биолошки центар, Петра Драпшина 1, 23000 Зрењанин и* [3]*Природно–математички факултет, Департман за хемију, Трг Д. Обрадовића 3, 21000 Нови Сад*

Применом GC–MS методе, испитан је хемијски састав екстраката листа *Stevia rebaudiana* Bertoni, по први пут експериментално гајене на плантажи у околини Зрењанина. Испитивани биљни материјал је пожњевен септембра 2002. године. За анализу хемијског састава липофилних компоненти листова стевије изоловано је етарско уље и етилацетатни екстракт. Квалитативном анализом етарског уља, добијеног хидродестилацијом, утврђено је да је богато моно- и сесквитерпенима, тј. да од 88 идентификованих компоненти 50 су моно- и сесквитерпени. Анализом хемијског састава етилацетатног екстракта домаће *Stevia rebaudiana* утврђено је да се она одликује присуством масних киселина (присутних у виду естара и слободних киселина), *n*-алкана, *n*-алкена, цикличних алкана, алкохола, алдехида, кетона и др. Од терпена (идентификовано 50 врста) доминирају сесквитерпени. Поред тога у етилацетатном екстракту су регистровани и стероли. Терпени нерол, *β*-циклоцитрал, сафранал, аромадендрен, *α*-аморфен и Т-муролол су први пут идентификовани у овој биљној врсти са слагањем добијених масених спектара са оним из Wiley библиотеке преко 90 %. Имајући у виду да су наведени терпени по први пут идентификовани у овој биљној врсти, очигледно је да *Stevia rebaudiana* гајена на нашим просторима поседује извесне специфичности које се могу приписати условима гајења на домаћој плантажи.

(Примљено 8. јуна, ревидирано 9. августа 2007)

REFERENCES

1. J. E. Brandle, A. N. Starratt, M. Gijzen, *Can. J. Plant Sci.* **78** (1998) 527, http://sci.agr.ca/ /london/faq/stevia_rev_e.htm (April 29, 2007)
2. D. J. Midmore, A. H. Rank, *A New Rural Industry – Stevia – To Replace Imported Chemical Sweeteners*, A report for the Rural Industries Research and Development Corpo-

ration, Australia, RIRDC Project No UCQ-16A, 2002, pp. 1-3, http://www.rirdc.gov.au/ /reports/NPP/02-022.pdf (June 2, 2007)

3. W. H. Lewis, *Econ. Bot.* **46** (1992) 336
4. D. Mowrey, *Life with Stevia: How Sweet it is!*, Nutritional and Medicinal Uses, Health Freedom Resources, 1992, http://www.formerfatguy.com/articles/stevia.asp (April 29, 2007)
5. P. Chan, B. Tomlinson, Y. J. Chen, J. C. Liu, M. H. Hsieh, J. T. Cheng, *Br. J. Clin. Pharmacol.* **50** (2000) 215
6. P. B. Jeppensen, S. Gregersen, S. E. D. Rolfsen, M. Jepsen, M. Colombo, A. Agger, J. Xiao, M. Kruhøffer, T. Ørntoft, K. Hermansen, *Metabolism* **52** (2003) 372
7. G. Planas Mazzei, J. Kuc, *Science* **162** (1968) 1007
8. F. Dozono, N. Sato, U. S. Patent, 5262161 (1993)
9. S. Fujita, K. Taka, Y. Fujita, *Yakugaku Zasshi* **97** (1977) 692 [C.A. **87**/1977 122621v]
10. A. Martelli, C. Frattini, F. Chialva, *Flavour Frag. J.* **1** (1985) 3
11. P. L. Cioni, I. Morelli, L. Andolfi, M. Macchia, L. Ceccarini, *J. Essent. Oil Res.* **18** (2006) 76
12. S. K. Yoda, M. O. M. Marques, A. J. Petenate, M. A. A. Meireles, *J. Food Eng.* **57** (2003) 125
13. http://www.rain-tree.com/stevia-chemicals.pdf (April 29, 2007)
14. M. Popović, N. Mimica-Dukić, S. Mezei, O. Gašić, M. Gavrilović, N. Mrkovački, *Arh. Farm.* **50** (2000) 304
15. H. Hosseinzadeh, H. R. Sadeghnia, *J. Pharm. Pharmaceut. Sci.* **8** (2005) 394
16. A. N. Assimpoulou, Z. Sinakos, V. P. Papageorgiou, *Phytother. Res.* **19** (2005) 997
17. O. Tzakou, H. Skaltsa, *Planta Med.* **69** (2003) 282
18. A. Ulubelen, G. Topcu, C. Eris, U. Soenmez, M. Kartal, S. Kurucu, C. Bozok-Johansson, *Phytochemistry* **36** (1994) 971
19. U. Nardi, *Erboristeria Domani* **6** (1996) 58
20. Y. M. A. W. Lamers, *Ph.D. Thesis*, Wageningen University, Wageningen, 2003
21. C. L. Wu, S. C. Chien, S. Y. Wang, Y. H. Kuo, S. T. Chang, *Holzforschung* **59 (**2005) 620
22. Y. Oshima, J. Saito, H. Hikino, *Tetrahedron* **42** (1986) 6443
23. Y. Oshima, J. Saito, H. Hikino, *Phytochemistry* **27** (1988) 624
24. A. Rajbhandari, M. F. Roberts, *J. Nat. Prod.* **46** (1983) 194
25. N. F. Komissarenko, A. I. Derkach, I. P. Kovalyov, N. P. Bublik, G. A. Chermeneva, A. G. Kotov, V. V. Zinchenko, *Rast. Resursy* **30** (1994) 53
26. S. Filip, *M.Sc. thesis*, University of Belgrade, Faculty of Chemistry, Beograd, 2001 (in Serbian)
27. Z. Zeković, I. Pfaf-Šovljanski, O. Grujić, *J. Serb. Chem. Soc.* **72** (2007) 81
28. A. García-Granados, E. Liñán, A. Martínez, F. Rivas, C. M. Mesa-Valle, J. J. Castilla--Calvente, A. Osuna, *J. Nat. Prod.* **60** (1997) 13
29. S. Hatziantoniou, K. Dimas, A. Georgopoulos, N. Sotiriadou, C. Demetzos, *Pharmacol. Res.* **53** (2006) 80
30. R. Palić, T. I. Eglinton, B. C. Benitez-Nelson, G. Eglinton, J. Veličković, G. Stojanović, *J. Serb. Chem. Soc.* **64** (1999) 443
31. C. A Vanstone, M. Raeini-Sarjaz, W. E. Parsons, P. J. H. Jones, *Am. J. Clin. Nutr.* **76** (2002) 1272
32. T. Y. P. Bonnie, Y. M. Choo, *J. Oil Palm Res.* **2** (1999) 62
33. J. S. Sinninghe Damsté, M. P. Koopmans, *Pure Appl. Chem.* **69** (1997) 2067
34. Q. Xian, H. Chen, H. Liu, H. Zou, D. Yin, *Environ. Sci. Pollut. Res.* **13** (2006) 233.

www.shd.org.yu

Journal of the Serbian Chemical Society
eVersion electronic
JSCS@tmf.bg.ac.yu • www.shd.org.yu/JSCS

J. Serb. Chem. Soc. 73 (3) 299–305 (2008) UDC **Teucrium montanum*:665.52/.54:615.281:547.261
JSCS–3711 *Original scientific paper*

The chemical composition of the essential oil and the antibacterial activities of the essential oil and methanol extract of *Teucrium montanum*

NENAD VUKOVIĆ[*], TANJA MILOŠEVIĆ[#], SLOBODAN SUKDOLAK
and SLAVICA SOLUJIĆ[#]

Department of Chemistry, Faculty of Science, University of Kragujevac, Radoja Domanovića 12,
P. O. Box 12, 34000 Kragujevac, Serbia

(Received 11 June, revised 3 September 2007)

Abstract: This study was designed to examine the chemical composition of the essential oil and the *in vitro* antibacterial activities of the essential oil and methanol extract of *Teucrium montanum*. The inhibitory effects of the essential oil and the methanol extracts of *Teucrium montanum* were tested against thirteen bacterial species using the disc-diffusion method. GC/MS analyses revealed that the essential oil contained mainly sesquiterpenes, such as δ-cadinene (17.19 %), β-selinene (8.16 %) and α-calacorene (4.97 %). The highest activities were obtained with the essential oil of *Teucrium montanum* against *K. pneumoniae*, *B. subtilis*, *B. mycoides*, *E. cloaceae* and *A. chlorococcum*. In addition, comparison of the antibacterial activities of the essential oil and the methanol extract showed that the essential oil exhibited the stronger antibacterial activities.

Keywords: essential oil; *Teucrium montanum*; antibacterial activity.

INTRODUCTION

The use of phytochemicals as natural antimicrobial agents, commonly called "biocides", is gaining in popularity.[1] There is growing interest in correlating the phytochemical constituents of a plant with its pharmacological activity.[2,3] The antimicrobial properties of essential oils have been recognized for many years[4,5] and their preparations have found applications as naturally occurring antimicrobial agents in the fields of pharmacology, pharmaceutical botany, phytopathology, medical and clinical microbiology, food preservation, *etc*. The preparations of essential oils possessing antimicrobial activities have been the subject of many investigations, which, in the screening of a wide variety of plant species, revealed structurally unique biologically active compounds. However, less attention was

---

[*] Corresponding author. E-mail: nvukovic@kg.ac.yu

[#] Serbian Chemical Society member.

doi: 10.2298/JSC0803299V

given to the activities of the main components in the tested oils. The main advantage of natural agents is that they do not enhance "antibiotic resistance", a phenomenon commonly encountered with long-term use of synthetic antibiotics. There are reports of active principles of essential oils from various plants with antibacterial or antifungal activity.[6–12] The antimicrobial activity of essential oils is assigned to a number of small terpenoids and phenolic compounds (thymol, carvacrol, eugenol), which also in pure form exhibit high antibacterial activity.[13–15] Essential oils and their components are known to be active against a wide variety of microorganisms, including Gram-negative[16,17] and Gram-positive bacteria.[18] Gram-negative bacteria were shown to be generally more resistant than Gram-positive ones to the antagonistic effects of essential oils because of the lipopolysaccharide present in the outer membrane[19] but this was not always the case.[15]

Teucrium montanum is a grass crop which has long been consumed both as an herbal medicine and as a nourishing food. It is widely used as a diuretic, stomachic, analgesic and antispasmodic agent, and also possesses antibacterial, antifungal, anti-inflammatory and anti-oxidative activity.[20–22]

Therefore, the objective of the present study was (a) to examine the chemical composition of the essential oil of *T. montanum* by GC–MS and (b) to evaluate the antibacterial activity of the essential oil and methanolic extract of *T. montanum*.

EXPERIMENTAL

Plant material and isolation of the essential oil

Teucrium montanum was collected from the mountain Jadovnik in August 2006. The species was identified and a voucher specimen deposited (16177, BEOU, Snežana Vukojičić) at the Department of Botany, Faculty of Biology, University of Belgrade. The essential oils were obtained from aerial parts of *Teucrium montanum* by hydrodistillation using a Clevenger-type apparatus for 3 h. The obtained oil was dried over anhydrous sodium sulfate overnight and kept in sterile sample tubes in a refrigerator. The yield of oil, calculated on a dry weight basis, was 0.47 %.

Gas chromatography–mass spectrometry (GC–MS)

The analyses were carried out in an Agilent 6890N (G 1530N) (Serial No. CN10702033) gas chromatograph fitted with an HP-5MS fused silica column (5 % phenyl methyl polysiloxane 30 m×0.25 mm i.d., film thickness 0.25 μm), interfaced with an Agilent mass selective detector 5975B (Agilent Technologies, USA) (G 3171A) (Serial No. US65125280) operated by HP Enhanced ChemStation software, G1701DA MSD ChemStation Rev. D.00.00.38. The operating conditions were as follows: oven temperature: 60–240 °C, at 3 °C min^{-1} (62 min analysis time); injector temperature: 250 °C; carrier gas: helium, adjusted to a column velocity of flow 1.1 ml min^{-1}; split ratio 25:1, whereas the split flow was 30.7 ml min^{-1}; interface temperature: 280 °C; standard electronic impact (EI) MS source temperature: 230 °C; MS quadrupole temperature: 150 °C; mass scan range: 50–500 amu at 70 eV; scan velocity: 3.12 scans s^{-1}; resulting EM voltage: 1200 V. One microliter of sample (dissolved in hexane 100 % v/v) was injected into the system.

Identification of the constituents of the essential oil

The identification of the components was based on comparison of their mass spectra with Wiley7Nist database through G1701DA mass spectrum ChemStation or with mass spectra reported in the literature. Also, the identification was assisted by comparison of their retention times with authentic samples. Quantitative analysis was performed by means of the direct peak area integration technique based on the TIC.

Microbial strains used

The test microorganism employed in this study were: *Agrobacterium tumefaciens* (PMFKg-B11), *Azotobacter chlorococcum* (PMFKg-B14), *Bacillus mucoides* (IPH), *Bacillus subtilis* (IPH), *Enterobacter cloaceae* (PMFKg-B22), *Erwinia carotovora* (PMFKg-B31), *Klebsiella pneumoniae* (PMFKg-B26), *Proteus* sp. (PMFKg-B34), *Pseudomonas aeruginosa* (PMFKg-B37), *Pseudomonas glycinea* (PMFKg-B40), *Pseudomonas fluorescens* (PMFKg-B28), *Pseudomonas phaseolicola* (PMFKg-B29), *Staphylococcus aureus* (PMFKg-B30).

All the tested bacteria cultures were obtained from the Institute for Health Protection (IPH) and the Faculty of Agriculture, University of Belgrade, Serbia. The Laboratory for Microbiology, Department of Biology, Faculty of Science, University of Kragujevac, Serbia confirmed the identification of all the tested microorganisms (PMF-Kg).

Antimicrobial analysis

The antibacterial activity of the essential oil and methanolic extract of the plant *Teucrium montanum* was investigated by the disc-diffusion method on Mueller–Hinton broth (NCCLS, 1990).[23] It was performed using a 24 h old bacterial culture at 37 °C reseeded on Nutrient broth. The cultures were adjusted to 5.6×10^6 CFU ml^{-1} with sterile water. One milliliter of the suspension was added over the plates containing the Mueller–Hinton broth to obtain a uniform microbial growth on both the control and test plates. The extracts of *Teucrium montanum* were dissolved in methanol (30 mg ml^{-1}) and sterilized. Under aseptic conditions, empty sterilized discs (Whatman No. 5, 6 mm diameter) were impregnated with 10 μl of the essential oil, methanol extract (300 μg ml^{-1}) and placed on the agar surface. The plates were left for 30 min at room temperature to allow the diffusion of the oil and extract before incubation at 37 °C. After the incubation period (24 h), the zone of inhibition was measured and presented in mm. Negative controls were prepared using the same solvents employed to dissolve the plant extract. Amracin was used as the standard antibiotic for comparison.

RESULTS AND DISCUSSION

The essential oil was extracted by hydrodistillation of the dried aerial parts of *Teucrium montanum* and the constituents were analyzed by GC–MS. The yield of oil was 0.47 %, calculated on a dry weight basis. The essential oil of *Teucrium montanum* was analyzed to determine its constituents (Table I). From the GC–MS analysis, 44 compounds were identified in the oil, representing 97.95 % of the total. GC–MS analysis of the oil showed the presence of *δ*-cadinene (17.19 %) and *β*-selinene (8.16 %), as the major constituents of the essential oil. The compounds *α*-calacorene (4.97 %), torreyol (3.91 %), 1,6-dimethyl-4-(1-methylethyl)naphthalene (4.91 %), copaene (4.23 %), 4-terpineol (3.90 %), cadina-1,4-diene (3,39 %), *τ*-cadinol (3.12 %), caryophyllene (3.34 %), *β*-sesquiphellandrene (3.98 %) and *α*-cedrene (2.90 %) were also identified as significant components in the oil of *T. montanum*. Sesquiterpene hydrocarbons were characteristic constituents of the oil of *T. montanum*. α-Pinene, 1-ethyl-3-methylbenzene, sabinene, 1-(2-methylprop-1-enyl)cyclohexa-1,3-diene, β-phellandrene, carvone, phellandral, 1(7),3,8-*o*-menthatriene, *p*-cymen-7-ol, carvacrol and γ-muurolene were found to be minor components of *T. montanum* oil in this study.

TABLE I. Chemical composition of *Teucrium montanum* essential oil

t / min	MS + t_{ret} identification	Content, %
5.953	α-Pinene	tr
6.755	1-Ethyl-3-methylbenzene	tr
7.419	Sabinene	tr
8.597	α-Terpinene	tr
8.889	*p*-Cimene	0.71
10.182	γ-Terpinene	0.41
12.717	β-Phellandrene	tr
13.295	1-(2-Methylprop-1-enyl)cyclohexa-1,3-diene	tr
14.245	5-(1-Methylethyl)-bicyclo[3.1.0]hexan-2-one	1.1
14.635	Unknown	1.73
15.074	4-Terpineol	3.90
15.910	Myrtenal	0.98
16.465	*cis*-Verbenone	1.09
17.964	Carvone	tr
19.286	Phellandral	tr
19.560	1(7),3,8-*o*-Menthatriene	tr
20.001	*p*-Cymen-7-ol	tr
20.493	Carvacrol	tr
22.507	Unknown	1.14
23.600	α-Cubebene	0.78
23.989	β-Damascenone	0.43
24.247	Zingiberene	1.34
25.368	Caryophyllene	4.35
26.078	α-Bergamotene	1.11
26.392	β-Sesquiphellandrene	3.34
26.638	Unknown	0.69
26.753	α-Caryophyllene	1.91
26.987	β-Farnesene	1.76
27.050	Aromadendrene	1.32
27.601	Unknown	1.54
27.874	Copaene	4.23
28.004	α-Curcumene	1.74
28.075	β-Selinene	8.16
28.303	(+)-Epi-bicyclosesquiphellandrene	1.64
28.418	Isoledene	1.62
28.664	α-Muurolene	1.73
28.813	*cis*-α-Bisabolene	0.53
29.007	β-Bisabolene	0.71
29.167	α-Cedrene	2.90

TABLE I. Continued

t / min	MS + t_{ret} identification	Content, %
29.242	Unknown	1.23
29.597	δ-Cadinene	17.19
29.917	1,2,3,4,4a,7-Hexahydro-1,6-dimethyl-4-(1-methylethyl)naphthalene	1.29
30.318	α-Calacorene	4.97
30.393	Unknown	1.87
33.562	Cadina-1,4-diene	3.39
34.083	Torreyol	3.91
34.243	γ-Muurolene	tr
34.523	τ-Cadinol	3.12
35.187	γ-Curcumene	3.18
35.256	1,6-Dimethyl-4-(1-methylethyl)naphthalene	4.91

According to the results given in Table II, the essential oil of *T. montanum* had great antibacterial activity against all the investigated microorganisms. The diameters of the growth inhibition zone ranged from 16 to 29 mm (including the 6 mm diameter of the disc) with the highest inhibition zone values observed against *K. pneumoniae* (29 mm). The largest level of resistance was shown by *A. tumefaciens* and *E. carotowora* (an inhibition zone of 16 mm). The essential oil showed similar activity on both Gram-positive and Gram-negative bacteria.

TABLE II. Antimicrobial susceptibility pattern of the essential oil (10 µl/disc) and methanol extract (300 µg ml^{-1}) of *T. montanum*

Microorganism	Inhibition zone diameter^{a,b}, mm		Antimicrobial agent
	Essential oil	Methanol extract	Amracin (300 µg ml^{-1})
	Gram(+)		
Bacillus mycoides	25 ± 0.5	19± 0.5	34 ± 0.5
Bacillus subtilis	26 ± 0.5	14± 0.3	29 ± 0.5
Staphylococcus aureus	10 ± 0.3	8 ± 0.3	30 ± 0.5
	Gram(–)		
Agrobacterium tumefaciens	16 ± 0.4	13 ± 0.5	32 ± 0.5
Azotobacter chlorococcum	24 ± 0.5	28 ± 0.5	34 ± 0.5
Enterobacter cloaceae	24 ± 0.5	16 ± 0.3	36 ± 0.5
Erwinia carotovora	18 ± 0.3	19 ± 0.5	31 ± 0.5
Klebsiella pneumoniae	29 ± 0.5	22 ± 0.5	35 ± 0.7
Proteus sp.	–	–	11± 0.5
Pseudomonas aeruginosa	–	–	17 ± 0.3
Pseudomonas glycinea	20 ± 0.5	16 ± 0.5	35 ± 0.7
Pseudomonas fluorescens	22 ± 0.5	12 ± 0.3	42 ± 0.7
Pseudomonas phaseolicola	23 ± 0.5	19 ± 0.5	35 ± 0.5

[a] Mean value ± *SD*, $n = 3$ (the zone of inhibition, in mm, includes the disc of 6 mm diameter); [b] Solvent controls (methanol) were negative

In general, the essential oil showed better activities than the methanol extract. The methanolic extract showed strong antibacterial activity against the bacteria *A. chlorococcum,* the inhibition zone was 28 mm. Both the essential oil and methanol extract had similar sizes of the zone of inhibition for *E. carotovora* (18 and 19 mm, respectively). On all other microorganism the methanol extract showed lower activity than the essential oil.

CONCLUSIONS

According to the obtained results, it is possible to conclude that *Teucrium montanum* had a strong and broad spectrum of antibacterial activity. To the best of our knowledge, this is the first study to provide data on the evaluation of the essential oil of *T. montanum* against bacteria.

The antibacterial activities of the essential oil and methanol extract reported here could be associated with the presence δ-cadinene (17.19 %) and β-selinene (8.16 %). The compounds present in oil indicated a preference of *T. monanum* to synthesize sesquiterpenes.

Based on the obtained results, *Teucrium montanum* essential oil could be used as a preservative in food products, to protect them from microbial spoilage.

ИЗВОД

ХЕМИЈСКИ САСТАВ ЕТАРСКОГ УЉА И АНТИБАКТЕРИЈСКА АКТИВНОСТ ЕТАРСКОГ УЉА И МЕТАНОЛСКОГ ЕКСТРАКТА *Teucrium montanum*

НЕНАД ВУКОВИЋ, ТАЊА МИЛОШЕВИЋ, СЛОБОДАН СУКДОЛАК и СЛАВИЦА СОЛУЈИЋ

Институт за хемију, Природноматематички факултет, Универзитет у Крагујевцу,
Радоја Домановића 12, 34000 Крагујевац

У овом раду је представљено испитивање хемијског састава етарског уља и антибактеријска активност етарског уља и метанолског екстракта *Teucrium montanum*. У највећем проценту етарско уље садржи сесквитерпенске угљоводонике. Забележена је јака антибактеријска активност етарског уља према испитиваним бактеријама. Генерално гледано, етарско уље показује већу активност од метанолског екстракта.

(Примљено 3. септембра 2007)

REFERENCES

1. E. J. Smid, L. G. M. Gorris, *Handbook of Food Preservation*, Marcel Dekker, New York, 1999, p. 285
2. A. B. Vaidya, V. D. S. Antarkar, *J. Assoc. Physicians India* **42** (1994) 221
3. S. S. Gupta, *Indian J. Pharmacol.* **26** (1994) 1
4. K. A. Hammer, C. F. Carson, T. V. Riley, *J. Appl. Microbiol.* **86** (1999) 985
5. D. J. Daferera, B. N. Ziogas, M. G. Polissiou, *J. Agric. Food. Chem.* **48** (2000) 2576
6. J. Hinou, C. Harvala, S. Philianos, *Ann. Pharm. Fr.* **47** (1989) 95
7. J. K. Oloke, B. O. Kolawole, W. O. Erhun, *Fitoterapia* **59** (1988) 384
8. F. J. Hammerschmidt, A. M. Clark, F. M. Soliman, E. S. El-Kashoury, A. M. Ab-El Kawy, M. el-Fishawy, *Planta Med.* **59** (1993) 68
9. C. F. Carson, T. V. Riley, *J. Appl. Bacteriol.* **74** (1995) 264
10. S. Barel, R. Segal, J. Yashphe, *J. Ethnopharmacol.* **33** (1991) 187

11. D. R. L. Caccioni, M. Guizzardi, D. M. Biondi, A. Renda, G. Ruberto, *Int. J. Food Microbiol.* **43** (1998) 73
12. S. Cosentino, C. I. G. Tuberoso, B. Pisano, M. Satta, V. Mascia, E. Arzedi, F. Palmas, *Lett. Appl. Microbiol.* **29** (1999) 130
13. D. E. Conner, *Antimicrobials in foods*, Marcel Dekker Inc., New York, 1993, p. 441
14. N. Didry, L. Dubreuil, M. Pinkas, *Pharmazie* **48** (1993) 301
15. M. Karapinar, S. E. Aktung, *Int. J. Food Microbiol.* **4** (1987) 161
16. I. M. Helander, H. L. Alakomi, K. L. Kala, T. M. Sandholm, I. Pol, E. J. Smid, L. G. M. Gorris, A. von Wright, *J. Agric. Food Chem.* **46** (1998) 3590
17. A. Sivropoulou, E. Papanikolaou, C. Nikolanou, S. Kokkini, T. Lanaras, M. Arsenakis, *J. Agric. Food Chem.* **44** (1996) 1202
18. J. Kim, M. R. Marshall, C. Vei, *J. Agricult. Food Chem.* **43** (1995) 2839
19. A. D. Russel, *J. Appl. Bacteriol.* **71** (1991) 191
20. R. Jančić, D. Stošić, N. Mimica-Dukić, B. Lakušić, *The Aromatic Plants from Serbia*, NIP Dečije novine, Gornji Milanovac, Serbia, 1995, p. 214 (in Serbian)
21. V. T. Tumbas, A. I. Mandić, G. S. Ćetković, S. M. Djilas, J. M. Čanadanović-Brunet, *Acta Periodica Technol.* **35** (2004) 265
22. S. M. Djilas, S. L. Markov, D. D. Cvetković, J. M. Čanadanović-Brunet, G. S. Ćetković, V. T. Tumbas, *Fitoterapia* **77** (2006) 401
23. NCCLS, Performance Standards for Antimicrobial Disk Susceptibility Tests, Approved Standard NCCLS Publication M2/A4, Villanova, PA, USA, 1990.

Journal of the Serbian Chemical Society

JSCS@tmf.bg.ac.yu • www.shd.org.yu/JSCS

www.shd.org.yu

J. Serb. Chem. Soc. 73 (3) 307–310 (2008)
JSCS–3712

UDC 635.71:581.19:665.52/.54(815.3)
Note

NOTE

Chemical composition of *Thymus vulgaris* L. (thyme) essential oil from the Rio de Janeiro State (Brazil)

ALEXANDRE PORTE[1]* and RONOEL L. O. GODOY[2]

[1]*Instituto de Tecnologia – Universidade Federal Rural do Rio de Janeiro, BR 465, km 47, Seropédica, Cep 23890-000, Rio de Janeiro and* [2]*Embrapa Agroindústria de Alimentos, Avenida das Américas, 29501, Guaratiba, Cep 23020-470, Rio de Janeiro, Brazil*

(Received 5 June 2007)

Abstract: The essential oil from fresh leaves of *Thymus vulgaris* L. from Rio de Janeiro State, Brazil, was isolated by hydrodistillation and analyzed through a combination of GC and GC/MS. Compounds representing 95.1 % of the oil were identified. Thirty-nine constituents were detected, of which twenty-eight were identified according to their chromatographic retention indices and mass spectra. The major constituents of the oil were thymol (44.7 %), *p*-cymene (18.6 %) and γ-terpinene (16.5 %).

Keywords: *Thymus vulgaris*; thyme; essential oil; thymol; *p*-cymene.

INTRODUCTION

Thymus vulgaris L., as *Rosmarinus officinalis* L. (rosemary) and other species of the Lamiaceae family, is native of Mediterranean countries, growing abundantly over wide areas in France, Spain, Portugal, Italy, Algeria and Morocco.[1] Moreover, it is also cultivated in other parts of Europe and North America, North Asia and Oceania.[2]

Thyme is employed to season and suppress offensive odors, such as trimethylamine odor, in foods.[2,3] The essential oil is well recognized for its medicinal properties in the treatment of bronchitis, whooping cough and tooth-ache. The herb or its infusion is also given for several disorders. It is possible that the flavonoids present may be important, such as in the spasmolytic activity of the smooth muscles of the guinea pig ileum and trachea.[2,3] It was found that the main components of the essential oil were thymol and carvacrol and that it had antimicrobial activity against fungi (some aflatoxins producers), viruses, helminths, Gram-positive bacteria (included *C. botulinum*) and Gram-negative bacteria.[3–8]

The aim of this study was to examine the composition of the essential oil of thyme from Rio de Janeiro, Brazil.

---

* Corresponding author. E-mail: alexandre_porte@yahoo.com.br

doi: 10.2298/JSC0803307P

EXPERIMENTAL

Plant material

The botanical material was collected in Petrópolis, Rio de Janeiro, Brazil. A voucher specimen of this plant has been deposited in the herbarium of the Departamento de Botânica do Instituto de Biologia da Universidade Federal Rural do Rio de Janeiro (RBR 4239).

Isolation of the essential oil

Fresh leaves were subjected to hydrodistillation in a Clevenger-type apparatus for 93 min, which gave the essential oil.

Gas chromatography

Chemical analysis was performed on a Hewlett–Packard 5890 series II gas chromatograph fitted with a HP-5 capillary column (25 m×0.20 mm, film thickness 0.33 μm). The carrier gas was hydrogen at a flow of 1.0 ml min^{-1} and a split ratio 1:100. The column temperature was programmed from 60–250 °C at 2.0 °C min^{-1}; the injector temperature was 250 °C and the detector (FID) temperature was 280 °C.

Gas chromatography/mass spectroscopy

The analysis was performed on a Hewlett–Packard 5890 series II gas chromatograph coupled to a HP 5970 mass selective detector using a fused silica capillary column HP-5 (25 m×0.20 mm, film thickness 0.33 μm). The column temperature was programmed from 60–250 °C at 2.0 °C min^{-1} using helium as the carrier gas at a flow rate of 1.0 ml min^{-1}. The ion source temperature was 300 °C and the electron energy 70 eV. Identification of components was based on comparison of their mass spectra with those found in the literature,[9] on retention indices,[9] the mass spectrometry data bank (NIST) and a computer search of the Wiley library.

RESULTS AND DISCUSSION

The yield of thyme essential oil from the Rio de Janeiro plant material was 1.1 % based on the dry mass. Other Brazilian work, but from South Brazil, found a yield of 0.25 %.[10] The compounds identified in the oil sample are presented in Table I.

GC and GC/MS analyses of the oil resulted in the identification of 28 constituents, accounting for 95.1 % of the oil. The chemical composition of the oil is characterized by high amounts of thymol, *p*-cymene and *γ*-terpinene. This composition is different to those found in some oils from Italy, Spain, France, Poland and New Zealand but is in accordance with the Food Chemical Codex requirement (*i.e.*, not less than 40 %, by volume of phenols).[11–18] Therefore, the thyme essential oil analyzed in this study was a thymol chemotype, while the essential oil from the above-mentioned countries could have been carvacrol chemotypes or other chemotypes, assuming that the essential oils investigated in these countries were obtained from *Thymus vulgaris*, and not other species (*e.g. T. zygis* – very spread in Spain and Portugal, *T. panonicus* – common in Poland or *T. satureoides*).[11,12]

The high concentration of thymol suggests that the thyme essential oil from Rio de Janeiro could have desirable phenols values for international trade, principally, if we will consider that plant material was collected during the Brazilian spring (*i.e.*, not flowering plants). In spring, the values of thymol trend to increase and the values of *p*-cymene and γ-terpinene are at their lowest, as pointed by other workers.[19,20]

TABLE I. Chemical composition of the essential oil from leaves of *Thymus vulgaris* L. from Rio de Janeiro State, Brazil

Compound	Content, %
1,3-Octadiene	0.3
1,7-Octadiene	0.1
2,4-Dymethyl-2,4-heptadiene	1.5
α-Pinene	0.8
Camphene	0.3
Sabinene	0.1
para-Menthene-1	1.8
para-Menthene-3	0.1
Myrcene	2.4
α-Phellandrene	0.3
α-Terpinene	1.8
p-Cymene	18.6
Limonene	0.8
(Z)-β-Ocimene	0.1
(E)-β-Ocimene	0.1
γ-Terpinene	16.5
Mentha-3,8-diene	0.4
α-Terpinolene	0.2
p-Cimenene	0.1
Borneol	0.5
trans-Dihydrocarvone	0.2
Thymol methyl ether	0.1
Thymol	44.7
Carvacrol	2.4
Carvacrol acetate	< 0.1
β-Caryophyllene	0.8
Calamenene	< 0.1
δ-Cadinene	0.1
Total	95.1

Due to the extent of the inhibitory effect of the oil on micro-organisms being attributed to the presence of aromatic nuclei containing a polar functional group, especially the thymol phenol group, it can be awaited that the studied essential oil would exhibit good antimicrobial properties, but this was not evaluated.

Acknowledgments. We are grateful to CAPES for financial support.

ИЗВОД

ХЕМИЈСКИ САСТАВ ЕТАРСКОГ УЉА БИЉКЕ *Thymus vulgaris* L. ИЗ ДРЖАВЕ РИО ДЕ ЖАНЕИРО, БРАЗИЛ

ALEXANDRE PORTE[1] и RONOEL L. O. GODOY[2]

[1]*Instituto de Tecnologia – Universidade Federal Rural do Rio de Janeiro, BR 465, km 47, Seropédica,*
Cep 23890-000, Rio de Janeiro и [2]*Embrapa Agroindústria de Alimentos, Avenida das Américas,*
29501, Guaratiba, Cep 23020-470, Rio de Janeiro, Brazil

Етарско уље свежих листова биљке *Thymus vulgaris* L. из државе Рио де Жанеиро, Бразил, изоловано је дестилацијом воденом паром и анализирано комбинацијом GC и GC/MS. Идентификована једињења чине 95,1 % уља. Детектовано је 39 састојака, од којих је 28 идентификовано на основу хроматографских ретенционих индекса и масених спектара. Главни састојци уља су били тимол (44,7 %), *p*-цимен (18,6 %) и γ-терпинен (16,5 %).

(Примљено 5. јуна 2007)

REFERENCES

1. A. Porte, R. L. O. Godoy, D. Lopes, M. Koketsu, S. L. Gonçalves, H. S. Torquilho, *J. Essent. Oil Res.* **12** (2000) 577
2. J. S. Pruthi, *Spices and Condiments*, National Book Trust, New Delhi, 1976, p. 199
3. N. Nakatani, K. Miura, T. Inagaki, *Agric. Biol. Chem.* **53** (1989) 1375
4. S. Perruci, F. Mancianti, P. L. Cioni, G. Flamini, I.Morelli, G. Macchioni, *Planta Med.* **60** (1994) 184
5. D. P. Thompson, C. Cannon, *Bull. Environ. Contam. Toxicol.* **36** (1986) 527
6. A. Ismaiel, M. D. Pierson, *J. Food Sci.* **55** (1990) 1676
7. R. S. Farag, Z. Y. Daw, S. H. Abo-Raya, *J. Food Sci.* **54** (1989) 74
8. R. S. Farag, Z. Y. Daw, F. M. Hewedi, G. S. A. El-Baroty, *J. Food Prot.* **52** (1989) 665
9. R. P. Adams, *Identification of essential oil components by gas chromatography/mass spectroscopy*, Allured Publ. Corp., Carol Stream, 1995, p. 467
10. A. C. Atti-Santos, M. R. Pansera, N. Paroul, L. Atti-Serafini, P. Moyna. *J. Essent. Oil Res.* **16** (2004) 294
11. B. M. Lawrence, *Perfum. Flavor* **7** (1982) 39
12. B. M. Lawrence, *Perfum. Flavor* **13** (1988) 60
13. B. M. Lawrence, *Perfum. Flavor* **17** (1992) 140
14. B. M. Lawrence, *Perfum. Flavor* **20** (1995) 67
15. B. M. Lawrence, *Perfum. Flavor* **23** (1998) 42
16. R. Picclagia, M. Marotti, *Flavour Fragr. J.* **6** (1991) 241
17. R. Picclagia, M. Marotti, *Flavour Fragr. J.* **8** (1993) 115
18. *Food Chemical Codex*, National Academy Press, Washington, 1981. p. 265
19. J. A. McGimpsey, M. H. Douglas, J. W. van Klink, D. A. Beauregard, N. B. Perry, *Flavour Fragr. J.* **9** (1994) 347
20. M. S. Karawya, M. S. Hifnawy, *J. AOAC Int.* **57** (1974) 997.

www.shd.org.yu

Journal of the Serbian Chemical Society

JSCS@tmf.bg.ac.yu • www.shd.org.yu/JSCS

J. Serb. Chem. Soc. *73* (3) 311–319 (2008)
JSCS–3713

UDC 539.6:517.58:519.17–124
Original scientific paper

Hosoya polynomial of zigzag polyhex nanotorus

MEHDI ELIASI and BIJAN TAERI*

Department of Mathematical Sciences, Isfahan University of Technology,
Isfahan 84156-83111, Iran

(Received 12, revised 22 September 2007)

Abstract: The Hosoya polynomial of a molecular graph G is defined as $H(G,\lambda)=\sum_{\{u,v\}\subseteq V(G)}\lambda^{d(u,v)}$, where $d(u,v)$ is the distance between vertices u and v. The first derivative of $H(G,\lambda)$ at $\lambda = 1$ is equal to the Wiener index of G, defined as $W(G)=\sum_{\{u,v\}\subseteq V(G)}d(u,v)$. The second derivative of $\frac{1}{2}\lambda H(G,\lambda)$ at $\lambda=1$ is equal to the hyper-Wiener index, defined as $WW(G)=\frac{1}{2}W(G)+\frac{1}{2}\sum_{\{u,v\}\subseteq V(G)}d(u,v)^2$. Xu *et al.*[1] computed the Hosoya polynomial of zigzag open-ended nanotubes. Also Xu and Zhang[2] computed the Hosoya polynomial of armchair open-ended nanotubes. In this paper, a new method was implemented to find the Hosoya polynomial of $G = HC_6[p,q]$, the zigzag polyhex nanotori and to calculate the Wiener and hyper Wiener indices of G using $H(G,\lambda)$.

Keywords: Wiener index; hyper-Wiener index; Hosoya polynomial; nanotubes.

INTRODUCTION

A topological index is a real number related to a structural graph of a molecule. It does not depend on the labeling or pictorial representation of graph. Among topological indices, the Wiener index[3] is certainly the most important one. This index was introduced by the chemist Harold Wiener, about 60 years ago to demonstrate correlations between physico-chemical properties of organic compounds and the topological structure of their molecular graphs. Wiener defined his index as the sum of the distances between two carbon atoms in the molecules, in terms of carbon–carbon bonds. The historical details and further bibliography on the chemical applications of the Wiener index are reviewed in the literature.[4,5]

The topological distance between a pair of vertices u and v of a molecular graph G, denoted by $d(u,v)$, is the number of edges on the shortest path joining u and v. Thus, the Wiener index of G is half the sum of distances between all vertices of the graph G:

---

* Corresponding author. E-mail: b.taeri@cc.iut.ac.ir

doi: 10.2298/JSC0803311E

$$W(G) = \sum_{\{u,v\} \subseteq V(G)} d(u,v)$$

where $V(G)$ is the set of vertices of G.

Another topological index is the hyper-Wiener index that was defined by Klein *et al.*[6] and others[7–12] applied it to cyclic structures as:

$$WW(G) = \frac{1}{2} W(G) + \frac{1}{2} \sum_{\{u,v\} \subseteq V(G)} d(u,v)^2$$

Haruo Hosoya[13] introduced a distance-based polynomial, which he called the Wiener polynomial, related to each connected graph G as:

$$H(G,\lambda) = \sum_{k \geq 0} d(G,k) \lambda^k$$

where $d(G,k)$ is the number of pair vertices of G that are at distance k of each other. However, today it is called the Hosoya polynomial.[14–15] It is easy to see that it is equal to:

$$H(G,\lambda) = \sum_{\{u,v\} \subseteq V(G)} \lambda^{d(u,v)}$$

In 1991, Iijima[16] discovered carbon nanotubes as multi-walled structures. Carbon nanotubes show remarkable mechanical properties. Experimental studies have shown that they belong to the stiffest and most elastic materials known. These mechanical characteristics clearly predestinate nanotubes for advanced composites. Diudea was the first chemist who considered the problem of computing topological indices of nanostructures.[1,2,17–24] Recently computing topological indices of nanostructures has been the subject of many papers. The reader is encouraged to consult papers[25–31] on computing topological indices of some nanotubes.

RESULTS AND DISCUSSION

Xu *et al.*[1] computed the Hosoya polynomials of zigzag open-ended nanotubes. Also Xu and Zhang[2] computed the Hosoya polynomial of polynomials of armchair open-ended nanotubes. In this paper, a new method was implemented to find the Hosoya polynomial of zigzag polyhex nanotorus. Throughout this paper, $G = HC_6[p,q]$ (see Fig. 1) denotes an arbitrary zigzag polyhex nanotorus in terms of the circumference p and the length q.

It should be noticed that p and q must be even. Also, a coordinate label for the vertices of $G = HC_6[p,q]$, as shown in Fig. 2, was chosen. The distances from x_{01} to all vertices are given in Fig. 3. Note that the graph is bipartite, or equivalently, the vertices can be colored with white and black, so that adjacent vertices have a different color. Since the graph is symmetric with respect to the line joining $x_{0,\frac{p}{2}+1}$ to $x_{1,\frac{p}{2}+1}$, one half of the numbers are shown in Fig. 3.

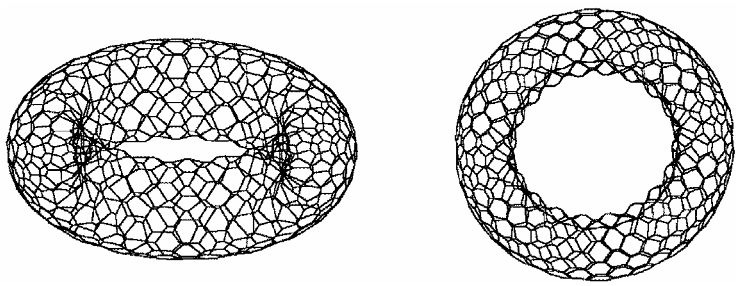

Fig. 1. $HC_6[20,40]$: Side view; top view.

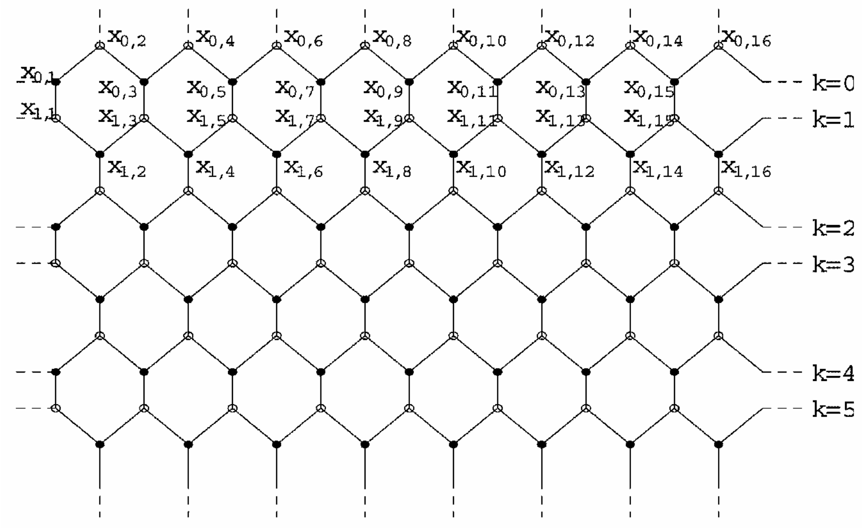

Fig. 2. A zigzag polyhex nanotorus lattice with $p = 16$ and $q = 6$.

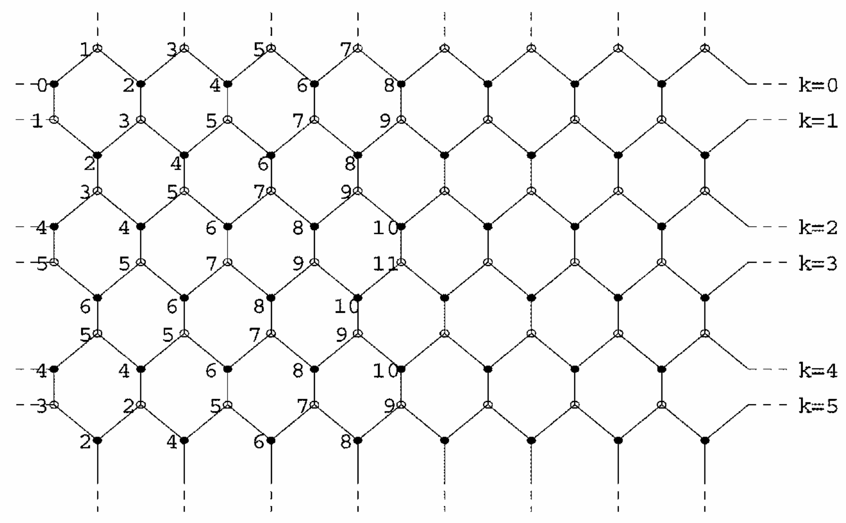

Fig. 3. Distances from x_{01} to each vertex of $HC_6[6,16]$.

CALCULATION PROCEDURE

For a vertex $u \in V(G)$,

$$d(u,\lambda) = \sum_{v \in V(G)} \lambda^{d(u,v)}$$

is defined and the work is commenced with the following key result.

Result 1. Let $u \in V(G)$ be a white vertex and the summation of $\lambda^{\alpha(u,x)}$, where x varies on the vertices of level k, is denoted by $w_k(\lambda)$. Then if $0 \le k < p/2$, one obtains:

$$\begin{aligned} w_k(\lambda) &= \sum_{x \in \text{level}\, k} \lambda^{d(x_{02},x)} \\ &= \sum_{x \in \text{level}\, k} \lambda^{d(x_{04},x)} \\ &\vdots \\ &= \frac{1}{\lambda-1}(\lambda^{k+\frac{p}{2}} - \lambda^{2k+1} + \lambda^{k+\frac{p}{2}+1} - k\lambda^{2k} - \lambda^{2k} + k\lambda^{2k+2}) \end{aligned}$$

and if $k \ge p/2$ then one has:

$$\begin{aligned} w_k(\lambda) &= \sum_{x \in \text{level}\, k} \lambda^{d(x_{02},x)} \\ &= \sum_{x \in \text{level}\, k} \lambda^{d(x_{04},x)} \\ &\vdots \\ &= \frac{p}{2}\lambda^{2k+1} + \frac{p}{2}\lambda^{2k} \end{aligned}$$

Similarly, suppose that $u \in V(G)$ is a black vertex and the summation of $\lambda^{\alpha(u,x)}$, where x varies on the vertices of level k, is denoted by $b_k(\lambda)$. Then if $0 \le k < p/2$, one has:

$$\begin{aligned} b_k(\lambda) &= \sum_{x \in \text{level}\, k} \lambda^{d(x_{01},x)} \\ &= \sum_{x \in \text{level}\, k} \lambda^{d(x_{03},x)} \\ &= \frac{1}{\lambda-1}(\lambda^{k+\frac{p}{2}} - \lambda^{2k+1} + \lambda^{k+\frac{p}{2}+1} + k\lambda^{2k+1} - \lambda^{2k} - k\lambda^{2k-1}) \end{aligned}$$

and if $k \ge p/2$, then one has:

$$\begin{aligned} b_k(\lambda) &= \sum_{x \in \text{level}k} \lambda^{d(x_{01},x)} \\ &= \sum_{x \in \text{level}k} \lambda^{d(x_{03},x)} \\ &= \frac{p}{2}\lambda^{2k-1} + \frac{p}{2}\lambda^{2k} \end{aligned}$$

Proof. $b_k(\lambda)$ is computed. It is suffices to consider x_{01}. For other black vertices, the argument is similar. Firstly, note that the lattice is symmetric with respect to the line joining x_{01} to x_{11}. Three cases can be distinguished:

Case 1. $p/2 \le k$ and k is even. In this case, for all $1 \le j \le p/2 + 1$, one has

$$d(x_{01}, x_{kj}) = \begin{cases} 2k-1 & \text{if } j \text{ is even} \\ 2k & \text{if } j \text{ is odd} \end{cases}$$

Now by considering these vertices and their symmetric vertices, one obtains $p/2$ vertices having a distance $2k - 1$ from x_{01}, and $p/2$ vertices having a distance $2k$ from x_{01}. Hence,

$$b_k(\lambda) = \frac{p}{2}\lambda^{2k-1} + \frac{p}{2}\lambda^{2k}$$

Case 2. $p/2 \le k$ and k is odd. In this case for all $1 \le j \le p/2+1$, one has:

$$d(x_{01}, x_{kj}) = \begin{cases} 2k & \text{if } j \text{ is even} \\ 2k-1 & \text{if } j \text{ is odd} \end{cases}$$

Now by considering these vertices and their symmetric vertices, one obtains $p/2$ vertices having distance $2k - 1$ from x_{01}, and $p/2$ vertices having a distance $2k$ from x_{01}. Hence,

$$b_k(\lambda) = \frac{p}{2}\lambda^{2k-1} + \frac{p}{2}\lambda^{2k} .$$

Case 3. $p/2 < k$. For all j's, such that $p + 1 \le j$ and $k + 1 < j$, one has:

$$d(x_{01}, x_{kj}) = k + j - 1$$

Thus, the summation of the distances between x_{01} and x_{kj} (for all j's, such that $p + 1 \le j$ and $k + 1 < j$) and their symmetric vertices is:

$$S_1 = 2\sum_{j=k+2}^{\frac{p}{2}} \lambda^{k+j-1} + \lambda^{k+\frac{p}{2}+1-1} = \frac{1}{\lambda - 1}(\lambda^{k+\frac{p}{2}} - 2\lambda^{2k+1} + \lambda^{k+\frac{p}{2}+1})$$

Also if $1 \le j \le k + 1$, then

$$d(x_{01}, x_{kj}) = \begin{cases} 2k & \text{if } k-j \text{ is odd} \\ 2k-1 & \text{if } k-j \text{ is even} \end{cases}$$

Therefore, the summation of the distances between x_{01} and x_{kj} (for all j such that $1 \le j \le k + 1$) and their symmetric vertices is:

$$S_2 = (k+1)\lambda^{2k} + k\lambda^{2k-1}$$

Hence,

$$b_k(\lambda) = S_1 + S_2 = \frac{1}{\lambda - 1}(\lambda^{k+\frac{p}{2}} - \lambda^{2k+1} + \lambda^{k+\frac{p}{2}+1} + k\lambda^{2k+1} - \lambda^{2k} - k\lambda^{2k-1})$$

The proof for $w_k(\lambda)$ is similar.

Result 2. For one white or black vertex x_{0j} of level 0, one has:

$$w_{\frac{q}{2}}(\lambda) = b_k(\lambda) := \sum_{x \in \text{level}\,\frac{q}{2}} \lambda^{d(x_{0j},x)} =$$

$$= \begin{cases} \frac{1}{\lambda - 1}(\lambda^{\frac{q}{2}+\frac{p}{2}} - \lambda^{2(\frac{q}{2})+1} + \lambda^{\frac{q}{2}+\frac{p}{2}+1} + \frac{q}{2}\lambda^{2(\frac{q}{2})+1} - \lambda^{2(\frac{q}{2})} - (\frac{q}{2})\lambda^{2(\frac{q}{2})-1}) \text{ if } \frac{q}{2} < \frac{p}{2} \\ \frac{p}{2}\lambda^{2(\frac{q}{2})-1} + \frac{p}{2}\lambda^{2(\frac{q}{2})} \text{ if } \frac{q}{2} \ge \frac{p}{2} \end{cases}$$

Proof. Since G is symmetric with respect to the line joining x_{01} to x_{11}, it is sufficient to prove the assertion for x_{01} and x_{02}. For x_{01}, the proof is exactly the proof of Result 1. Considering tori that can be built up from two halves collapsing at level 0, the top part x_{02} is a black vertex, hence by the proof of Result 1, one can calculate $b_{\frac{q}{2}}(\lambda)$.

Result 3. For each $u \in V(G)$, one has:

$$D(\lambda) := d(u,\lambda) = b_0(\lambda) + b_1(\lambda) + \cdots + b_{\frac{q}{2}}(\lambda) + w_1(\lambda) + \cdots + w_{\frac{q}{2}-1}(\lambda)$$

Proof. Firstly, note that the lattice is symmetric (with respect to the level k). Hence, it suffices to consider x_{01} and x_{02}. For other black (white) vertices, the argument is similar. Now, beginning with x_{01}, let $B_1 = \{k \mid 0 \le k \le \frac{q}{2}\}$ and $B_2 = \{k \mid \frac{q}{2} < k \le q-1\}$. Then one has:

$$d(x_{01},\lambda) = \sum_{v \in V(G)} \lambda^{d(x_{01},v)} = \sum_{v \in B_1} \lambda^{d(x_{01},v)} + \sum_{v \in B_2} \lambda^{d(x_{01},v)}$$

However,

$$\sum_{v \in B_1} \lambda^{d(x_{01},v)} = \sum_{v \in level0_1} \lambda^{d(x_{01},v)} + \sum_{v \in level1_1} \lambda^{d(x_{01},v)} + \cdots + \sum_{v \in level_1 \frac{q}{2}-1} \lambda^{d(x_{01},v)} = b_0(\lambda) + b_1(\lambda) + \cdots + b_{\frac{q}{2}}(\lambda)$$

For computing the last sum, tori that can be built up from two halves collapsing at level 0 are considered. The top part is formed of the lines of B_2 such that x_{01} are a black vertex. Hence, by changing the index and using the proof of Lemma 1, one obtains:

$$\sum_{v \in B_2} \lambda^{d(x_{01},v)} = \sum_{v \in \mathrm{level} q-1_1} \lambda^{d(x_{01},v)} + \sum_{v \in \mathrm{level} q-2_1} \lambda^{d(x_{01},v)} + \cdots + \sum_{v \in \mathrm{level}_1 \frac{q}{2}+1} \lambda^{d(x_{01},v)} = w_1(\lambda) + \cdots + w_{\frac{q}{2}-1}(\lambda)$$

which completes the proof.

Theorem. The Hosoya polynomial, $H(G,\lambda)$, of $G = HC_6[p,q]$, nanotorus is given by:

$$\begin{cases} H_1(G,\lambda) & \text{if } q \le p \\ H_2(G,\lambda) & \text{if } q > p \end{cases}$$

where

$$H_1(G,\lambda) = \frac{pq}{4\lambda(\lambda-1)^2}(-2\lambda^{q+2} + 2\lambda^{\frac{p}{2}+\frac{q}{2}+2} - 2\lambda^{\frac{p}{2+2}} + 4\lambda^2 + q\lambda^{q+2} +$$
$$+4\lambda^{\frac{p}{2}+\frac{q}{2}+1} - 4\lambda^{\frac{p}{2}+1} - 2\lambda^{q+1} - 2\lambda - 2\lambda^{\frac{p}{2}} - 2\lambda^q + 4 - q\lambda^q + 2\lambda^{\frac{p}{2}+\frac{q}{2}})$$

and

$$H_2(G,\lambda) = \frac{pq}{4\lambda(\lambda-1)^2}(-2\lambda^{\frac{p}{2}+3} + p\lambda^{q+3} + 4\lambda^3 - 4\lambda^{p+2} - p\lambda^{p+2} -$$
$$-4\lambda^{\frac{p}{2}++2} - 2\lambda^2 + p\lambda^{p+1} + 4\lambda^{p+2} + 4\lambda^{p+1} + 4\lambda - 2\lambda^{\frac{p}{2}+1} - 4\lambda^{p+1} - p\lambda^{q+1})$$

Proof. One has:

$$H(G,\lambda) = \frac{1}{2}\sum_{u \in V(G)}\sum_{v \in V(G)} \lambda^{d(u,v)} + \frac{1}{2}\sum_{u \in V(G)} \lambda^{d(u,u)} = \frac{1}{2}\sum_{v \in V(G)} d(v,\lambda) + \frac{1}{2}|V(G)| = \frac{1}{2}\sum_{v \in V(G)} D(\lambda) + \frac{1}{2}pq =$$
$$= \frac{pq}{2}D(\lambda) + \frac{1}{2}pq$$

First suppose that $q \le p-2$. In this case, $q < p$, hence by Result 3 and Result 1, one has:

$$
\begin{aligned}
D(\lambda) &= b_o(\lambda)+b_1(\lambda)+\cdots+b_{\frac{q}{2}}(\lambda)+w_1(\lambda)+\cdots+w_{\frac{q}{2}-1}(\lambda)\\
&= \sum_{k=0}^{\frac{q}{2}} \frac{1}{\lambda-1}(\lambda^{k+\frac{p}{2}}-\lambda^{2k+1}+\lambda^{k+\frac{p}{2}+1}+k\lambda^{2k+1}-\lambda^{2k}-k\lambda^{2k-1})\\
&\sum_{k=1}^{\frac{q}{2}-1} \frac{1}{\lambda-1}(\lambda^{k+\frac{p}{2}}-\lambda^{2k+1}+\lambda^{k+\frac{p}{2}+1}-k\lambda^{2k}-\lambda^{2k}+k\lambda^{2k+2}) =\\
&= \frac{1}{2\lambda(\lambda-1)(\lambda^2-1)}(2\lambda+4\lambda^2+q\lambda^{q+3}-4\lambda^{q+2}+2\lambda^4+4\lambda^3-\\
&-2\lambda^{q+4}-4\lambda^{q+3}+2\lambda^{\frac{p}{2}+4+\frac{q}{2}}+6\lambda^{\frac{p}{2}+3+\frac{q}{2}}+6\lambda^{\frac{p}{2}+2+\frac{q}{2}}-6\lambda^{\frac{p}{2}+3}-\\
&-6\lambda^{\frac{p}{2}+2}-2\lambda^{\frac{p}{2}+1}-q\lambda^{2+q}+q\lambda^{q+4}-q\lambda^{1+q}-2\lambda^{q+1}+2\lambda^{\frac{p}{2}+3+\frac{q}{2}}-2\lambda^{\frac{p}{2}+4})
\end{aligned}
$$

Hence, in this case $H(G,\lambda) = H_1(G,\lambda)$.

Now suppose that $p \le q-2$. In this case, $p/2-1 \le q/2-1$, hence by Result 3 and Result 1, one has:

$$
\begin{aligned}
D(\lambda) &= b_0(\lambda)+b_1(\lambda)+\cdots+b_{\frac{q}{2}}(\lambda)+w_1(\lambda)+\cdots+w_{\frac{q}{2}-1}(\lambda) =\\
&= b_0(\lambda)+b_1(\lambda)+\cdots+b_{\frac{p}{2}-1}(\lambda)+b_{\frac{p}{2}}(\lambda)+\cdots+b_{\frac{q}{2}}(\lambda)+\\
&\quad + w_1(\lambda)+\cdots+w_{\frac{p}{2}-1}(\lambda)+w_{\frac{p}{2}}(\lambda)+\cdots+w_{\frac{q}{2}-1}(\lambda) =\\
&\quad = \sum_{k=0}^{\frac{p}{2}-1} \frac{1}{\lambda-1}(\lambda^{k+\frac{p}{2}}-\lambda^{2k+1}+\lambda^{k+\frac{p}{2}+1}+k\lambda^{2k+1}-\lambda^{2k}-k\lambda^{2k-1})+\\
&\quad + \sum_{k=\frac{p}{2}}^{\frac{q}{2}} (\tfrac{p}{2}\lambda^{2k-1}+\tfrac{p}{2}\lambda^{2k}) + \sum_{k=1}^{\frac{p}{2}-1} \frac{1}{\lambda-1}(\lambda^{k+\frac{p}{2}}-\lambda^{2k+1}+\lambda^{k+\frac{p}{2}+1}-k\lambda^{2k}-\lambda^{2k}+k\lambda^{2k+2})+\\
&\quad + \sum_{k=\frac{p}{2}}^{\frac{q}{2}-1} (\tfrac{p}{2}\lambda^{2k+1}+\tfrac{p}{2}\lambda^{2k})
\end{aligned}
$$

After calculation of these summations, one obtains:

$$H(G,\lambda) = H_2(G,\lambda)$$

Finally, if $p = q$, then by Result 3 and Result 1, for each $u \in V(G)$, one has:

$$
\begin{aligned}
D(\lambda) &= b_0(\lambda)+b_1(\lambda)+\cdots+b_{\frac{q}{2}}(\lambda)+w_1(\lambda)+\cdots+w_{\frac{q}{2}-1}(\lambda) =\\
&= b_0(\lambda)+b_1(\lambda)+\cdots+b_{\frac{p}{2}-1}(\lambda)+w_{\frac{p}{2}}(\lambda)+w_1(\lambda)+\cdots+w_{\frac{p}{2}-1}(\lambda) =\\
&= \sum_{k=0}^{\frac{p}{2}-1qp} \frac{1}{\lambda-1}(\lambda^{k+\frac{p}{2}}-\lambda^{2k+1}+\lambda^{k+\frac{p}{2}+1}+k\lambda^{2k+1}-\lambda^{2k}-k\lambda^{2k-1})+(\tfrac{p}{2}\lambda^{2(\frac{p}{2})-1}+\tfrac{p}{2}\lambda^{2(\frac{p}{2})})\\
&\quad \sum_{k=1}^{\frac{p}{2}-1} \frac{1}{\lambda-1}(\lambda^{k+\frac{p}{2}}-\lambda^{2k+1}+\lambda^{k+\frac{p}{2}+1}-k\lambda^{2k}-\lambda^{2k}+k\lambda^{2k+2})
\end{aligned}
$$

Hence, in this case, $H(G,\lambda) = H_1(G,\lambda)$.

One of the most frequent applications of the Hosoya polynomial is the calculation of the Wiener and hyper-Wiener indices. In fact

$$W(G) = \frac{d}{d\lambda} H(G,\lambda)\Big|_{\lambda=1}$$

and

$$WW(G) = \frac{1}{2}\frac{d^2}{d\lambda^2}[\lambda H(G,\lambda)]\Big|_{\lambda=1}$$

Since the polynomials are a continuity function, hence for the obtained polynomials one has:

$$W(G) = \lim_{\lambda\to 1} \frac{d}{d\lambda}[H(G,\lambda)]$$

and

$$WW(G) = \lim_{\lambda\to 1} \frac{1}{2}\frac{d^2}{d\lambda^2}[\lambda H(G,\lambda)]$$

Thus, one can calculate:

Result 4. The Wiener index of $HC_6[p,q]$ nanotori is given by:

$$\begin{cases} \frac{pq^2}{24}(-4+3p^2+3pq+q^2) \text{ if } q \le p \\ \frac{p^2q}{24}(-4+p^2+6q^2) \text{ if } q > p \end{cases}$$

Result 5. The hyper-Wiener index of $HC_6[p,q]$ nanotori is given by:

$$\begin{cases} \frac{1}{192} pq^2(-16+16p-20q+4p^3+6p^2q+4pq^2+12p^2+5q^3+4q^2+12pq) \text{ if } q \le p \\ \frac{1}{192} p^2q(3p^3+4p^2-12p-6+16q^3+24q^2+8q) \text{ if } q > p \end{cases}$$

CONCLUSION

A method has been developed which is usually very useful for calculating the Hosoya polynomials of C_6 nanotubes and nanotorus. As a consequence of calculating the Hosoya polynomials of zigzag polyhex nanotorus, the Wiener and hyper-Weiner of such nanotorous were computed.

Acknowledgement. The second author was partially supported by the Center of Excellence of Mathematics of the Isfahan University of Technology (CEAMA).

ИЗВОД

HOSOYA ПОЛИНОМ ЦИК-ЦАК ПОЛИХЕКС НАНОТОРУСА

MEHDI ELIASI и BIJAN TAERI

Department of Mathematical Sciences, Isfahan University of Technology,Isfahan 84156-83111, Iran

Hosoya полином молекулског графа G је дефинисан као $H(G,\lambda) = \sum_{\{u,v\}\subseteq V(G)} \lambda^{d(u,v)}$, где је $d(u,v)$ растојање између чворова u и v. Први извод од $H(G,\lambda)$ за $\lambda = 1$ једнак је Винеровом индексу графа G, који је дефинисан као $W(G) = \sum_{\{u,v\}\subseteq V(G)} d(u,v)$. Други извод

од $\frac{1}{2}\lambda H(G,\lambda)$ за $\lambda = 1$ једнак је хипер-Винеровом индексу, дефинисаном као $WW(G) = \frac{1}{2}W(G) + \frac{1}{2}\sum_{\{u,v\}\subseteq V(G)} d(u,v)^2$. Xu *et al.*[1] су израчунали Hosoya полином незатворених цик-цак наноцеви. Xu и Zhang[2] су израчунали Hosoya полином “armchair” незатворених наноцеви. У овом раду развијена је нова метода за одређивање Hosoya полинома за $G = HC_6[p,q]$, тј. за цик-цак полихекс наноторусе. Користећи $H(G,\lambda)$, израчунати су Винеров и хипер-Винеров индекс ових наноторуса.

(Примљено 12., ревидирано 22. септембра 2007)

REFERENCES

1. Sh. Xu, H. Zhang, M. Diudea, *MATCH Commun. Math. Comput. Chem.* **57** (2007) 443
2. S. Xu, H. Zhang, *Int. J. Quantum Chem.* **107** (2007) 586
3. H. Wiener, *J. Am. Chem. Soc.* **69** (1947) 17
4. I. Gutman, *Chem. Phys. Lett.* **364** (2002) 352
5. I. Gutman, O. E. Polansky, *Mathematical Concepts in Organic Chemistry*, Springer-Verlag, Berlin, 1986
6. D. J. Klein, I. Lukovits, I. Gutman, *J. Chem. Inf. Comput. Sci.* **35** (1995) 50
7. J. Devillers, A. T. Balaban, *Topological Indices and Related Descriptors in QSAR and QSPR*, Gordon and Breech, Amsterdam, 1999
8. I. Gutman, *J. Serb. Chem. Soc.* **68** (2003) 949
9. I. Gutman, B. Furtula, J. Belić, *J. Serb. Chem. Soc.* **68** (2003) 943
10. I. Gutman, *Croat. Chim. Acta* **77** (2004) 61
11. I. Gutman, B. Furtula, *Monatsh. Chem.* **134** (2003) 975
12. S. Klavzar, P. Zigert, I. Gutman, *MATCH Commun. Math. Comput. Chem.* **24** (2000) 229
13. H. Hosoya, *Discr. Appl. Math.* **19** (1988) 239
14. I. Gutman, *Publ. Elektrotehn. Fak.* (Beograd), Ser. Mat. **10** (1999) 53
15. D. Stevanovic, *Discr. Math.* **235** (2001) 237
16. S. Iijima, *Nature* **354** (1991) 56
17. M. V. Diudea, I. Silaghi-Dumitrescu, B. Parv, *MATCH Commun. Math. Comput. Chem.* **44** (2001) 117
18. M. V. Diudea, *MATCH Commun. Math. Comput. Chem.* **45** (2002) 109
19. M. V. Diudea, A. Graovac, *MATCH Commun. Math. Comput. Chem.* **44** (2001) 93
20. M. V. Diudea, I. Silaghi-Dumitrescu, B. Parv, *MATCH Commun. Math. Comput. Chem.* **44** (2001) 117
21. M. V. Diudea, P. E. John, *MATCH Commun. Math. Comput., Chem.* **44** (2001) 103
22. M. V. Diudea, *Bull. Chem. Soc. Jpn.* **75** (2002) 487
23. M. V. Diudea, *MATCH Commun. Math. Comput. Chem.* **45** (2002) 109
24. M. V. Diudea, M. Stefu, B. Parv, P. E. John, *Croat. Chim. Acta* **77** (2004) 111
25. A. R. Ashrafi, A. Loghman, *MATCH Commun. Math. Comput. Chem.* **55** (2006) 447
26. A. R. Ashrafi, S. Yousefi, *MATCH Commun. Math. Comput. Chem.* **57** (2007) 403
27. A. Heydari, B. Taeri, *MATCH Commun. Math. Comput. Chem.* **57** (2007) 665
28. A. Heydari, B. Taeri, *J. Comput. Theor. Nano Sci.* **4** (2007) 158
29. S. Yousefi, A. R. Ashrafi, *MATCH Commun. Math. Comput. Chem.* **56** (2006) 169
30. E. Eliasi, B. Taeri, *MATCH Commun. Math. Comput. Chem.* **56** (2006) 383
31. A. Heydari, B. Taeri, *MATCH Commun. Math. Comput. Chem.* **57** (2007) 463.

www.shd.org.yu

Journal of the Serbian Chemical Society

JSCS@tmf.bg.ac.yu • www.shd.org.yu/JSCS

J. Serb. Chem. Soc. 73 (3) 321–331 (2008)
JSCS–3714

UDC 54–36:541.183.1+547.639:543.4
Original scientific paper

Modification of nano-sized layered double hydroxides by long-chain organic aliphatic surfactants

RAMASAMY ANBARASAN[1]*, WANDUC LEE[2] and SEUNG SOON IM[2]

[1]Department of Polymer Technology, Advanced Nanotechnology Research Laboratory,
Kamaraj College of Engineering and Technology, Virudhunagar – 626 001,
Tamil Nadu, India and [2]Department of Fiber and Polymer Engineering,
Hanyang University, Seoul-133 791, South Korea

(Received 17 July 2007)

Abstract: The inter-layer anion of layered double hydroxides (LDH) with a hydrotalcite (HT)-like structure was ion-exchanged with various organic surfactants, particularly with long chain aliphatic surfactants. After the ion-exchange process, the basal spacing of the LDH was increased and the increase of the basal spacing depended on various factors, such as the intercalation capacity functionality and orientation capability of the surfactant. Of the employed surfactants, stearic acid intercalated LDH showed the highest increase of the basal spacing, which was confirmed by XRD analysis. FTIR results supported the interaction of the surfactants with the LDH. In addition, an increase in the thermal stability of the dodecanedioic acid intercalated HT was evidenced by the TGA method.

Keywords: hybrid; ion-exchange method; XRD; FTIR spectroscopy; TGA.

INTRODUCTION

Recently layered double hydroxides (LDH), synthetic clays with a hydrotalcite (HT)-like structure, have tempted both industrialists and academics due to their versatile applications as ion-exchangers, catalysts and electrolytes.[1–3] Nevertheless, their applications are limited due to their incompatibility with organic materials. In such a way their physical and chemical activities are frozen. This problem can be overcome by the introduction of a surfactant with mono- or multi-functionality into the HT structure through the ion-exchange method, with the surfactant playing the role of combatibilizer. The hydrophobicity of the HT is increased after modification with organic surfactants. Selection of the surfactant is very important because it not only increases the hydrophobicity but also increases the thermal and catalytic activities of the LDH.

---

* Corresponding author. E-mail: anbu_may3@yahoo.co.in

doi: 10.2298/JSC0803321A

A literature search revealed a number of papers related to the present topic. You *et al.*[4] modified a HT (containing Mg and Al as the divalent and trivalent metal ions with Cl ions as the interlayer anion) using various long chain aliphatic sulfates and aromatic sulfonates. In that study, a perpendicular approach of the surfactant into the HT was proposed. LDHs with various Mg/Al ratios were synthesized in which the Cl^- ion was the interlayer anion and the obtained LDHs were ion-exchanged with stearate anions.[5] A poly(ethylene oxide) (PEO) intercalated Mg–Al LDH was reported by Wypych and co-workers.[6] A paratungstate grafted (Mg/Al = 2) LDH was reported.[7] An acrylate anion intercalated Ni-based LDH was prepared and polymerized by an *in situ* method.[8] Steven and co-workers[9] modified an LDH by the ion-exchange method with carboxylates, sulfonates, phosphonates, porphyrins and phthalocyanin for certain catalysis and electrochemical applications. Recently Narita *et al.*[10] published a calixarene-*p*-sulfonate intercalated LDH. Anbarasan *et al.*[11] communicated results on the modification of a LDH by various sulfonates. A phosphonate intercalated LDH was also prepared.[12] Mg/Al and Zn/Al LDHs were intercalated with metallic oxalato complexes and the resulting hybrids were characterized by FTIR spectroscopy and XRD analysis.[13] An L-aspartic acid intercalated LDH was prepared and characterized by various analytical techniques.[14] Intercalation of bio-molecules, such as hexose, pentose, nucleotide, deoxyribonucleic acid, amino acids and polypeptides into LDH was reported by different authors.[15–20] A tetradecanoic acid intercalated LDH was reported by Changwen *et al.*[21] A report of a 4-hydroxy-3-methoxy cinnamic acid intercalated LDH is also available in the literature.[22]

The present communication reports the modification of an Mg/Al LDH with different long-chain organic aliphatic surfactants with various structural aspects discussed. The hybrids were characterized by FTIR, XRD and TGA methods.

EXPERIMENTAL

Materials

HT (nano-sized material), an LDH with carbonate anions as the inter-layer anion (Mg/Al = = 2.1, with a layer thickness of 0.48 nm) was a gift sample from KICET (Korea) and was used as received. Dodecane-1,12-diol (DDDIOL), dodecanedioic acid (DDDA), heptadecanoic acid (HDA) and octadecanoic acid (stearic acid) (SA) (Aldrich Chemicals, Korea) were used for the purpose of modification. The employed olive oil (OO) (Junsei Chemicals Co. Ltd., Japan) consisted of 85 % oleic acid (OA) (octadec-9-enoic acid), 9 % linoleic acid and 1.5 % of linolenic acid. In this study, the activity due to OA was considered due to its high content in OO. These surfactants were purchased and used without any further purification.

Method

HT (5 g) was placed in a 500 ml three-necked round-bottomed flask containing 250 ml of de-ionized water. The middle neck was used to attach a stirrer and the other two were used as the nitrogen inlet and outlet. Surfactant (10 g) was added under vigorous stirring to the content of the flask under inert atmosphere at 70 °C. Stirring in the alkaline medium was continued for 48 h. The ratio of carbonate to surfactant must be 1:2 because the divalent carbonate anions were ion-exchanged by the monovalent surfactant. After 48 h, the content of the flask was filtered and the precipitate was washed several times with de-ionized water to remove the sodium carbonate formed during the ion-exchange reaction and dried at room temperature overnight. The thus obtained white solid was ground and stored in a vial bottle.

Characterization

The HT powder before and after the ion-exchange reaction was characterized by XRD analysis using a Rigaku Rint 2000 (Japan) diffractometer at room temperature with CuKα1 radiation, in the 2θ angle range from 2 to 70° and by FTIR spectroscopy (KBr pellet technique) using a Nicolet 760 magna FTIR spectrometer. The thermal stability of the HT before and after modification was checked by thermogravimetric analysis (TGA), performed under a dynamic air atmosphere at a heating rate of 10 °C min^{-1} using an SDT 2960 TGA instrument.

The basal spacing (*d*) (from the Bragg equation), the inclined angle (ϕ) and the gallery height (*L*) can be calculated from Eqs. (1), (2) and (3), respectively.

$$d = \frac{\lambda}{2\sin\theta} \tag{1}$$

$$\sin\phi = \frac{\text{Basal spacing of } d_{003} \text{ plane} - \text{Thickness of layer}}{\text{Length of the organic anionic surfactant}} \tag{2}$$

$$L = d - \text{Thickness of layer} \tag{3}$$

where *d* is the basal spacing, θ the diffraction angle, λ the wavelength, ϕ the contact angle and *L* is the gallery height. The chain lengths of the organic aliphatic surfactants were calculated based on Isupov's[23] semi-empirical formula.

RESULTS AND DISCUSSION

The FTIR spectrum of pure HT is shown in Fig. 1 (curve a). It exhibited four peaks: *i.e.*, a peak at 3500 cm^{-1}, due to OH stretching (from interlayer water molecules); a bending vibration of water at 1641 cm^{-1}; carbonate stretching at 1377 cm^{-1}, as a sharp peak, and metal–hydroxide stretching at 679 cm^{-1}. The FTIR spectrum of HT–DDDIOL is shown in Fig. 1(curve b), from which it can be seen that some new peaks are present in addition to the HT peaks, *i.e.*, a twin peak at 2924 and 2836 cm^{-1}, due to C−H antisymmetric and symmetric stretching, peaks at 1453, 1044 and 990 cm^{-1}, due to CH_2 bending, alcoholic C−O antisymmetric stretching and chain folding, respectively. The appearance of the new peaks confirms the interaction between HT and DDDIOL. The FTIR spectra of HT–DDDA, HT–HDA, HT–SA, and HT–OO are shown in Fig. 1 (curves c–f, respectively). The same peaks as mentioned above were also present in these spectra. These FTIR spectra are, however, not sufficient to prove the existence of interaction between HT and surfactants and they cannot clearly explain the type of interaction. A peak due to carbonyl stretching of the long chain carboxyl group (≈ 1730 cm^{-1}) is not visible in Fig. 1 (curves c–e). Normally, FTIR spectra for long chain carboxyl compounds do not show the carbonyl peak clearly. In the case of HT–OO (Fig. 1, curve f), a peak at 1742 cm^{-1} due to carbonyl stretching of the unsaturated long-chain aliphatic carboxylic acid can be seen. This is an entirely new peak and different from the other long chain carboxylic acids. The reason for this will be discussed in detail in the following XRD and TGA section. Nevertheless, in all the FTIR spectra, including HT–OO, one can observe a peak at ≈ 1365 cm^{-1} due to carbonate stretching. This indicates that even after modification of HT with the organic surfactants, complete removal of carbonate anion from the gallery space was not possible. This is because of the high charge density of the HT layer and the rapid uptake of CO_2 from the atmosphere by the water molecules and very fast re-substitution reactions.

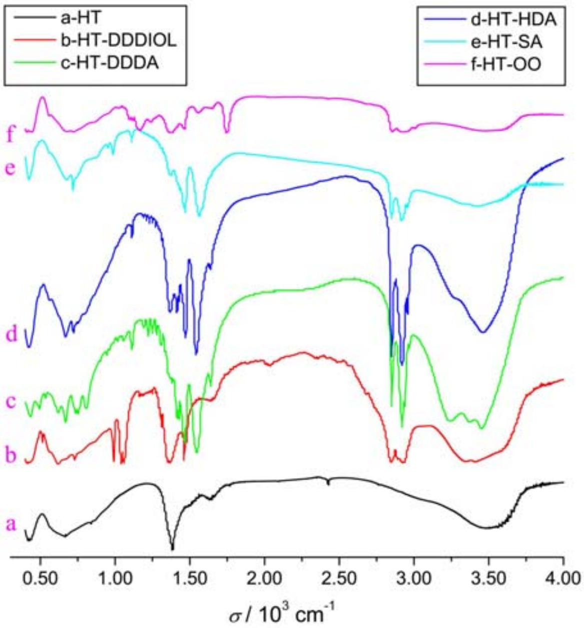

Fig. 1. FTIR spectrum of a) HT, b) HT–DDDIOL, c) HT–DDDA, d) HT–HDA, e) HT–SA and f) HT–OO.

The XRD profiles of HT before and after modification are shown in Fig. 2 and the data given in Table I. The crystalline peaks of HT are represented in Fig. 2 (curve a), in which the d_{003}, d_{006}, d_{012}, d_{015}, d_{018}, d_{110} and d_{113} plane peaks are visible. The original HT showed a gallery height of 0.289 nm, corresponding to the length of the carbonate anion. After modification with DDDIOL (Fig. 2, curve b), the gallery height was increased to 1.176 nm. This can be confirmed by the appearance of a small peak at the 2θ value of 7.21°, with the corresponding basal spacing of 1.224 nm. DDDIOL approached the hydroxyl layer of HT at 21° (parallel approach), with the formation of a mono-layer structure. It is possible to form a bi-layer structure because DDDIOL has an OH group at both ends of its molecule. However, the XRD results showed no formation of a bi-layer structure (*i.e.*, no pillar-like structural arrangement). The intensity (normalized intensity) of the d_{006} plane peak was greatly enhanced due to the presence of DDDIOL. The other small peaks are due to crystalline peaks of DDDIOL. The important point noted here is the maintenance of the layered arrangement even after the modification with long chain aliphatic surfactant. The XRD pattern of HT–DDDA is shown in Fig. 2, curve c (normalized intensity), with a gallery height of 1.544 nm with a monolayer structure. The orientation angle was calculated as 39°. Two new peaks appeared at low 2θ values, *i.e.*, at 4.36 and 6.86°, which correspond to the d_{001} and d_{002} planes, respectively. Other small shoulders which appeared in the XRD pattern are due to DDDA. DDDA has a better intercalation capacity than DDDIOL. In the case of organic–inorganic hybrids, the length of a surfactant is an important factor. In the present system, both DDDIOL, and DDDA have very similar chain lengths but their intercalation capacity is different due to their different functionalities. DDDA form a mono-layer structure with HT (Scheme 1). Hence, the alignment of the surfactant in the gallery space is also of primary importance. However, sometimes the layered structure may be delaminated due to improper alignment of the surfactant molecules in the interlayer space of HT. Moreover, both are bi-functional in nature but their intercalation capacities and orientation capabilities are different. This is because of the nature of the functional groups, which tend to form ionic structures.

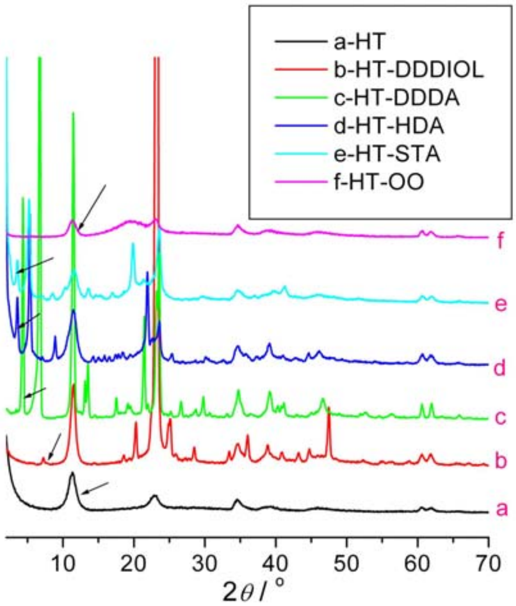

Fig. 2. XRD Pattern of a) HT, b) HT–DDDIOL, c) HT–DDDA, d) HT–HDA, e) HT–SA and f) HT–OO.

The XRD patterns of HT–HDA and HT–SA are shown in Fig. 2 (curves d and e), with gallery heights of 1.987 nm and 2.192 nm, respectively. These surfactants differ by only one $-CH_2-$ group. Their orientation angle increases from 44° for HDA to 54° for SA. However, their chemical activities coincide by forming a mono-layer structure because they have only one functional group at their chain ends. Comparing their intercalation capacities, SA exhibited a better intercalation capacity by increasing the basal spacing than HDA, DDDIOL or DDDA. The XRD results indicated that with increasing chain length of the surfactant, the basal spacing and orientation angle are also increased. The highest basal spacing exhibited by the HT–SA system indicated that SA had the best intercalation capacity of the four above-mentioned surfactants.

TABLE I. XRD analysis of HT before and after modification with various surfactants

System	2θ / °	Basal spacing nm	Orientation angle ϕ / °	Layer structure	Gallery height nm
HT	11.49	0.769	–	–	0.289
HT–DDDIOL	7.21	1.224	21	Monolayer	1.176
HT–DDDA	4.36	2.024	39	Monolayer	1.544
HT–HDA	3.57	2.467	44	Monolayer	1.987
HT–SA	3.30	2.672	54	Monolayer	2.192
HT–OO(OA)	11.49	0.769	–	–	0.289

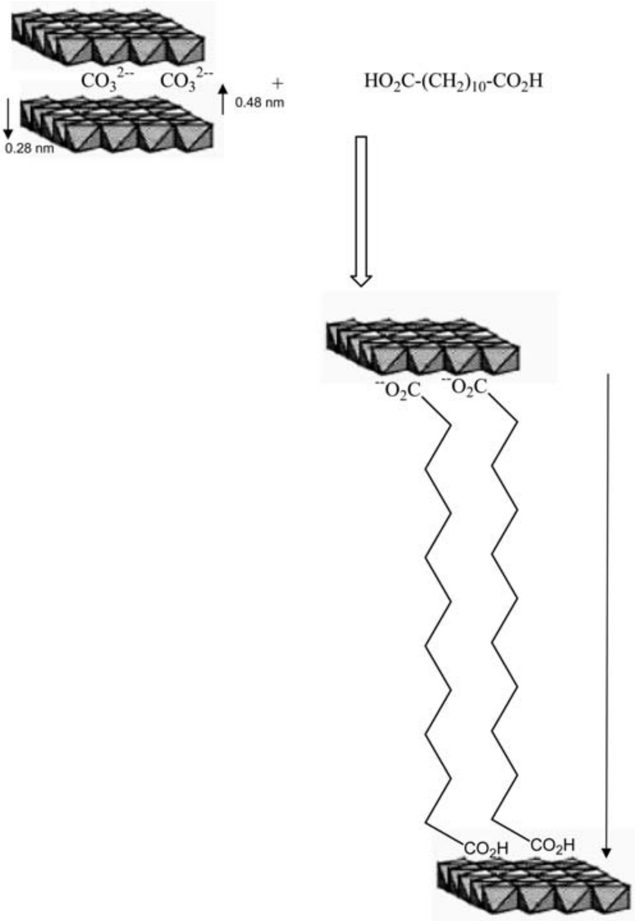

Scheme 1.

In the case of the HT–OO system (Fig. 2, curve f), the gallery height was not increased even after the ion-exchange process with OO. This indicates that OO was not intercalated into the HT structure. On the contrary, the FTIR spectrum showed a possible interaction between HT and OO. This controversy can be explained as follows. The FTIR results of the HT–OO system inferred the presence of carbonyl stretching but the XRD indicated a zero increase in the gallery height. As mentioned in the experimental part, OO contains different compounds with different chain lengths and different numbers of double bonds. The ion-exchange process was carried out at 70 °C under a nitrogen atmosphere with vigorous stirring. Under these experimental conditions, polymerization, oligomerization or at least dimerization could be thermally initiated as a result of which the size and chain length of the surfactants were increased and hence unable to intercalate into the HT gallery space. In OO, polymerization occurred in two different ways, *i.e.*, homo and copolymerization, because OO consists of 85 % OA (containing one double bond), 9 % linoleic acid (containing two double bonds) and 1.5 % linolenic acid. OA leads to homopolymerization because of its higher content in OO. Simultaneously, it is possible to form copolymers with other double bond-containing compounds. In this case, intercalation and polymerization are competitive reactions. The XRD results confirmed that polymerization was the dominant reaction through the zero increase in the basal spacing of HT. Polymer, either homo or copolymer, formed in the reaction medium may restrict the interaction between HT and the single linear double bond containing surfactants by increasing the viscosity of the reaction medium. Formation of polymer or oligomer during the ion-exchange process could be visually seen by the gel-like appearance of the hybrid. Secondly, the FTIR spectrum did not show a peak due to C=C around 1680 cm^{-1}. Hence, the FTIR and XRD results combined led to the proposal of interaction *via* the hydrogen bonding mechanism, *i.e.*, OO interacts with HT through the only possible way of hydrogen bonding. There is no other chemical force between them.

The XRD results of the hybrids indicated on comparing all that SA acts as a better intercalating agent than the other surfactants, even though it is a mono-functional compound, as the basal spacing of HT increased without layer degradation. All intercalants, except OO, interacted with HT through ionic bonding. OO prefers hydrogen bonding because polymerization or oligomerization led to a bulky size and very long chain length. Recently, the hydrogen bonding mechanism was proposed for the HT–hydroxyethanesulfonic acid hybrid system.[10]

The thermal stabilities of HT and its hybrids are presented and compared in Fig. 3 and Table II. Nominally, HT showed a four-step degradation mechanism (Fig. 3, curve a). The first and second steps corresponded to the removal of physisorbed and interlayer water molecules, respectively. The major and important step is the removal of water molecules through the dehydroxylation process. The last minor step was the degradation of carbonate inter-layer anions. Up to 400 °C, HT showed a mass loss of 29.63 % (Table II). The residual mass at 700 °C was 56.95 %. In the case of the HT–DDDIOL hybrid system (Fig. 3, curve b), a two-step degradation process was evidenced. The first major degradation step corresponds to the degradation of DDDIOL from the HT, followed by a dehydroxylation process. The second minor step was the dehydroxylation process alone. For pure HT, the dehydroxylation occurred at around 350 °C. However, in the present system (HT–DDDIOL), dehydroxylation occurred at ≈ 250 °C. This is due to the poor intercalation capacity of DDDIOL. Once the DDDIOL had been removed, dehydroxylation immediately occurred. At 400 °C, it showed a 22.52 % mass loss. The residual mass at 700 °C was 19.45 %, due to the formation of mixed metal oxides.

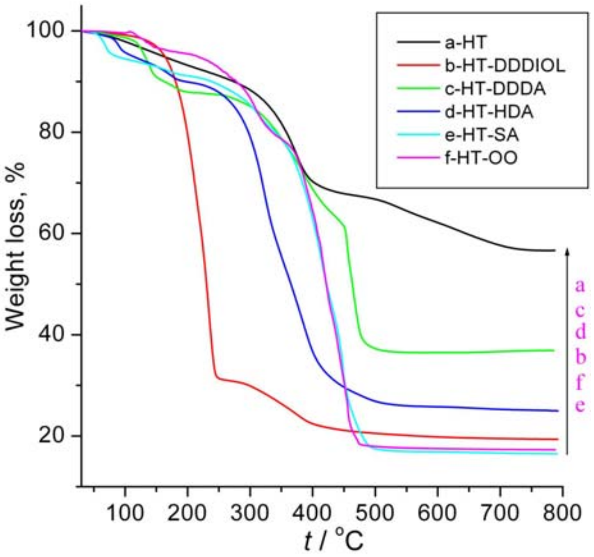

Fig. 3. TGA of a) HT, b) HT–DDDIOL, c) HT–DDDA, d) HT–HDA, e) HT–SA and f) HT–OO.

TABLE II. TG Analysis of HT before and after modification with various surfactants

System	Weight loss at 200 °C, %	Weight loss at 400 °C, %	Weight loss at 500 °C, %	Weight loss at 600 °C, %	Residual mass %
HT	93.01	70.37	66.80	61.97	56.95
HT–DDDIOL	80.42	22.52	20.62	19.92	19.45
HT–DDDA	87.67	69.04	37.21	36.53	36.53
HT–HDA	89.99	36.76	26.78	25.77	25.34
HT–SA	91.08	63.46	17.44	16.76	16.57
HT–OO(OA)	95.34	64.80	17.78	17.40	17.08

In the case of HT–DDDA (Fig. 3, curve c), the first and second steps were as usual the removal of physisorbed and interlayer water molecules. Third step at 385 °C was due to the degradation of DDDA. The fourth major mass loss was due to the dehydroxylation process (at 457 °C). At 400 °C, it showed only 30.96 % mass loss (Table II). Above 700 °C, the residual mass was 36.53 %. Comparing the thermal stability of HT, HT–DDDIOL and HT–DDDA, the last one exhibited the highest thermal stability. This may be due to the strong intercalation capacity of the bi-functional DDDA. The increase in thermal stability confirms the existence of strong ionic forces between HT and DDDA. The TG curve of HT–HDA is shown at Fig. 3 (curve d). In this hybrid system, dehydroxylation occurred at temperatures between those of pure HT and HT–DDDIOL. The residual mass above 700 °C was 25.34 %. The thermal degradation stability of HT–SA is shown in Fig. 3 (curve e). In this case, dehydroxylation occurred around 425 °C, which is higher than that of pristine HT. At 400 °C, it exhibited a mass loss of 36.54 %. The residue above 700 °C was 16.57 %. Comparing the thermal stability of HT–HDA and HT–SA, it can be seen that the latter hybrid showed a higher thermal stability, although the surfactants have a very similar chain length with structural identity. It showed the second highest thermal stability after the HT–DDDA hybrid system.

The TG curve of HT–OO is shown in Fig. 3 (curve f). At 400 °C, a 35.20 % mass loss was observed while the residue above 700 °C was 17.08 % (Table II). The dehydroxylation of HT–OO occurred at 416 °C. This system showed higher thermal stability for the dehydroxylation process than the pristine HT, HT–DDDIOL and HT–HDA systems. As mentioned earlier, only hydrogen bonding exists between HT and OO, but nevertheless this system showed a slightly higher thermal stability. This may be due to the following reason, *i.e.*, at 350 °C, it showed an initial dehydroxylation process but immediately the free carboxyl groups of the polymerized or oligomerized OO interacted with the HT through ionic linkage. Hence, the dehydroxylation temperature was increased. The dissociation of HT–OO linkages and dehydroxylation could be simultaneous processes.

In an overall discussion of the TGA results it should be mentioned that separate decomposition step due to carbonate decomposition in the modified HT was not evidenced, although the FTIR spectra confirmed the presence of carbonate anions in the hybrids. From these two results, it can be concluded that carbonate ions may be present only in trace amounts, which may not be sufficient to appear on the TG curves. Secondly, the long chain diol is not suitable for hybrid preparation because of its lower thermal stability. Finally, the mono-functional acid surfactants with similar structures showed different thermal stabilities.

CONCLUSIONS

Organic–inorganic hybrids were prepared *via* the ion-exchange method with various long chain organic aliphatic surfactants. FTIR spectroscopy supported the presence of the long chain anionic aliphatic surfactants in the LDH structure. The XRD results showed that the mono-carboxylic (SA) surfactant exhibited a higher basal spacing than the dicarboxylic acid surfactants and the diol surfactant without degradation of the layer structure. OO interacted with HT through hydrogen bonding whereas the diol and other surfactants interacted with LDH through ionic linkage. XRD analysis also confirmed that no pillar-like structure was formed during the modification. TGA results revealed that the di-carboxylic acid containing surfactant DDDA showed a higher thermal stability than the alcohol and mono-carboxylic acid containing surfactants.

Acknowledgements. I would like to express my sincere thanks to B.K.21 office and Hanyang University Office for their financial support during my postdoctoral research period in South Korea.

ИЗВОД

МОДИФИКАЦИЈА НАНОДИМЕНЗИОНИХ ДВОСТРУКИХ СЛОЈЕВИТИХ ХИДРОКСИДА ДУГОЛАНЧАНИМ ПОВРШИНСКИ АКТИВНИМ СУПСТАНЦАМА

RAMASAMY ANBARASAN[1], WANDUC LEE[2] и SEUNG SOON IM[2]

[1]*Department of Polymer Technology, Advanced Nanotechnology Research Laboratory, Kamaraj College of Engineering and Technology, Virudhunagar – 626 001, Tamil Nadu, India and* [2]*Department of Fiber and Polymer Engineering, Hanyang University, Seoul-133 791, South Korea*

Међуслојни анјон у структури двоструког слојевитог хидроксида (LDH) типа хидро-талка (HT) је јонском изменом замењен различитим дуголанчаним алифатичним површински активним супстанцама. После јонске измене базално међуслојно растојање (LDH) је расло у зависности од интеркалационе способности, оријентације и функционалних група коришћених површински активних супстанци. Резултати XRD потврђују да се највеће повећање базалног растојања постиже интеркалацијом стеаринске киселине. Резултати FTIR потврђују интеракцију површински активних супстанци са LDH. TGA анализа је потврдила да се термална стабилност HT повећава интеркалацијом додекан-дикиселине.

(Примљено 17. јула 2007)

REFERENCES

1. S. K. Yun, T. J. Pinnavaia, *Chem. Mater.* **7** (1995) 348
2. H. B.Friedrich, M. Govender, O. Onani, *Chem. Commun.* **23** (2003) 2922
3. C. S. Liao, W. B. Ye, *J. Polym. Res.* **10** (2003) 241
4. Y. You, H. Zhao, F. Vance, *Colloids Surf. A.* **205** (2002) 161
5. T. Itoh, M. Ohta, T. Schichi, T. Yui, K. Tagaki, *Langmuir* **19** (2003) 9120
6. G. A. Bubniak, W. H. Schreiner, N. Mattoso, F. Wypych, *Langmuir* **18** (2002) 5967
7. M. Arco, D. Carriazo, C. Martin, V. Rives, *Inorg. Chem.* **43** (2004) 375
8. C. Vaysse, C. Delmas, E. Duguet, *Macromolecules* **37** (2004) 45
9. P. Steven, W. Jones, *New J. Chem.* **2** (1998) 105
10. S. Sasaki, S. Aisawa, E. Narita, *Chem. Lett.* **790** (2004) 204
11. R. Anbarasan, S. S. Im, *Indian J. Chem. Technol.* **12** (2005) 259
12. R. Anbarasan, S. S.Im, *Bull. Mater. Sci.* **28** (2005) 145
13. P. Beaudot, M. E. Roy, J. P. Besse, *Chem. Mater.* **16** (2004) 935
14. Q. Yuan, M. Wei, Z. Wang, G. Wang, Z. Duan, *Clay Clay Miner.* **52** (2004) 40
15. S. Aisawa, H. Hirahara, Y. Umetsu, E. Narita, *Chem. Lett.* **33** (2004) 306

16. J. H. Choy, S. Y. Kwak, Y. J. Jeong, J. Portier, *J. Am. Chem. Soc.* **121** (1999) 1399
17. A. Fudala, I. Palinko, I. Kiricsi, *Inorg. Chem.* **38** (1999) 4653
18. H. J. Choy, S. Y. Kwak, Y. J. Jeong, J. S. Park, *Angew. Chem. Int. Ed.* **39** (2000) 4041
19. S. Y. Kwak, Y. J. Jeong, J. S. Park, H. J. Choy, *Solid State Ionics* **151** (2002) 229
20. H. J. Choy, S. Y. Kwak, J. S. Park, Y. J. Jeong, *J. Mater. Chem.* **11** (2001) 1671
21. H. U. Changwen, L. I. Dangeng, G. Yihang, E. Wang, *Chin. Sci. Bull.* **46** (2001) 1061
22. A. H. He, S. Yin, T. Sato, *Solid State Chem. V* **77** (2003) 51
23. V. P. Isupov, V. G. Kostrovsky, V. A. Poluboyarov, *Solid State Ionics* **141** (2001) 231.

Journal of the Serbian Chemical Society
JSCS@tmf.bg.ac.yu • www.shd.org.yu/JSCS

J. Serb. Chem. Soc. *73* (3) 333–339 (2008) UDC 546.719+66–914:541.183.1:546.33'131:66.049.2
JSCS–3715 *Original scientific paper*

Concentration of rhenium from dilute sodium chloride solutions

DRAGOLJUB M. LUKIĆ[1], JURIJ L. VUČINA[1*#] and SLOBODAN K. MILONJIĆ[2#]

[1]Laboratory for Radioisotopes and [2]Chemical Dynamics Laboratory, Vinča Institute of Nuclear Sciences, 11001 Belgrade, P. O. Box 522, Serbia

(Received 24 May 2007)

Abstract: The conditions for the desorption of rhenium from the anion exchange resin Dowex 1-x8 by HNO_3, HCl, H_2SO_4 and NaOH were determined. The solution (5.0×10^{-3} mol dm^{-3} Re in 0.15 mol dm^{-3} NaCl) was passed through a column containing 0.10 g of the resin. The total sorbed amount of rhenium was 0.20 g/g of the resin. It was then eluted by the corresponding eluent in the concentration range up to about 3.0 mol dm^{-3}. The highest elution efficiency and the most favourable elution profile were found with 3.0 mol dm^{-3} HNO_3. Over 77 % of the sorbed rhenium was found in the first 5 ml of the eluate. Practically all the rhenium was recovered with 20 ml of the acid. Under the given experimental conditions, HCl and H_2SO_4 were less favourable while NaOH was not applicable, due to very low efficiency of rhenium elution.

Keywords: ion exchange; concentration; rhenium; elution efficiency; elution profile.

INTRODUCTION

Low concentrations of elements often restrict their intended use. The recovery of a given element from very dilute solutions is often not simple. For routine practice, the procedure should preferably be simple, rapid and effective. There are reports in the literature describing several approaches to solve this problem. One of the most promising is based on ion exchange. The dilute solution is passed through a column containing either an inorganic or organic ion exchanger onto which the desired element is firmly sorbed.[1,2] Then, it is recovered in a much higher concentration by elution from the resin with an as small as possible volume of an appropriate eluent. The efficacy is determined by the elution efficiency, *i.e.*, by the ratio of the desorbed element in the first fractions of the eluate and by the elution profile representing the total volume of the eluent required to desorb practically the whole quantity of the element from the resin.

Such concentration procedures find wide application. They are also used in radiochemistry to achieve, for example, a high radioactive concentration of a given

---

* Corresponding author. E-mail: vucina@vin.bg.ac.yu

\# Serbian Chemical Society member.

doi: 10.2298/JSC0803333L

radioisotope necessary for the preparation and the application of radiopharmaceuticals.[3,4]

The procedure under examination is based on the anion exchange resin Dowex 1-x8, onto which rhenium, in the form of perrhenate anions, was sorbed. The paper presents the results of the determination of the conditions of its effective desorption using mineral acids, *i.e.*, HNO_3, HCl and H_2SO_4, and sodium hydroxide. The determinations of rhenium elution profiles and of the total elution volume in dependence on the concentration of the eluents, are given.

The results of these experiments find application in the development and improvement of procedures for the production of concentrated solutions of the radioisotope ^{188}Re, the physical properties of which are suitable for employment in therapeutic nuclear medicine.[3,5,6]

EXPERIMENTAL

Reagents

Potassium perrhenate ($KReO_4$, p.a., Aldrich) and the resin Dowex 1-x8, 100–200 mesh (Aldrich) were commercially purchased.

Chemical analyses

The content of rhenium in the solutions was determined by direct current argon arc plasma atomic emission spectroscopy (DCP–AES) with an aerosol supply. The procedure was described in earlier papers.[6-8]

The experiments, repeated twice, were performed at room temperature.

Experiments

The experiments were performed in a glass column (5.5 mm I.D., 40 mm length) containing 0.1 g of Dowex 1-x8. The bed height, l, was 0.69 cm. A freshly prepared Re solution containing 5.0×10^{-3} mol dm^{-3} in 0.15 mol dm^{-3} NaCl was passed through the column. The total amount of sorbed rhenium was 0.20 g/g of resin. The flow rate was 3.0 ml min^{-1}.

The elution of rhenium was performed using various concentrations of HNO_3 (0.16, 0.9, 1.6, 3.0, 6.0 and 7.2 mol dm^{-3}), HCl (0.16, 1.6 and 3.0 mol dm^{-3}), H_2SO_4 (0.08, 0.16, 0.8, 1.5 and 3.0 mol dm^{-3}) and NaOH (0.16, 1.6 and 3.0 mol dm^{-3}).

The volume of the effluent solution was 5.0 ml. The flow rate (3.0 ml min^{-1}) was kept constant using a Masterflex C/L pump (Cole Palmer Instrument Company).

Total experimental error is up to 1 %.

RESULTS AND DISCUSSION

The main residence or contact time (τ_c) between the solution and the resin can be calculated by:[9]

$$\tau_c = \varepsilon\, l/u \qquad (1)$$

where: ε is the extra particle bed porosity or void fraction of the sorbent bed (for the resin, the calculated value of ε was ≈ 0.33) and u is the linear or interstitial velocity (m s^{-1}).

For a value of u of 12.5 cm min^{-1} (*i.e.*, a flow rate of 3.0 ml min^{-1}), the calculated contact time τ_c is 1.1 s.

It can be seen that the contact time between the solution and the resin is very short in comparison with the value between the solution and alumina, which was found to be about ten seconds.[6]

The calculated theoretical sorption capacities of the resin Dowex 1-x8 (100–200 mesh) for the corresponding anions are given in Table I. In practice, the values are about 50 % lower than those calculated.

TABLE I. The theoretical sorption capacities of the resin Dowex 1-x8 (100–200 mesh) for the corresponding anions

Anion	Theoretical capacity, g/g of the resin
ReO_4^-	0.85
NO_3^-	0.21
Cl^-	0.12
SO_4^{2-}	0.16
OH^-	0.06

Experimentally, the dependence of the elution efficiency of rhenium from the resin on the nature and the concentration of the influent solution were examined. The elution profiles of Re, *i.e.*, the ratio of the total sorbed rhenium found in the first 5.0 ml of the eluate and in the total volume of the eluate (20 ml) was determined for the different concentrations of the chosen eluents. The results obtained with nitric acid in the concentration range of 0.16–7.2 mol dm^{-3} are given in Table II.

TABLE II. The dependence of the elution efficiency of rhenium from Dowex 1-x8 on the concentration of the eluent HNO_3

Sample No.	V / ml	Eluted rhenium, %					
		c_M (HNO_3) / mol dm^{-3}					
		0.16	0.9	1.6	3.0	6.0	7.2
1	5.0	5.6	55.4	65.7	77.2	63.2	66.4
2	5.0	12.2	24.6	20.9	15.9	20.7	21.5
3	5.0	12.6	10.4	9.2	5.7	10.1	4.9
4	5.0	11.8	5.3	4.5	2.1	5.2	2.3
Total	20	42.2	95.7	100.3	100.9	99.2	95.1

From the results presented in Table II, it can be seen that the best results are obtained when the rhenium was eluted by 3.0 mol dm^{-3} HNO_3. In this case, the highest amount of rhenium was desorbed and found in both the first 5.0 ml and in the total volume of the eluate (20 ml).

The effect of the concentration of HNO_3 on the elution efficiency of rhenium is presented in Fig. 1, from which it can be seen that the efficiency first rises, reaches the highest levels at about 3.0 mol dm^{-3} HNO_3 and then decreases with the further increase in the concentration of the acid.

The results obtained with HCl, H_2SO_4 and NaOH are given in Tables III–V.

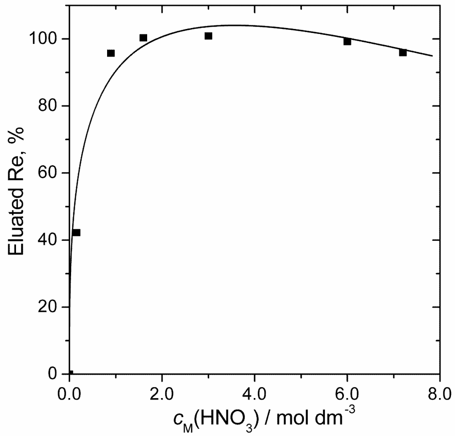

Fig. 1. The dependence of the efficiency of rhenium elution on the concentration of the eluent HNO_3.

TABLE III. The dependence of the elution efficiency of rhenium from Dowex 1-x8 on the concentration of the eluent HCl

Sample No.	V / ml	Eluted rhenium, %		
		c_M (HCl) / mol dm^{-3}		
		0.16	1.6	3.0
1	5	0.5	12.6	34.0
2	5	1.6	12.2	19.3
3	5	3.0	8.7	10.7
4	5	3.9	6.4	7.1
Total	20	9.0	39.9	71.1

According to the data given in Tables II–V, it can be concluded that both the elution efficiency and the profile depend on the nature and the concentration of the eluent. The most favourable results were obtained with 3.0 mol dm^{-3} HNO_3. In this case, the highest amount of rhenium was found in the first 5.0 ml of the eluate. The total sorbed rhenium was recovered with 20 ml of the eluent. The shape of the dependence of the elution efficiency on the concentration of nitric acid is shown in Fig. 1.

TABLE IV. The dependence of the elution efficiency of rhenium from Dowex 1-x8 on the concentration of the eluent H_2SO_4

Sample No.	V / ml	Eluted rhenium, %					
		c_M (H_2SO_4) / mol dm^{-3}					
		0.08	0.16	0.80	1.5	1.6	3.0
1	5	0.5	1.7	12.2	21.4	22.6	19.4
2	5	1.5	3.0	14.4	14.7	15.2	13.3
3	5	2.4	3.8	11.5	9.6	10.3	9.4
4	5	3.0	4.1	9.2	7.7	8.0	6.9
Total	20	7.4	12.6	44.3	53.4	56.1	49.0

For the other employed eluents, except for HCl, the pattern of the dependence of the efficiency of rhenium elution on concentration was the same as that shown in Fig. 1. The concentration of 3.0 mol dm^{-3} HCl was found to be too low to reach the maximal elution efficiency. However, higher concentrations of the acid would be very unsuitable for further handling.

TABLE V. The dependence of the elution efficiency of rhenium from Dowex 1-x8 on the concentration of the eluent NaOH

Sample No.	V / ml	Eluted rhenium, %		
		c_M (NaOH) / mol dm^{-3}		
		0.16	1.6	3.0
1	5	0.24	0.64	0.25
2	5	0.11	0.53	0.11
3	5	0.09	0.55	0.11
4	5	0.09	0.59	0.14
Total	20	0.53	2.31	0.61

In the case of NaOH, the elution efficiency of rhenium was very low. Hence, this eluent can be neglected in the further considerations.

The elution efficiencies of rhenium when 20 ml of 3.0 mol dm^{-3} HNO_3, HCl and H_2SO_4, respectively, were passed through the column at a flow rate of 3.0 ml min^{-1} are presented in Table VI.

TABLE VI. Elution efficiency of rhenium when 20 ml of 3.0 mol dm^{-3} HNO_3, HCl and H_2SO_4 were employed as the eluents

Eluent	c_M / mol dm^{-3}	Eluted Re, %
HNO_3	3.0	100.9
HCl	3.0	71.1
H_2SO_4	3.0	49.0
H_2SO_4	1.5	53.4

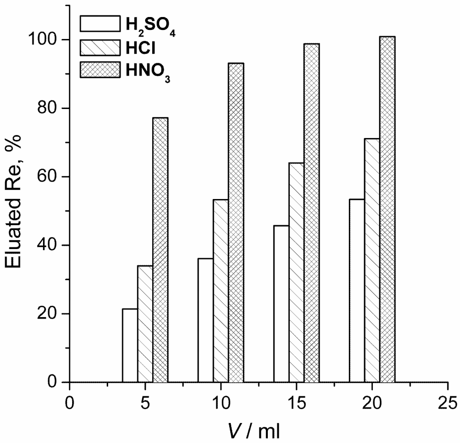

Fig. 2. Elution efficiency of rhenium in dependence on the volume of HNO_3, HCl and H_2SO_4.

By comparing the results obtained with acids of the same concentration, it can be seen that the highest elution efficiency was obtained when nitric acid was the eluent. The anions are bound on the resin in the following order: $NO_3^- > Cl^- > SO_4^{2-}$.

The same conclusions were obtained when the other concentrations of the acids, given in Tables II–V, are compared. In all cases, the highest elution yield of rhenium was obtained with nitric acid.

The dependences of the elution efficiency of rhenium on the elution volume of the acid eluents are presented in Fig. 2, from which it can be seen that the most favourable elution profile was obtained with nitric acid. Much higher volumes of the other eluents were required for the recovery of rhenium.

CONCLUSIONS

The results presented in this paper showed that perrhenate anions sorbed on Dowex 1-x8 can be desorbed by the mineral acids HNO_3, HCl and H_2SO_4. The experiments were performed with concentrations of the eluent up to 3.0 mol dm^{-3}. The total elution volume of the corresponding eluate was 20 ml. In the examined range of concentrations, the highest efficiency of rhenium elution and the most favourable elution profile were obtained when using 3.0 mol dm^{-3} HNO_3. In this case, practically all the sorbed rhenium was eluted in 20 ml of the acid. The elution yields were lower if HCl or H_2SO_4 of the same concentrations were used. In addition, the elution profiles were less favourable. The results showed that NaOH, under the given experimental conditions, was not useful for the intended purpose due to very low efficiency of rhenium elution.

Thus, the applicability of the proposed concept of concentration based on the sorption of rhenium from dilute solutions on an anion exchanger and its subsequent elution by acid was confirmed. However, further investigations are required before its introduction into routine practice.

Acknowledgements. This work was financially supported by the Ministry of Science of the Republic of Serbia, under Project No.142004B.

ИЗВОД

КОНЦЕНТРИСАЊЕ РЕНИЈУМА ИЗ РАЗБЛАЖЕНИХ РАСТВОРА НАТРИЈУМ-ХЛОРИДА

ДРАГОЉУБ М. ЛУКИЋ[1], ЈУРИЈ Л. ВУЧИНА[1] и СЛОБОДАН К. МИЛОЊИЋ[2]

[1]*Лабораторија за радиоизотопе и* [2]*Лабораторија за хемијску динамику, Институт за нуклеарне науке «Винча», п. пр. 522, 11001 Београд*

Одређивани су услови десорпције ренијума са анјонске измењивачке смоле Dowex 1-x8 са HNO_3, HCl, H_2SO_4 и NaOH. Раствор ренијума (5,0×10^{-3} mol dm^{-3} Re у 0,15 mol dm^{-3} NaCl) је пропуштан кроз колону са 0,10 g смоле. Укупна сорбована количина ренијума била је 0,20 g по граму смоле. Ренијум је затим елуиран одговарајућим елуентом у опсегу концентрација до 3,0 mol dm^{-3}. Највећа ефикасност елуирања и најповољнији профил елуирања добијени су са HNO_3 концентрације 3,0 mol dm^{-3}. У првих 5 ml елуата налази се преко 77 % сорбованог ренијума. Практично сва количина се елуира са 20 ml киселине. Под датим експерименталним условима, примена HCl и H_2SO_4 је мање повољна док NaOH није примењив због врло ниске ефикасности елуирања.

(Примљено 24. маја 2007)

REFERENCES

1. A. Mushtag, *J. Radioanal. Nucl. Chem*. **262** (2004) 797
2. R. M. Lambrecht, K. Tomiyoshi, T. Sekine, *Radiochim. Acta* **77** (1997) 103
3. F. F. Knapp, Jr., A. L. Beets, S. Guhlke, P. O. Zamora, H. Bender, H. Palmedo, H.-J. Biersack, *Anticancer Res.* **17** (1997) 1783
4. A. Mushtag, *Appl. Radiat. Isotopes* **58** (2003) 309
5. J. L. Vučina, D. M. Lukić, M. M. Stoiljković, *J. Serb. Chem. Soc*. **69** (2004) 683
6. J. L. Vučina, D. M. Lukić, S. K. Milonjić, M. M. Stoiljković, *J. Radioanal. Nucl. Chem.* **267** (2006) 67
7. F. M. Marinković, T. J. Vickers, *Appl. Spectroscopy* **25** (1971) 319
8. D. M. Lukić, J. L. Vučina, S. K. Milonjić, *J. Serb. Chem. Soc*. **72** (2007) 555
9. S. K. Milonjić, Dj. M. Čokeša, R. V. Stevanović, *J. Radioanal. Nucl. Chem*. **158** (1992) 79.

Journal of the Serbian Chemical Society

JSCS@tmf.bg.ac.yu • www.shd.org.yu/JSCS

J. Serb. Chem. Soc. *73* (3) 341–350 (2008)

UDC 546.482+66.061:541.12.012–
–032.2:549.451.1:547.441–036.7

JSCS–3716

Original scientific paper

Cd(II) extraction in PEG (1550)–$(NH_4)_2SO_4$ aqueous two-phase systems using halide extractants

LAURA BULGARIU[1]* and DUMITRU BULGARIU[2]

[1]Department of Environmental Engineering and Management, Faculty of Chemical Engineering, Technical University "Gh. Asachi", D. Mangeron 71A, 700050 Iaşi and [2]Department of Geology – Geochemistry, Faculty of Geography and Geology, "Al. I. Cuza" University, Carol I 20A, 700050 Iaşi, Romania

(Received 30 May, revised 30 August 2007)

Abstract: The extraction of Cd(II) was studied in an aqueous PEG–$(NH_4)_2SO_4$ two-phase system, formed from a water-soluble polymer (poly(ethylene glycol), PEG) and an inorganic salt ($(NH_4)_2SO_4$), in the presence of halide ions. In the absence of a suitable extracting agent, Cd(II) remains predominantly in the salt-rich phase of the extraction system. By addition of halide ions as extractants, Cd(II) is extracted into the PEG-rich phase due to the formation of cadmium halide species. The efficiency of the extractants increased in the order: $Cl^- < Br^- < I^-$. From the distribution coefficients determined as a function of the concentration of the halide ions, the compositions of the extracted species were assumed and the "conditional" extractions constants calculated. The experimental results indicate that the extractability of Cd(II) in such extraction systems depends on the type of Cd(II) halide species (which is mainly determined by the acidity of salt stock solution) and of their stability.

Keywords: aqueous two-phase system; Cd(II) extraction; halide ions; poly(ethylene glycol); $(NH_4)_2SO_4$.

INTRODUCTION

Traditionally, extraction and recovery of metal ions from aqueous solutions were performed using solvent extraction, where the formation of two immiscible phases involved the mixing of an organic solvent with an aqueous solution.[1,2] However, most of the organic solvents used in the extraction methods are toxic, flammable, volatile and cause many problems to the environment. For this reason, the employment of aqueous two-phase systems for the same purpose has commenced.

The aqueous two-phase systems, formed from a water-soluble organic polymer and a certain inorganic salt, are mild and efficient extraction of metal ions

---

* Corresponding author. E-mail: lbulg@ch.tuiasi.ro

doi: 10.2298/JSC0803341B

techniques, which do not use any organic solvents, being thus friendly to the environment.

From a large variety of different water-soluble polymers which may be utilized for the preparation aqueous two-phase systems, poly(ethylene glycol) (PEG) has received the most attention.[3,4] PEG in combination with an inorganic salt, such as $(NH_4)_2SO_4$ determine the separation of two immiscible phases: a top phase – rich in PEG, which plays the role of the organic phase in traditional extraction systems, and a bottom phase – with a high content of inorganic salt.

The utilization of aqueous PEG-based two-phase systems for the extraction of metal ions has several advantages, *i.e.*, they are considered virtually non-toxic and non-flammable and all the components are commercially available. In addition, PEG is biodegradable, which makes the risk of environmental contamination relatively low.[5,6]

Metal ion extraction in such aqueous two-phase systems depends both on the characteristics of the formed aqueous two-phase system (determined by the nature and concentration of the inorganic salt and the molecular mass and concentration of PEG) and on the stability and degree of hydration of the metallic species formed in the extraction system.[7–9] If the optimum characteristics of the aqueous two-phase system (system stability, phase separation time, clear interface) can be obtained by a suitable selection of the phase forming components, the second condition requires the utilization of some extracting agent, which will provide for the selectivity of the extraction process.

Some metal ions (Bi(III), Hg(II), Pb(II), Zn(II), Cu(II), *etc.*) can be extracted into the PEG-rich phase using halide or pseudo-halide ions, by an ion-pair extraction mechanism, similar to the extraction of metal halide complexes with ethers or ketones.[10–16] It has also been shown that in presence of halide ions, Cd(II) partitioning into the PEG-rich phase of aqueous PEG-based two-phase systems occurs and the extracted species were assumed to be CdX_4^{2-}, in all cases.[14,17] However, our experimental results have shown that the number of halide ions associated with Cd(II) depends on the acidity of the salt stock solution and on the stability of the extracted cadmium halide species.

In this work, the extraction of Cd(II) in an aqueous PEG (1550)–$(NH_4)_2SO_4$ two-phase system was studied, as a function of the type and concentration of the halide ions extractants. The effect of the acidity of the salt stock solution on the extraction efficiency was also considered. The results are discussed, based on the elementary equilibria involved in extraction process.

EXPERIMENTAL

The reagents $(NH_4)_2SO_4$, NaI, NaBr, NaCl (from Aldrich) and PEG (1550) (from Serva Feinbiochema GmbH & Co) were of analytical grade and used without purification. The stock solution of 40 % (w/w) PEG (1550) was obtained by dissolving solid PEG in a certain mass of water. The 40 % (w/w) $(NH_4)_2SO_4$ salt stock solution was prepared similarly using water (salt stock solution with pH 4.65) or 10^{-3} M H_2SO_4 (salt stock solution with pH 3.03). The solution of ≈ 1.0 mg Cd(II) ml^{-1} was prepared by dissolving cadmium nitrate (from Fluka) in distilled water, followed by standardization of the solution.[18] The solutions of the extractants, containing 1 M NaX ($X^- = Cl^-$, Br^- or I^-) was obtained by dilution of a know mass of sodium halide salt to volume with the required salt stock solution.

The Cd(II) extraction experiments were performed in the following manner: for each determination, an aqueous two-phase system was prepared by mixing equal volumes of PEG (1550) stock solution and $(NH_4)_2SO_4$ salt stock solutions with the selected pH in a glass centrifuge tube. The pH values of the $(NH_4)_2SO_4$ salt stock solutions were measured with a Radelkis pH/ion-meter OK-271 type, equipped with a combined glass electrode. The Cd(II) stock solution (0.50 ml) and 1 M NaX solution (0.10–0.70 ml) were added. The system was centrifuged for 10 min at 2000 rpm. Centrifugation ensures an energetic mixing of the components of the system, which lowers the time necessary for phase separation. Just before analysis, the phases were carefully separated and placed into separated tubes. Equal volumes (1.0 ml) from each phase were measured spectrophotometrically using *p*,*p*'-dinitro-sym-diphenylcarbazide (S 104 D Digital Spectrophotometer; λ = 630 nm, 1.0 cm glass cell).[19] The Cd(II) content in each phase was determined in duplicate using a prepared calibration graph. The distribution coefficients (D_{Cd}) were calculated as the ratio of the Cd(II) concentration in the PEG-rich phase to that in the salt-rich phase. The concentration of halide ions in the PEG-rich phase was determined by conductometric titration with $AgNO_3$, using a Radelkis OK-109 conductometer.

RESULTS AND DISCUSSION

In a previous studies, it was shown that $(NH_4)_2SO_4$ can be used as the phase forming salt because it exerts a strong salting-out effect on PEG and has a high solubility in water.[20,21] Thus, an efficient extraction system can be prepared in which the differences in the concentration of PEG and the concentration of the inorganic salt concentrations in the two formed phases are large.

In the absence of a suitable extracting agent, the experimental results showed that the cadmium ions remained almost exclusively in the salt-rich phase. The low values of the distribution coefficients (D_{Cd} = 0.281 in case of the salt stock solution with pH 3.03 and D_{Cd} = 0.182 in case of the salt stock solution with pH 4.65) indicate that extraction of Cd(II) does not involve direct chemical interactions between the metal ions and the PEG molecules from the PEG-rich phase of extraction system.

Under the conditions of the prepared aqueous two-phase systems (the SO_4^{2-} concentration in salt-rich phase was 3.45 M), calculations showed that predominant species in the system were $Cd(SO_4)_2^{2-}$ ions (89.2 %), $CdSO_4$ was only 10.7 % and free Cd^{2+} ions were practically non-existent (≈ 0.01 %). The $Cd(SO_4)_2^{2-}$ species formed from a metal ion with a highly negative Gibbs free energy of hydration ($\Delta G_{hydr.} = -1722$ kJ mol^{-1}) and an anion with a strong salting-out effect will preferably remain in the salt-rich phase of the extraction system.[22]

Under these conditions, the extraction of Cd(II) can be enhanced by changing the nature of the Cd(II) species using a suitable extracting agent, which should have a lower degree of hydration and form a more stable species with Cd(II) than is $Cd(SO_4)_2^{2-}$.

The halide ions (Cl^-, Br^- and I^-) were used as inorganic complexing extractants and the extraction of Cd(II) was investigated in dependence of the type of halide ion and the concentration of NaX in the extraction system, for both values of pH of the salt stock solution. Comparatively, the Cd(II) distribution coefficients are given in Figs. 1 and 2.

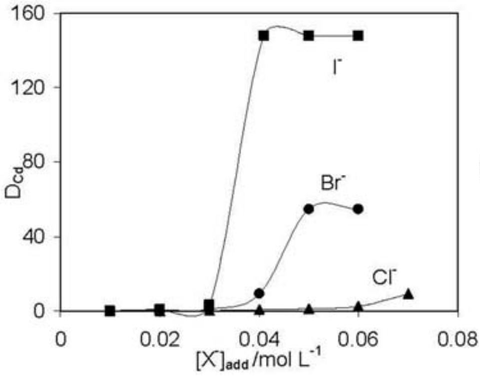

Fig. 1. The D_{Cd} *vs*. $[X^-]_{add}$ dependence for the salt stock solution of pH 3.03. (Cd_i = 57 μg ml^{-1}; t = 21 °C).

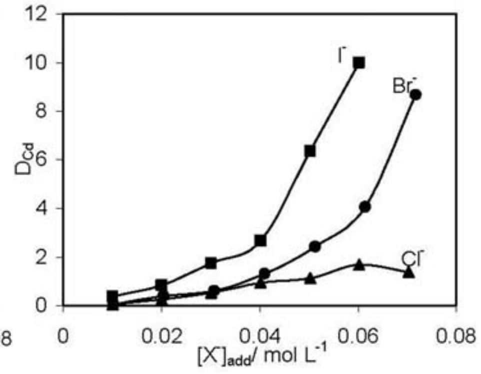

Fig. 2. D_{Cd} vs. $[X^-]_{add}$ dependence for the salt stock solution of pH 4.65. (Cd_i = 57 μg ml^{-1}; t = 21 °C).

An increase of Cd(II) extraction into the PEG-rich phase with increasing concentration of halide ions was observed for pH values. The Cd(II) distribution coefficients (D_{Cd}) followed the order: $Cl^- < Br^- < I^-$, which is in agreement with data from the literature.[14,17] It can also be observed that, although the $X^- = I^-$, Br^- and Cl^- systems all exhibit similar partitioning behaviour at low concentrations, the Cd(II) distribution coefficients increase earlier for I^- than for Br^- and those for Br^- increase earlier than for Cl^-. This order could be simply explained by the increasing stability of the cadmium halide species going from Cl^- to I^-; the more polarisable halide ions form stronger complexes with Cd(II).[23]

On the other hand, the presence of H_2SO_4 in the extraction system (salt stock solution with pH 3.03) enhanced the efficiency of Cd(II) extraction, and the maximum values of D_{Cd} were obtained at significant lower concentrations of halide ions than was the case of the systems prepared in the absence of H_2SO_4 (salt stock solution with pH 4.65). Increasing the acidity of the salt stock solution resulted in an increase of the hydrophobicity of the PEG-rich phase and, consequently, the extracted metal species should have a lower degree hydration and, hence, a larger number of halide ions in their molecules.[24]

The different extraction behaviour of Cd(II) in presence of halide ions for the two different pH values can be attributed to the formation of different cadmium halide species, depending on both the nature of the added halide ion extractant and the acidity of the salt stock solution.

Under these conditions, it can be assumed that the elementary equilibria, summarized in Table I, should be considered in the Cd(II) extraction process using halide ions extractants in the employed two-phase system.

TABLE I. The main elementary equilibriums involved in Cd(II) extraction in the aqueous PEG(1550)–$(NH_4)_2SO_4$–NaX two-phase system

Elementary equilibrium	Reaction of equilibrium	Constant of equilibrium
Formation of anionic sulphates	$Cd^{2+} + 2\,SO_4^{2-} \leftrightarrows Cd(SO_4)_2^{2-}$	$\beta_{Cd(SO_4)_2^{2-}} = \frac{[Cd(SO_4)_2^{2-}]}{[Cd^{2+}]\cdot[SO_4^{2-}]^2}$
Formation of halide species	$Cd^{2+} + nX^- \leftrightarrows CdX_n^{(n-2)-}$	$\beta_{CdX_n^{(n-2)-}} = \frac{[CdX_n^{(n-2)-}]}{[Cd^{2+}]\cdot[X^-]^n}$
Halide partitioning	$X^- \leftrightarrows (X^-)_{PEG}$	$D_{X^-} = \frac{[X^-]_{PEG}}{[X^-]}$
Halide species partitioning	$CdX_n^{(n-2)-} \leftrightarrows (CdX_n^{(n-2)-})_{PEG}$	$D_{CdX_n^{(n-2)-}} = \frac{[CdX_n^{(n-2)-}]_{PEG}}{[CdX_n^{(n-2)-}]}$
Anionic sulphates partitioning	$Cd(SO_4)_2^{2-} \leftrightarrows (Cd(SO_4)_2^{2-})_{PEG}$	$D_{Cd(SO_4)_2^{2-}} = \frac{[Cd(SO_4)_2^{2-}]_{PEG}}{[Cd(SO_4)_2^{2-}]}$

In this table, the chemical species from the PEG-rich phase are denoted by the subscript “PEG”, while those in the salt-rich phase are given without a subscript.

The Cd(II) distribution coefficient can be written as:

$$D_{Cd} = \frac{[Cd(SO_4)_2^{2-}]_{PEG} + \sum[CdX_n^{(n-2)-}]_{PEG}}{[Cd(SO_4)_2^{2-}] + \sum[CdX_n^{(n-2)-}]} \tag{1}$$

Under the given experimental conditions, only $CdX_n^{(n-2)-}$ species partition into the PEG-rich phase (the extractants concentration is 10^2 times larger than that of Cd(II) and the formation of intermediary cadmium halide species can be neglected). In addition, it is reasonable to assume that $[Cd(SO_4)_2^{2-}]_{PEG} << [CdX_n^{(n-2)-}]_{PEG}$, since the number of metal ions extracted into the PEG-rich phase is lower in the absence of extracting agent.

On the other hand, in salt-rich phase, the SO_4^{2-} concentration is more higher than that of the added halide ions and considering the comparable values of the stability constants for $Cd(SO_4)_2^{2-}$ and cadmium halide species, it can be assumed that the predominant Cd(II) species in this phase is $Cd(SO_4)_2^{2-}$.

Based on these observations, Eq. (1) can be rewritten as:

$$\begin{aligned} D_{Cd} &= \frac{[CdX_n^{(n-2)-}]_{PEG}}{[Cd(SO_4)_2^{2-}]} = \\ &= \frac{1}{\beta_{Cd(SO_4)_2^{2-}}[SO_4^{2-}]^2} \frac{\beta_{CdX_n^{(n-2)-}} D_{CdX_n^{(n-2)-}}}{(D_{X^-})^n} [X^-]_{PEG}^n \end{aligned} \tag{2}$$

where: n is the number of halide ions from the extracted species and K_{ex} is the extraction constant, which is given by the expression:

$$K_{\text{ex}} = \frac{1}{\beta_{\text{Cd(SO}_4)_2^{2-}}[\text{SO}_4^{2-}]^2} \frac{\beta_{\text{CdX}_n^{(n-2)-}} D_{\text{CdX}_n^{(n-2)-}}}{(D_{\text{X}^-})^n} \tag{3}$$

In the given aqueous two-phase system, where $[\text{SO}_4^{2-}]$ is constant and, for a particular metal ion, the term: $\beta_{\text{Cd(SO}_4)_2^{2-}}[\text{SO}_4^{2-}]^2$ is also constant, the "conditional extraction constant" (K_{ex}') has the expression:

$$K_{\text{ex}}' = K_{\text{ex}}\beta_{\text{Cd(SO}_4)_2^{2-}}[\text{SO}_4^{2-}]^2 = \frac{\beta_{\text{CdX}_n^{(n-2)-}} D_{\text{CdX}_n^{(n-2)-}}}{(D_{\text{X}^-})^n} \tag{4}$$

Eq. (2) indicates that the slope of a log–log plot of D_{Cd} against $[\text{X}^-]_{\text{PEG}}$, will give the number of halide ions associated with Cd(II) in the extracted species and the straight line intercept gives the "conditional extraction constant". The dependences of log D_{Cd} *vs.* log $[\text{X}^-]_{\text{PEG}}$ for the two studied media are presented in Figs. 3 and 4.

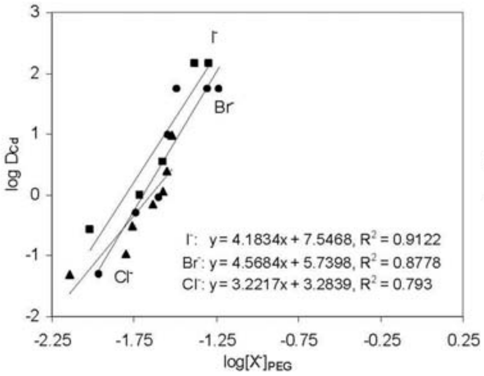

Fig. 3. The log D_{Cd} *vs.* log $[\text{X}^-]_{\text{PEG}}$ dependence for the salt stock solution of pH 3.03.

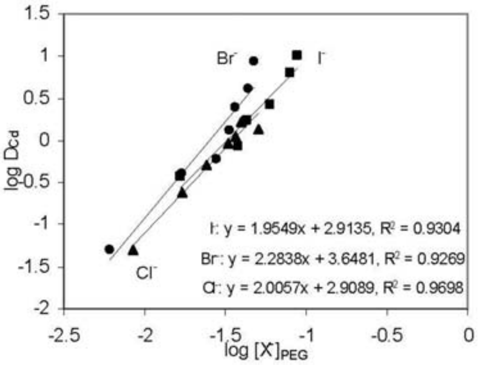

Fig. 4. The log D_{Cd} *vs.* log $[\text{X}^-]_{\text{PEG}}$ dependence for the salt stock solution of pH 4.65.

It should be observed that the slope of the obtained straight lines depends on the pH value of salt stock solution. Decreasing the pH of salt stock solution resulted in an increase of the number of halide ions in the extracted species from 2 to 4. In the presence of H_2SO_4 (pH 3.03), Cd(II) is predominantly extracted as anionic complexes (CdX_4^{2-}), while in the absence of H_2SO_4 (the salt stock solution with pH 4.65), the main extracted species are neutral halides (CdX_2). A different behaviour was observed in case of Cd(II) extraction with chloride ions, when at pH 3.03 the probable extracted species is CdCl_3^- and not CdCl_4^{2-}, as in case of I^- or Br^- extractants. This difference is probably due to the higher stability constant of CdCl_3^- ($\log\beta_{\text{CdCl}_3^-} = 2.4$) than of CdCl_4^{2-} ($\log\beta_{\text{CdCl}_4^{2-}} = 1.35$).[23]

The extraction of cadmium halide anionic complexes in case of the systems with pH 3.03 (prepared in the presence of H_2SO_4), had higher stability and lower hydration, as determined by the accentuated hydrophobicity of the PEG-rich phase of these systems. In case of systems with salt stock solution of pH 4.65 (in the absence of H_2SO_4), in which the polymeric phase had a lower hydrophobicity, the formation of such anionic complexes was not necessary, the neutral molecules CdX_2 being sufficient.

Using the Cd(II) species found to be extracted, the "conditional extraction constants" were calculated according to Eq. (4). These are compared with those obtained from the straight-line intercept (Figs. 3 and 4) in Table II.

TABLE II. The $\log K'_{\mathrm{ex}}$ values in case of Cd(II) extraction in presence of halide ions, in the considered aqueous two-phase system

Halide ion	Salt stock solution pH	Extracted species	$\log \beta_{\mathrm{CdX}_n^{(n-2)-}}$ [23]	$\log K'_{\mathrm{ex}}$ (Graphic, Figs. 3 and 4)	$\log K'_{\mathrm{ex}}$ (Calculated, Eq. (4))
I^-	3.12	CdI_4^{2-}	6.10	7.546	7.327
	4.53	CdI_2	3.04	2.913	3.097
Br^-	3.12	$CdBr_4^{2-}$	2.93	5.738	5.506
	4.53	$CdBr_2$	3.92	3.648	3.621
Cl^-	3.12	$CdCl_3^-$	2.41	3.284	3.411
	4.53	$CdCl_2$	2.74	2.908	2.783

The agreement of the "conditional extraction constants" obtained graphically and calculation shows that the extraction of Cd(II) in presence of halide ions in the aqueous PEG (1550)–$(NH_4)_2SO_4$ two-phase system can be satisfactory described by the elementary equilibria given in Table I and by the approximations presented above.

The obtained experimental results indicate that the efficiency of Cd(II) extraction in the aqueous PEG (1550)–$(NH_4)_2SO_4$ two-phase system depended on both the acidity of the salt stock solution used for the preparation of the aqueous two-phase system (which influenced the hydrophobicity of the PEG-rich phases[24] and, thus, the nature of the extracted species) and the stability of the chemical species formed between Cd(II) and the halide ions extractants.

The efficiency Cd(II) extraction increased in the order: $Cl^- < Br^- < I^-$, corresponding to the increasing stability of the cadmium halides (Figs. 5 and 6). Although, this dependence cannot be considered a linear one, its existence shows that the formation of extracted species plays an important role in the extraction mechanism.

A schematic representation of Cd(II) extraction in the presence of halide ions in the considered aqueous two-phase system is presented in Fig. 7. According to this, for partition Cd(II), processes which occur at the PEG-rich phase/salt-rich phase interface are essential: Cd(II) complexation with halide ions and the transformation of cadmium halide species into complex species towards the PEG-rich phase have a higher affinity under the employed conditions.

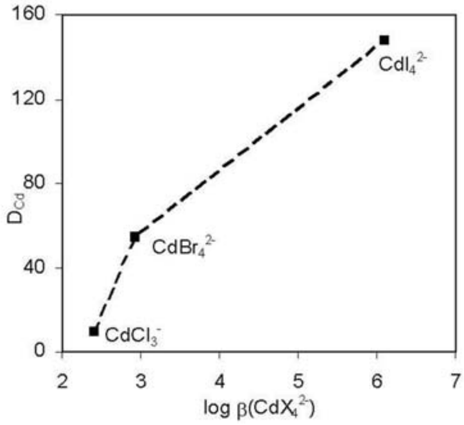

Fig. 5. Cd(II) distribution ratio *vs*. log β values^{23} for the formation of CdX_4^{2-} at pH 3.03.

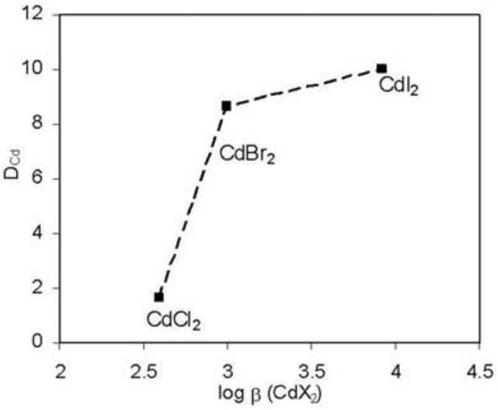

Fig. 6. Cd(II) distribution ratio *vs*. log β values^{23} for the formation of CdX_4^{2-} at pH 4.65.

The anionic species formed at the interface cross into the PEG-rich phase, where they will interact, predominantly by ionic forces, with the ether oxygen atoms of PEG. An equivalent ionic transfer process ensures the electroneutrality of the two phases.

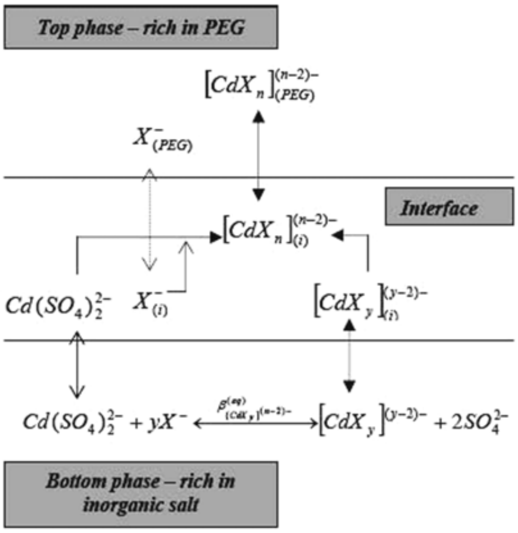

Fig. 7. Schematic representation of the main processes involved in Cd(II) extraction in the considered aqueous two-phase system.

In case of extraction of Cd(II) anionic complexes, the SO_4^{2-} ions which are present in the PEG-rich phase after formation of the aqueous two-phase system are expelled into the salt-rich phase, due to the incompatibility of the hydration environments. Thus, the phases are kept neutral from an electrical point of view and the hydrophobicity of the PEG-rich phase is maintained during of extraction process. The NH_4^+ cations can participate in such ionic transfer processes as counterions.

In case of neutral halide extraction, such an ionic transfer process is less important and the extraction occurs until the hydrophobicity of the PEG-rich phase is diminished by the presence of extractible species.

CONCLUSIONS

The extraction of Cd(II) in aqueous PEG (1550)–$(NH_4)_2SO_4$ two-phase system was investigated as a function of the type and concentration of halide ions extractants, at two different values of pH of the salt stock solution.

In the absence of a suitable extracting agent, the extraction of Cd(II) was insignificant, its preference for the salt-rich phase was determined by the formation of $Cd(SO_4)_2^{2-}$ species, which are stable and with high degree of hydration. The addition of halide ions, as inorganic complexing extractants, resulted in an increase of the extraction of Cd(II) into the PEG-rich phase with increasing halide concentration, due to the formation of metal halide species, more stable than $Cd(SO_4)_2^{2-}$ and with a lower degree of hydration. The efficiency of extractants follows the order: $Cl^- < Br^- < I^-$, which is in agreement with the data from the literature.

On the other hand, the experimental results showed that the extraction of Cd(II) was more effective in the presence of H_2SO_4 (salt stock solution of pH 3.03), when the main extracted species were cadmium anionic halide complexes, than in the absence of H_2SO_4 (salt stock solution of pH 4.65), when Cd(II) was extracted predominantly as neutral molecules (CdX_2).

Based on the experimental results, the nature of the extracted metal species was assumed and the "conditional extraction constants" obtained from the intercepts of straight lines and by calculation were compared. The concordant values of "conditional extraction constants" indicate that the extraction of Cd(II) in the presence of halide ions was mainly determined by two factors: (1) the acidity of the salt stock solution used for the preparation of the aqueous two-phase system and (2) the stability of the extracted species.

ИЗВОД

Cd(II) ЕКСТРАКЦИЈА У PEG (1550)–$(NH_4)_2SO_4$ ДВОФАЗНОМ СИСТЕМУ КОРИШЋЕЊЕМ ХАЛОГЕНИДА КАО ЕКСТРАКТАНАТА

LAURA BULGARIU[1] и DUMITRU BULGARIU[2]

[1]Department of Environmental Engineering and Management, Faculty of Chemical Engineering, Technical University "Gh. Asachi", D. Mangeron 71A, 700050 Iaşi, и [2]Department of Geology – Geochemistry, Faculty of Geography and Geology, "Al. I. Cuza" University, Carol I 20A, 700050 Iaşi, Romania

Екстракција Cd(II) је испитивана у воденим двофазним растворима PEG–$(NH_4)_2SO_4$ који настају растварањем полимера (полиетилен гликола, PEG) и неорганске соли ($(NH_4)_2SO_4$), у присуству халогених јона. У одсуству одговарајућег екстракционог агенса, Cd(II) јон заостаје у фази која је богата солима. Додатком халогених јона Cd(II) бива екстрахован у фазу богату PEG формирајући кадмијум-халогениде. Ефикасност екстракције расте на следећи начин: $Cl^- < Br^- < I^-$. Из дистрибуционих коефицијената одређених као функције концентрације халогених јона израчунате су константе екстракције. Експериментални резултати указују на то да екстрактибилност Cd(II) у датом систему зависи од стабилности Cd(II), формираног халогенида и киселости средине.

(Примљено 30. маја, ревидирано 30. августа 2007)

REFERENCES

1. I. Sarghie, *Mecanismul extractiei chelatilor metalici*, Gh. Asachi, Iasi, 1995, p. 5 (in Romanian)
2. Y. Zolotov, N. M. Kuz'min, O. M. Petrukim, B. Y. A. Spivakov, *Anal. Chim. Acta* **180** (1986) 137
3. B. Y. Zaslavsky, *Aqueous two-phase partitioning. Physical Chemistry and Bioanalytical Applications*, Marcel Dekker, New York, 1995, p. 75
4. J. G. Huddleston, H. D. Willauer, S. T. Griffin, R. D. Rogers, *Ind. Eng. Chem. Res*. **38** (1999) 2523
5. J. Chen, S. K. Spear, J. G. Huddleston, R. D. Rogers, *Green Chem*. **7** (2005) 64
6. L. Li, C. Y. He, S. H. Li, F. Liu, S. Su, X. X. Kong, K. A. Li, *Chin. J. Chem.* **22** (2004) 1313
7. K. P. Ananthapadmanabhan, E. D. Goddar, *Langmuir* **3** (1987) 25
8. H. Cabezas Jr., *J. Chromatogr. B* **680** (1996) 3
9. M. Shibukawa, K. Matsuura, Y. Shinazuka, K. Oguma, *Anal. Sci.* **16** (2000) 1039
10. R. D. Rogers, A. H. Bond, C. B. Bauer, *Sep. Sci. Tech.* **28** (1993) 1091
11. L. Bulgariu, D. Bulgariu, *Sep. Sci. Tech*. **42** (2007) 1093
12. L. Bulgariu, D. Bulgariu, *J. Serb. Chem. Soc.* **72** (2007) 289
13. L. Bulgariu, D. Bulgariu, *Central Eur. J. Chem*. **4** (2006) 246
14. M. Shibukawa, N. Nakayama, T. Hayashi, D. Shibuya, Y. Endo, S. Kawamura, *Anal. Chim. Acta* **427** (2001) 293
15. R. D. Rogers, A. H. Bond, C. B. Bauer, *Solvent Extraction in the Process Industries*, Elsevier, London and New York, 1993, p. 1641
16. T. A. Graber, B. A. Andrews, J. A. Asenjo, *J. Chromatogr. B* **743** (2000) 57
17. R. D. Rogers, A. H. Bond, C. B. Bauer, J. Zhang, S. T. Griffin, *J. Chromatogr. B* **680** (1996) 221
18. J. A. Dean, *Analytical Handbook,* McGraw-Hill, New York, 1995, pp. 3, 104
19. L. Bulgariu, D. Bulgariu, I. Sarghie, *Anal. Lett.* **38** (2005) 2365
20. L. Bulgariu, I. Sarghie, *Anal. St. Univ. "Al.I.Cuza" Iasi,* tom **XII** (2005) 27 (in Romanian)
21. D. I. Seracu, *Indreptar de chimie analitica,* Ed. Tehnica, Bucharest, 1989, p. 64 (in Romanian)
22. Y. Marcus, *J. Chem. Soc. Faraday Trans*. **87** (1991) 2995
23. J. Lurie, *Handbook of Analytical Chemistry,* Mir Publisher, Moscow, 1975, p. 283
24. L. Bulgariu, D. Bulgariu, I. Sarghie, T. Malutan, *Central Eur. J. Chem.* **5** (2007) 291.

www.shd.org.yu

Journal of the Serbian Chemical Society

JSCS@tmf.bg.ac.yu • www.shd.org.yu/JSCS

J. Serb. Chem. Soc. 73 (3) 351–367 (2008)

UDC 621.315.59.004.12:541.135.5–
–0.34.293:546.33–36+544.3

JSCS–3717

Original scientific paper

Semiconducting properties of oxide films formed onto an Nb electrode in NaOH solutions

VLADIMIR D. JOVIĆ*# and BORKA M. JOVIĆ#

Institute for Multidisciplinary Research, 11030 Belgrade, P. O. Box 33, Serbia

(Received 26 June, revised 27 August 2007)

Abstract: In this paper, the results of the potentiostatic formation of homogeneous and heterogeneous, nano-crystalline passive films of Nb_2O_5 onto an Nb electrode in NaOH solutions of different concentrations at potentials lower than 3.0 V *vs.* SCE are presented. The semiconducting properties of such films were investigated by EIS measurements. After fitting the EIS results by appropriate equivalent circuits, the space charge capacitance (C_{sc}) and space charge resistance (R_{sc}) of these films were determined. The donor density (N_{sc}), flat band potential (E_{fb}) and thickness of the space charge layer (d_{sc}) for such oxide films were determined from the corresponding Mott–Schottky (M–S) plots. It is shown that all oxide films were n-type semiconductors in a certain potential range.

Keywords: nano-crystalline; Nb_2O_5; passive film; Mott–Schottky plot; n-type semiconductor.

INTRODUCTION

Among transition metal oxides representing materials having interesting properties, such as superconductivity, colossal magneto-resistance and piezoelectricity, niobium oxides are one of the most interesting. For instance, Nb_2O_5 possesses outstanding dielectric properties, NbO_2 is a semiconductor, while NbO is a metallic conducting material.[1] Due to such properties, they are of high interest for application as devices, optical coatings,[2] solar control and electrochromic films,[3,4] oxygen sensors[5] and capacitors.[6–8] Therefore, procedures for their preparation and evaluation of their properties have attracted considerable attention in recent years. Most of the available data from the materials science approach consider the synthesis of Nb_2O_5 thin films.[9–11]

On the other hand, considerable amount of literature data are available in the field of electrochemical formation, stability and properties of Nb_2O_5 passive films on an Nb electrode in different electrolytes.[12–43] It was shown that a thin passive film, originally formed on an Nb electrode in air, can easily be thickened

---

* Corresponding author. E-mail: vladajovic@ibiss.bg.ac.yu

\# Serbian Chemical Society member.

doi: 10.2298/JSC0803351J

by anodization,[12–16] whereby this process occurs by high-field, ionic migration in the thin film,[12–15] either by metal ions outwards or oxygen ions inwards.[16] It was also shown that the passive oxide film formed on the Nb electrode consists mainly of amorphous Nb_2O_5.[12–14] Its density was determined[17,18] to be 4.74 g cm^{-3}, while its dielectric constant[12] was estimated to be about 45 and that such a film possessed a rather high donor density of the order of 10^{19} cm^{-3} (recently it was found that its value should be 41).[7,8] The value of donor density was ascribed to oxygen vacancies making such a passive oxide film an n-type semiconductor.[19,20] As shown in the book of R. Morrison,[20] an n-type Nb_2O_5 passive film is characterized by a band-gap of 3.4 eV and by a flat band potential of −0.75 V *vs.* SHE at pH 13.0.[22] Some studies have been devoted to the kinetics of the dissolution of naturally formed oxide films[24,25] and to the kinetics of the formation of passive oxide film.[23,26–31] In some cases, EIS[27,32,33] and photoelectrochemical[34] measurements were performed in order to analyze the properties of Nb_2O_5 passive films. An ellipsometric study revealed that with increasing anodic potential in the range from 2.0 to 10.0 V *vs.* SHE in 1.0 M H_2SO_4, the thickness of the Nb_2O_5 film increased linearly from about 10 nm to about 28 nm,[28] with the simultaneous evolution of oxygen at potentials higher than 2.0 V *vs.* SHE. Most recently it was shown that by combination of anodization – annealing – anodization techniques, porous Nb_2O_5 films of thickness of more than half a micrometer could be formed onto an Nb electrode in 1.0 M H_3PO_4 with the addition of 1.0 wt. % HF at 5.0 °C at 2.5 V *vs.* Ag|AgCl (3.0 M KCl) followed by annealing under a nitrogen atmosphere at different temperatures for 3 h.[35] It is important to note that the electrochemical behavior of Nb (corrosion and passive oxide film formation) were mainly investigated in a relatively narrow potential range, from about –1.3 to about 1.0 V *vs.* SCE,[23–31] while the properties of Nb_2O_5 passive films were mainly investigated for the films obtained under high-voltage anodized Nb.[12–20,27,33,34] The semiconducting properties of passive oxide films formed at potentials lower than 2.0 V *vs.* SCE have practically not been reported in the literature hitherto.

In this study an attempt was made to grow potentiostatically Nb_2O_5 passive films in NaOH electrolyte of different concentrations at potentials lower than 3.0 V *vs.* SCE and to investigate their semiconducting properties by analysis of EIS results and M–S plots.

EXPERIMENTAL

All experiments were carried out in a three-compartment standard electrochemical cell at room temperature in an atmosphere of purified nitrogen. Before each experiment, the electrolyte was purged with N_2 for 30 min. The same N_2 atmosphere was maintained over the solution during the experiment to minimize oxygen contamination. A platinum mesh counter electrode and the reference, saturated calomel electrode (SCE), were placed in separate compartments. The latter was connected to the working electrode by a Luggin capillary. All solutions were made from analytical grade NaOH (Merck) and extra pure UV water (Smart2PureUV, TKA).

Polarization, chronoamperometric and EIS measurements were performed by a computer-controlled Gamry potentiostat (Reference 600) using Corrosion Software DC 105, Physical Electrochemistry Software PHE 200 and Electrochemical Impedance Software EIS 300.

Contact of the Nb (99.9% Goodfellow) sample (1.0×1.0×0.2 cm^3) with a copper wire on the back side of the electrode was made with silver conductive epoxy paste (Alfa Aesar) and electrode was sealed in an epoxy resin so that only an area of 1.0 cm^2 was exposed to the solution. Once mounted, the electrode was polished first on emery papers (1200, 2400 and 4000) and then on polishing clothes impregnated with alumina down to 0.05 μm (1, 0.3 and 0.05 μm), cleaned in an ultrasonic bath for 10 min (to remove traces of polishing alumina), thoroughly washed with extra pure UV water and transferred to the electrochemical cell in which the chronoamperometric, polarization and EIS measurements were performed.

Before the polarization measurements, the Nb electrode was kept at the open circuit potential for 10 s and cathodic limit was set at −1.35 V. The polarization diagrams were recorded at a sweep rate of 1.0 mV s^{-1} starting from the cathodic limit and finishing at 3.0 V in 0.25 M NaOH and at 2.0 V in 2.50 M and 5.00 M NaOH. The formation of passive oxide films was performed by the following procedures: in 0.25 M NaOH, the potential was first set at 1.0 V for 1 h and then at 3.0 V for 2 h; in 2.50 M NaOH, the potential was first set at 1.0 V for 1 h and then at 2.0 V for either 3 h or 6 h; in 5.00 M NaOH, the potential was first set at 1.0 V for 1 h and then at 2.0 V for 1 h. The corresponding current density *vs.* time responses were also recorded. After passive oxide film formation, EIS spectra were recorded at different potentials, covering the potential region B (see Fig. 1), starting from the most positive one (usually 2.0 V, except for 0.25 M NaOH where the starting potential was 2.7 V) down to a potential of 0.5 or 0.6 V. All EIS spectra were recorded in the 0.1 Hz to 40 kHz frequency range with ac amplitude of 10 mV. After completion of these measurements, EIS spectra for certain potentials in the range 0.6–2.0 V (for example 1.0 V, 1.5 V and 2.0 V) were recorded again to determine whether the property of the passive film had changed during this procedure. It was found that the maximum difference between the first and repeated experiments was in the range of ±5 %, confirming that the properties of the passive film remained the same during the impedance measurements.

Scanning electron microscopy was performed using a VEGA TS 5130 MM (TESCAN) microscope.

RESULTS

The polarization diagrams recorded in three concentrations of NaOH (marked in the Figure) are shown in Fig. 1. As can be seen, all the diagrams are characterized by a corrosion potential (being more negative at higher concentrations of NaOH) followed by a sharp increase and a peak of the current density. This peak is seen to be more pronounced at higher concentrations of NaOH. At more positive potentials (region B on the diagram), all polarization curves are characterized by a current density plateau up to the potential of region C (dashed line in Fig. 1). In the potential region C, a second current density increase is seen to occur in all solutions, followed again by a current density plateau up to the upper applied potential limit (2.0 or 3.0 V).

The current density *vs.* time responses (j *vs.* t) for the formation of passive films in 0.25, 2.50 and 5.00 M NaOH are presented in Fig. 2a, 2b and 2c, respectively. The first applied potential of 1.0 V was approximately the potential of the second peak (second current density increase) in all solutions, while the second applied potential was the maximum potential recorded on the polarization diagrams (Fig. 1). As can be seen, the *j vs. t* transients recorded in 0.25 and 2.50 M NaOH solutions were monotonously falling transients for both applied potentials, while in the case of 5.00 M NaOH, first transient (1.0 V) was characterized by a current density increase after about 1000 s.

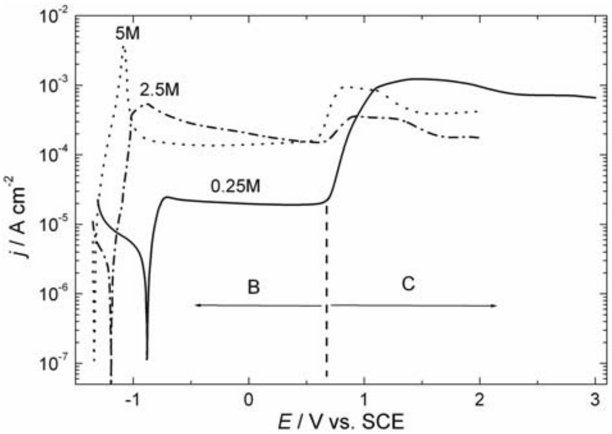

Fig. 1. Polarization diagrams recorded onto Nb electrode at a sweep rate of 1.0 mV s^{-1} in NaOH solutions of different concentrations (marked in the Figure).

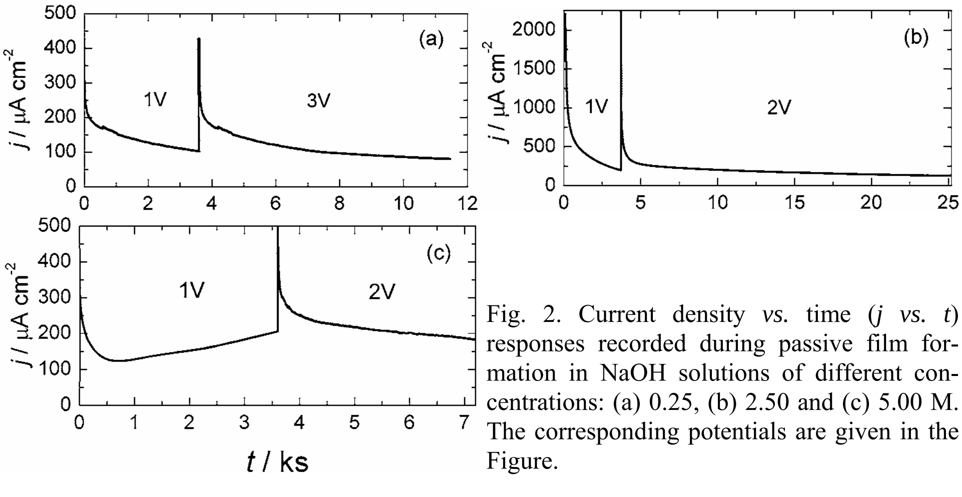

Fig. 2. Current density *vs.* time (*j vs. t*) responses recorded during passive film formation in NaOH solutions of different concentrations: (a) 0.25, (b) 2.50 and (c) 5.00 M. The corresponding potentials are given in the Figure.

The equivalent circuits used for fitting the EIS results are presented in Fig. 3. In all cases for 0.25 and 2.50 M NaOH, the best fit was obtained with the equivalent circuit (a). For the highest NaOH concentration of 5.00 M, the EIS results were of a different shape, characteristic for the surface charge approach[35–37] and these results were fitted with the equivalent circuit (b), used in the literature for such an approach.[31,33,35–37] The parameters of the corresponding equivalent circuits are: (a) R_s – solution resistance; CPE_{sc} – constant phase element corresponding to the space charge capacitance[38] ($Z_{CPE} = Y_0(j\omega)^{\alpha}$); R_{sc} – space charge resistance; (b) R_s – solution resistance; C_0 – Faradaic pseudocapacitance; C_b – barrier film capacitance; R_b – resistance of defect migration; R_{SC} and L_{SC} – elements associated with the negative surface charge at the film/solution interface.[31,33,35–37]

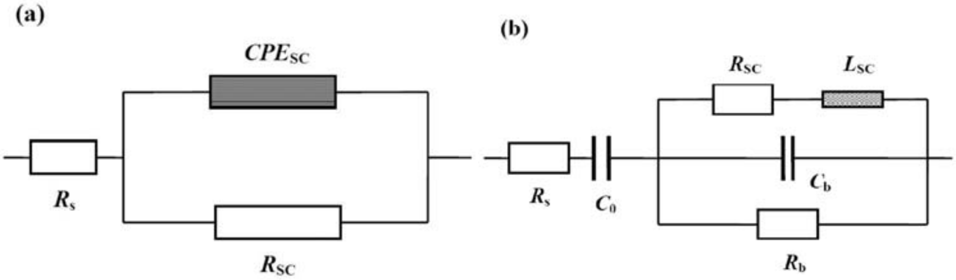

Fig. 3. Equivalent circuits used for fitting the EIS results.

Typical experimental EIS results (squares, circles, triangles, *etc.*) together with the fitting curves (solid lines) obtained in 0.25 and 2.50 M solutions are presented in Fig. 4. Actually, Fig. 4 represents the results obtained with the passive oxide film formed for 1 h at 1.0 V and for 3 h at 2.0 V in 2.50 M NaOH. The *Z*’–*Z*’’ diagrams recorded at each potential are presented in Fig. 4 and the corresponding potentials are marked in V (a – potentials from 2.0 to 1.3 V and b – potentials from 1.2 to 0.6 V). In general, the shape of all diagrams recorded in 0.25 and 2.50 M NaOH were identical to those in Fig. 4, except that the values of *Z*’ and *Z*’’ were different for different cases. A characteristic of the fitting results for these *Z*’–*Z*’’ diagrams is that the heterogeneity factor in the *CPE*s (α) is, in all cases, very close to unity (varying between 0.95 and 0.98), indicating that the space charge of the oxide films was almost homogeneously distributed in the film (see Discussion).

The EIS results obtained for the oxide film formed in 5.00 M NaOH are shown in Fig. 5 (the squares, circles, triangles, *etc.* are experimental points, the solid lines are the fitting results). The shape of the *Z*’–*Z*’’ diagrams is characteristic for the surface charge approach and, accordingly, the experimental results were fitted with the equivalent circuit developed for such an approach, presented in Fig. 3b. All the *Z*’–*Z*’’ diagrams were recorded in the range from 2.0 to 0.8 V and the low frequency limit was set at 0.50 Hz (some of the diagrams are shown in Fig. 5a). One *Z*’–*Z*’’ diagram, recorded for a potential of 1.4 V, was repeated (after the whole set of experiments were finished) with the low frequency limit set at 0.10 Hz. This diagram is presented in Fig. 5b. The experimental results in Fig. 5 were fitted by the equivalent circuit presented in Fig. 3b (dotted line) and by the same equivalent circuit where C_0 was replaced by *CPE* (solid line). As can be seen, a much better fit was obtained with *CPE*. Hence, all the experimental results were fitted by both equivalent circuits and the small difference was recorded for the parameters plotted in Fig. 7a and 7b. On the other hand, the values of C_0 varied between 2259 and 3761 μF cm^{-2}, most likely indicating a high roughness of the electrode surface and the possible adsorption of anions onto the passive film. At the same time, when fitting the EIS results with *CPE* instead of C_0, the heterogeneity factor in the *CPE*s (α) was found to vary between 0.613 and 0.762, also indicating a heterogeneous distribution of charge at the oxide/electrolyte interface.

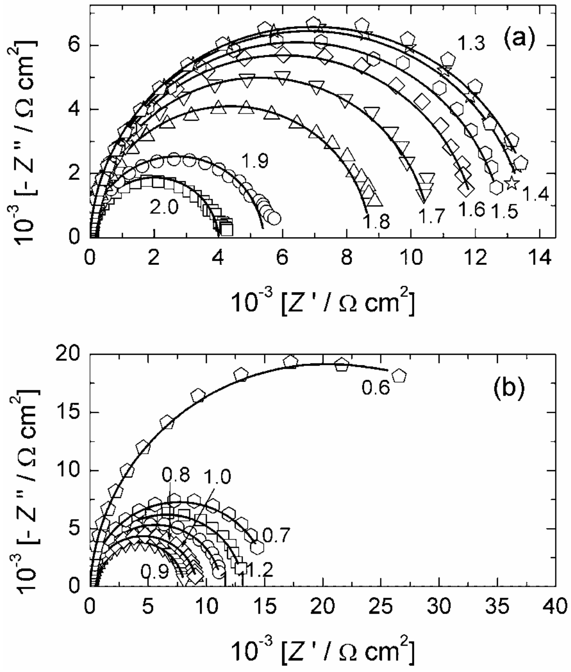

Fig. 4. *Z*'–*Z*'' Diagrams recorded in 2.50 M NaOH after passive film formation for 1 h at 1.0 V and 3 h at 2.0 V. The corresponding potentials are marked in V: (a) from 2.0 to 1.3 V; (b) from 1.2 to 0.6 V. The experimental points are presented by squares, circles, triangles *etc*., while the solid lines represent the fitted curves obtained using the equivalent circuit presented in Fig. 3(a). Frequency range: from 40 kHz to 0.10 Hz.

The M–S plots shown in Fig. 6 were obtained by analysis of the EIS results for: (a) 0.25, (b) 2.50 and (c) 5.00 M NaOH. As can be seen in Fig. 6a, linear M–S plot were obtained for the concentration of 0.25 M in the potential range from 2.5 to 1.4 V, while in the case of 2.50 and 5.00 M NaOH, well defined M–S plots were obtained over the whole investigated range of potentials for both passive films. These results indicate that n-type semiconducting oxide films are formed in all cases.

The results presented in Fig. 7 were obtained by analysis of the *Z*'–*Z*'' diagrams shown in Fig. 5. The squares represent the results obtained by fitting the *Z*'–*Z*'' diagrams using the equivalent circuit presented in Fig. 3b, while the circles represent the results obtained by the fitting *Z*'–*Z*'' diagrams using the same equivalent circuit with C_0 being replaced by *CPE*. As can be seen in Fig. 7a and 7b, linear dependences (predicted by the model) were obtained for C_b^{-1} *vs*. *E* and $R_{b}j$ *vs.* E. The steady-state current density used to plot $R_{b}j$ *vs.* E is the current density recorded at the end of the pulse presented in Fig. 2c. To obtain all the model parameters (see discussion), the (R_{b}/R_{sc}) *vs.* E and $(L_{sc}j/R_{sc})$ *vs.* E dependences are plotted in Fig. 7c and 7d, respectively, for all the investigated potentials. Although the model of surface charge approach does not consider a linear dependence for C_{b}^{-2} *vs.* E (M–S plot), this dependence was also recorded, as shown in Fig. 6c.

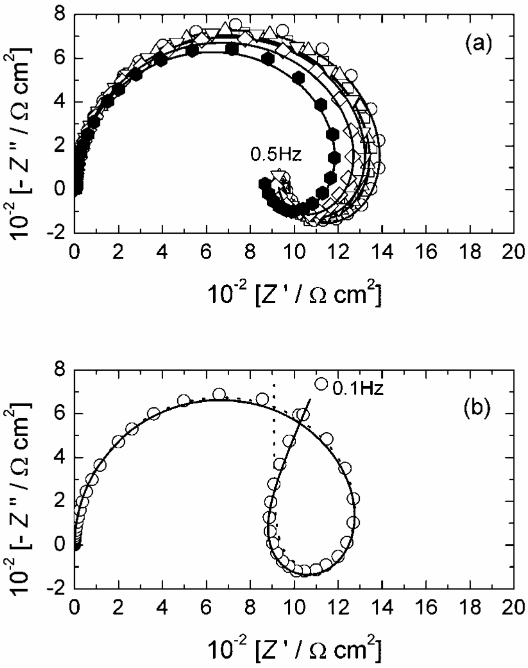

Fig. 5. (a) *Z'–Z''* Diagrams recorded in 5.00 M NaOH after passive film formation for 1 h at 1.0 V and 1 h at 2.0 V. The corresponding potentials: □ 1.9, ○ 1.7, △ 1.5, ▽ 1.3, ◇ 1.1 and ⬢ 0.9 V. The experimental points are presented by squares, circles, triangles *etc.*, while the solid lines represent the fitted curves obtained using the equivalent circuit presented in Fig. 3(b). Frequency range: from 40 kHz to 0.50 Hz. (b) *Z'–Z''* Diagram in the same solution under the same conditions of passive film formation: potential 1.4 V. The experimental points are presented by circles. The dotted line represents the fitted curve obtained using the equivalent circuit presented in Fig. 3(b), while the solid line represents the fitted curve obtained using the same equivalent circuit but with C_0 being replaced by *CPE*. Frequency range from 40 kHz to 0.10 Hz.

The SEM micrographs of the surface of the oxide films formed in 2.50 M NaOH by the pulse procedure (b), Fig. 2, and in 5.00 M NaOH by the pulse procedure (c), Fig. 2, are presented in Fig. 8a and 8b, respectively.

The M–S plots obtained by analysis of the EIS results recorded in 2.50 M NaOH are presented in Fig. 9a and 9b, assuming that the impedance of the process occurring in the semiconducting oxide film could be presented by the parallel connection of C_{sc} and R_{sc} or the serial connection of C_{sc} and R_{s}, respectively (see Discussion).

The properties of the space charge layer (slopes of the M–S plots, donor densities, N_{sc}, flat band potentials, E_{fb}, and thicknesses of the space charge layer, d_{sc}), obtained by the analysis of M–S plots presented in Fig. 6, as a function of the NaOH concentration and the conditions of the formation of Nb_2O_5 film are presented in Table I.

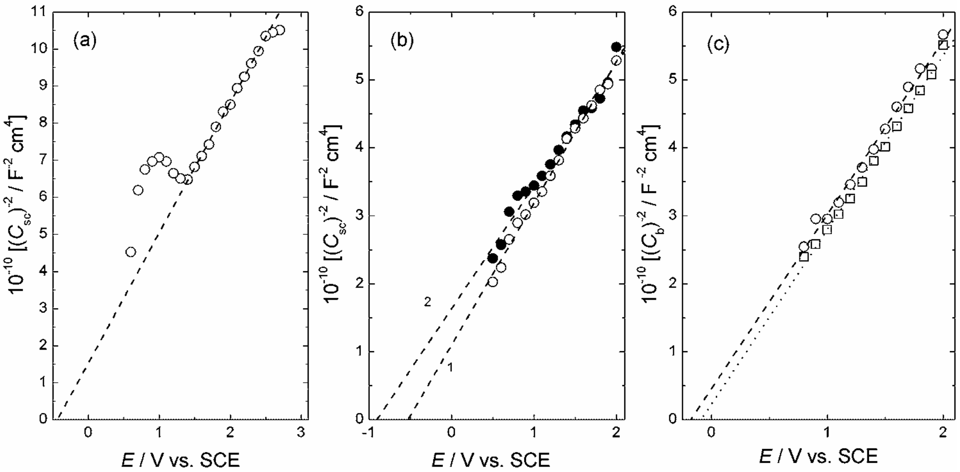

Fig. 6. M–S plots for the passive films formed in: (a) 0.25, (b) 2.50 (1 – 1 h at 1.0 V followed by 3 h at 2.0 V; 2 – 1 h at 1.0 V followed by 6 h at 2.0 V) and (c) in 5.00 M NaOH (□ – C_b values obtained by fitting the EIS results using the equivalent circuit presented in Fig. 3(b); ○ – C_b values obtained by fitting the EIS results using the same equivalent circuit but with C_0 being replaced by *CPE*).

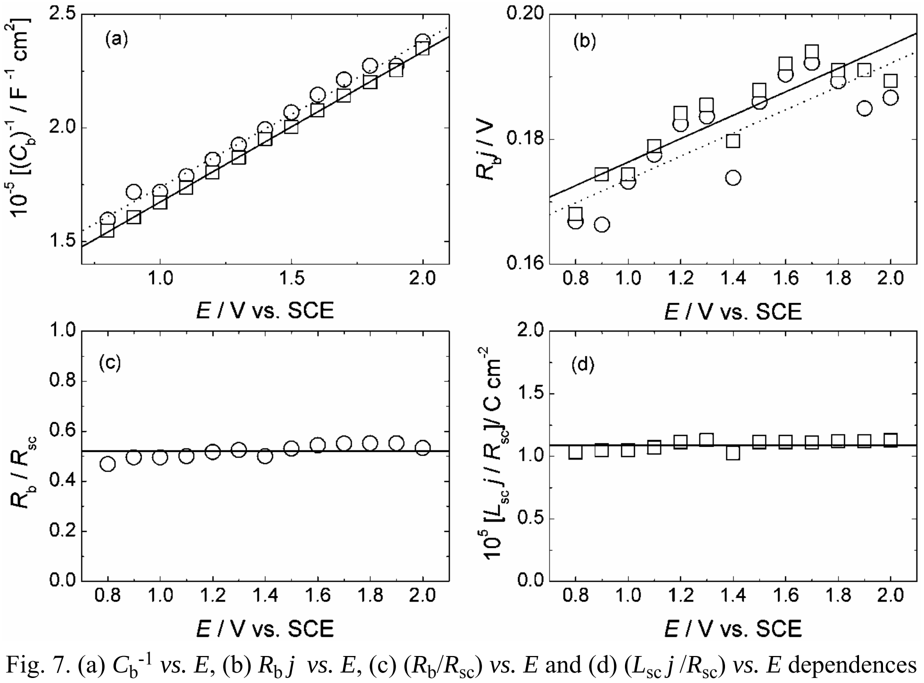

Fig. 7. (a) C_b^{-1} *vs. E*, (b) $R_b j$ *vs. E*, (c) (R_b/R_{sc}) *vs. E* and (d) ($L_{sc} j / R_{sc}$) *vs. E* dependences obtained by fitting the EIS results presented in Fig. 5. (□) C_b, R_b, R_{sc} and L_{sc} values obtained by fitting the EIS results using the equivalent circuit presented in Fig. 3b; (○) C_b, R_b, R_{sc} and L_{sc} values obtained by fitting the EIS results using the same equivalent circuit but with C_0 being replaced by *CPE*.

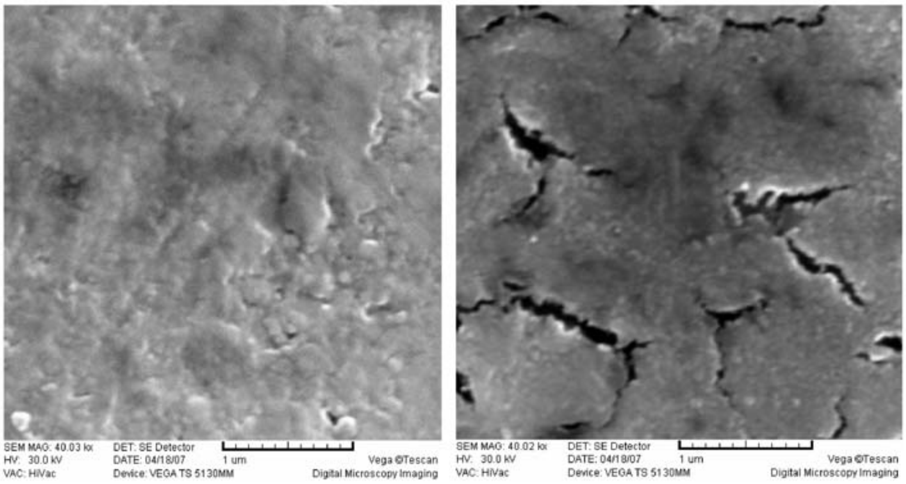

(a) (b)

Fig. 8. (a) SEMs of the Nb_2O_5 surface formed in 2.50 M NaOH by pulse procedure (b) in Fig. 2; (b) SEMs of the Nb_2O_5 surface formed in 5.00 M NaOH by pulse procedure (c) in Fig. 2.

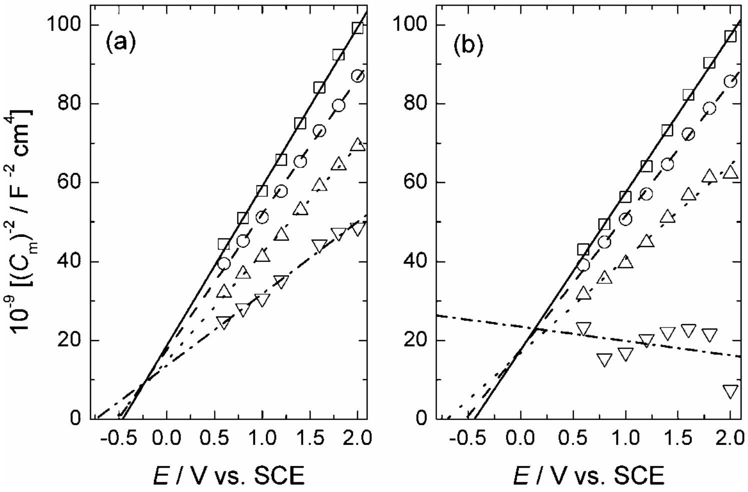

Fig. 9. M–S plots calculated from the EIS data recorded in 2.50 M NaOH for the film formed with 1 h at 1.0 V and 3 h at 2.0 V, assuming (a) parallel connection of C_{sc} and R_{sc} and (b) serial connection of C_{sc} and R_{sc} for different frequencies: □ – 10 kHz; ○ – 1 kHz; △– 100 Hz and ▽– 10 Hz.

DISCUSSION

Polarization diagrams

According to the available literature, the formation of a passive film on Nb is very sensitive to the pre-treatment of the electrode.[30] In order to avoid the formation of Nb hydrides[40,41] of a wide non-stoichiometric composition[42] which are usually formed at about −1.5 V *vs.* SHE,[30] all polarization diagrams were recorded starting from the same cathodic potential limit of −1.35 V *vs.* SCE, *i.e.*, about −1.0 V *vs.* SHE (after 10 s at the open circuit potential). As can be seen in Fig. 1, with increasing NaOH concentration, the corrosion potential becomes more negative, which is in accordance with previous investigations.[26] Simultaneously, the peak of Nb dissolution and Nb_2O_5 oxide formation,[26] appearing at slightly more positive potentials than the corrosion potential, was found to increase with increasing NaOH concentration. At more positive potentials than the peak potential, the sudden decrease in the current density indicates a well-defined passive behavior of Nb (Nb_2O_5 passive film) and this is characteristic for the potential region marked B in Fig. 1. With further increase of the potential in all three solution concentrations, a further increase in current density could be detected, indicating that a new process occurs at the passive Nb_2O_5 film. Such a behavior was detected in a few previously published papers,[30,32,34] but none of the authors attempted to explain it. Characteristic for the potential region C is that after the increase in current density a more or less well defined current density plateau could be detected in all the investigated solutions, with the one in 0.25 M NaOH being the best defined. Since a break-down of passive Nb_2O_5 film was found not to occur to 10 V[30] and even up to 80 V,[6] this current density increase could be ascribed to either further oxidation of the passive Nb_2O_5 layer or some other process, such as the accumulation of oxygen vacancies in the oxide film, since it was shown that oxygen vacancies are donors in such an n-type semiconducting film.[19,20] It is most likely that this process represents the accumulation of oxygen vacancies in the oxide film, since all three oxides of Nb should be formed at negative potentials (NbO at −1.57, NbO_2 at −1.46 and Nb_2O_5 at −1.128 V *vs.* SHE[43]) and, simultaneously, the only oxide detected by the X-ray diffraction technique[32] at potentials more positive than 2.0 V *vs.* SCE was Nb_2O_5.

Passive oxide film formation at constant potentials

As can be seen in Fig. 2, in all cases, passive oxide films were formed by applying two potentials: first at 1.0 V (approximately the potential of the current density maximum in the potential region C) for 1 h and then at the potential of the upper limit on the polarization curves for different time durations (2, 3, 6, and 1 h). Such a procedure was employed in order to obtain an as homogeneous as possible oxide film and it is obvious that this was achieved since the factor of the space charge layer homogeneity α was very close to 1 (see results). Also, with such a procedure of passive oxide film formation the possibility for Nb hydride formation[30] was avoided. It is characteristic for Fig. 2 that only in 5.00 M NaOH did the current density commence to increase after about 1000 s at the potential of 1.0 V, indicating a possible increase of the surface area, most likely by an increase of the roughness of the electrode surface, which was confirmed by the values for the Faradaic pseudocapacitance values (C_0), which varied between 2259 and 3761 μF cm^{-2} for such a passive oxide film (Fig. 5 – see discussion of the EIS results) and by the SEM presented in Fig. 8b, with the passive oxide film surface being characterized by the presence of a significant number of open pores (cracks) of length about 0.5 μm and width about 0.1 μm. As can be seen in Fig. 8a, the surface of the passive oxide film formed in 2.50 M NaOH (pulse procedure (b) – Fig. 2) was homogeneous, while the one formed in 5.00 M NaOH (pulse procedure (c) – Fig. 2) was heterogeneous. The crystals of both films are extremely small, being of the order of about 20 nm maximum (this could be estimated at higher magnification, but the picture was not very clear and is not presented here).

EIS Results analysis

As can be seen in Fig. 4, all the EIS spectra recorded in 0.25 and 2.50 M NaOH solutions in the frequency range 0.10–40 kHz were characterized by well defined semi-circles on the Z'–Z'' diagrams. After fitting them with the equivalent circuit presented in Fig. 3a, very good fits were obtained, indicating that in the given frequency range, a double layer capacitance could be neglected and that the whole process is dominated by a space charge capacitance and a resistance. In order to obtain the dimensionally correct value for the space charge capacitance (C_{sc}), the following Equation was used:[44]

$$C_{\mathrm{sc}} = (Y_0 R_{\mathrm{sc}}^{1-\alpha})^{\frac{1}{\alpha}} \tag{1}$$

which is derived from the Equation:[45]

$$C_{\mathrm{sc}} = Y_0 (\omega_{\mathrm{m}}'')^{\alpha-1} \tag{2}$$

where Y_0 represents the constant in the equation for the constant phase element[39] in all commercially available software (given in Ω^{-1} cm^{-2} s^{α}), ω_{m}'' is the frequency of the maximum on the $-Z''$ *vs.* log ω dependence (independent of the value of α) and α is the factor of the charge distribution homogeneity in the passive oxide film. It is important to note that in such approach it is assumed that both components of the space charge layer (C_{sc} and R_{sc}) are dependent on α (these equations are generally developed for parallel connection of *CPE* and R[44–46]). After the fitting procedure and calculation of C_{sc}, these values were used to plot the dependences shown in Fig. 6. From the slopes of the M–S plots, the values of the donor densities (N_{sc}) were calculated using the dielectric constant for Nb_2O_5, $\varepsilon = 41$.[7] These values are given in Table I for all the passive oxide films together with the values of the flat band potential (E_{fb}), obtained from the intercept at the potential axis. As can be seen, the lowest value of N_{sc} was obtained for the oxide film formed in 0.25 M NaOH, while the highest value was obtained for the film formed in 2.50 M NaOH with the duration of the second pulse at 2.0 V being 6 h, indicating that the number of donors (in this case oxygen vacancies) increased with the time of electrode polarization at a given anodic potential. Also, it should be noted that the increase of N_{sc} was accompanied by a more negative value of E_{fb}, which is in accordance with the theory of semiconducting processes[19,20] (an increase in N_{sc} lowers the slope of the M–S plot and accordingly the intercept at the potential axis is shifted to more negative potentials).

TABLE 1. Conditions of Nb_2O_5 film formation and oxide semiconducting properties

NaOH Conc.	Condition of oxide film formation	Slope of M–S plot $F^{-2}\ m^4\ V^{-1}$	$N_{sc}\times10^{-20}$ cm^{-3}	E_{fb} V *vs.* SCE	d_{sc} nm
0.25 M	1 h at 1.0V + 2 h at 3.0V	351	0.98	–0.44	12.56
2.50 M	1 h at 1.0V + 3 h at 2.0V	208	1.65	–0.54	8.30
2.50 M	1 h at 1.0V + 6 h at 2.0V	180	1.91	–0.92	8.28
5.00 M	1 h at 1.0V + 1 h at 2.0V	256	1.34	–0.19	8.54

The thickness of the space charge layer, d_{sc}, was calculated using the Equation:[47,48]

$$d_{sc} = \left[\frac{2\varepsilon\varepsilon_0}{eN_{sc}}(E - E_{fb} - \frac{kT}{e})\right]^{1/2} \tag{3}$$

where ε_0 represents the permittivity of free space, E is the potential of the passive oxide film formation (the value of the second pulse, either 2.0 or 3.0 V), while e, k and T have their usual meanings. As can be seen, the highest value of the space charge layer thickness was obtained at the most positive potential of 3.0 V (in accordance with the literature[6,28]), while with the duration of the second pulse, the thickness of the space charge layer does not change but the donor density increases and the flat band potential becomes more negative (line 2 in Fig. 6b).

In the case of 5.00 M NaOH solution, a completely different shape of Z'–Z'' diagrams, characterized by the presence of an inductive loop, was obtained (Fig. 5). According to Bojinov *et al.*[36–38], such EIS results are typical for the surface charge approach, *i.e.*, film growth is limited by both high-field assisted bulk migration and relaxation of the charge carrier density (in this case oxygen vacancies) at the metal/film interface. During such a process, a thin continuous barrier-like layer of a wide band-gap semiconductor is formed. This theory predicts several linear dependences for the parameters obtained by fitting the EIS results using the equivalent circuit shown in Fig. 3b, two of them being: C_b^{-1} *vs.* E and $R_b j$ *vs.* E. As can be seen in Fig. 7a and 7b, respectively, both of them are linear in the investigated potential range. Simultaneously, as the model predicts (see Eqs. (6) and (7)), the functions (R_b/R_{sc}) *vs.* E and ($L_{sc} j/R_{sc}$) *vs.* E are independent of potential (Fig. 7c and 7d, respectively). For the same system, Nb in 5.00 M NaOH, but at more positive potentials (2.0 V > E > 10.0 V) and a high temperature of 50 °C, similar dependences were obtained.[32]

According to the literature,[32,36–38] the parameters for the surface charge model can be calculated from the following Equations:

$$\frac{\mathrm{d}(R_\mathrm{b} j)}{\mathrm{d}E} = \frac{RT}{zFaE_\mathrm{f}} \tag{4}$$

$$\frac{\mathrm{d}(C_\mathrm{b}^{-1})}{\mathrm{d}E} = \frac{(1-\delta)}{\varepsilon\varepsilon_0 E_\mathrm{f}} \tag{5}$$

$$\frac{R_\mathrm{b}}{R_\mathrm{sc}} = \frac{\delta}{(1-\delta)} \tag{6}$$

$$\frac{L_\mathrm{sc} j}{R_\mathrm{sc}} = S \tag*{(7)^{38}}$$

and

$$\frac{L_\mathrm{sc} j}{R_\mathrm{sc}} = \frac{1}{S}* \tag*{(7a)^{32}}$$

$$C_0 = \frac{nF(1-\delta)}{V_\mathrm{m}\lambda E_\mathrm{f}} \tag{8}$$

where E_f is the electric field in the film bulk; a, the half-jump distance of the oxygen vacancies; S, the capture cross-section for positive defects by the negative surface charge; δ, the polarizability of the film/solution interface; λ, the current efficiency for film formation under transient conditions; V_m, the molar volume of the oxide; n, the number of elementary changes necessary to grow an oxide (for Nb_2O_5, $n = 10$) and z is the electric charge of the mobile species (in this case $z = 2$, charge transport occurs by oxygen vacancies, since it is assumed that the transport of oxygen vacancies is much faster than that of metal ones). Using the parameters of the surface charge model obtained from above Equations, it is possible to calculate the formation ratio dx/dE, which in this case does not simply coincide with the reciprocal of the electric field (traditional high field model[49]), but, according to Chao *et al.*,[50] is linked to the electric field and the polarizability of the oxide film/solution interface (point defect model) by the Equation:

$$\frac{\mathrm{d}x}{\mathrm{d}E} = \frac{1-\delta}{E_\mathrm{f}} \tag{9}$$

The model parameters obtained using Eqs. (4)–(9) and the results presented in Fig. 7 are: $E_\mathrm{f} = 2.83\times10^6$ V cm^{-1}; $S = 1.1\times10^{-5}$ C cm^{-2} (according to Ref. 38), or $S = 91$ mC^{-1} cm^2 (according to Ref. 32); $\delta = 0.34$; $\lambda_\mathrm{av.} \approx 1$; $a = 4.88$ nm and dx/dE = 2.33 nm V^{-1}. Hence, if the results obtained in Ref. 32 are compared with those presented in this paper, it could be concluded that, except for S and λ, the other parameters are in good agreement. It should be emphasized here that λ_av presented in this paper (calculated from Eq. (8)) was obtained as an average value, since the Faradaic pseudocapacitance value (C_0) varied between 2259 and 3761

---

* It should be noted that in both references[38,32] the value of S is given in C^{-1} cm^2.

μF cm^{-2} in the investigated potential range, with no indication of any linearity, indicating 100 % current efficiency for the formation of the oxide film under the given conditions. It is important to mention here that a significant difference in the surface of the passive oxide films obtained in Ref. 32 and in this paper exists. In Fig. 6 of Ref. 32, well-defined needle-like crystals (several tens of microns long and about 1 μm wide, randomly oriented) were detected on the Nb_2O_5 surface after 60 min of polarization at 4.0 V *vs.* SCE in 5.00 M NaOH at 50 °C, while in the present case, after 1 h at 1.0 V and 1 h at 2.0 V at 25 °C, a heterogeneous (with the presence of cracks – open pores), nano-crystalline Nb_2O_5 surface was obtained. Such a difference in the morphology of the Nb_2O_5 surface is the most likely reason for the difference in the parameters S and λ given in Ref. 32 and in this paper. It is also important to note that a much better fit of the experimental results presented in Fig. 5a would be obtained using *CPE* instead of C_0, which indicates that the calculation of λ would be more accurate after fitting the experimental results with *CPE*. Unfortunately, since there was no parallel resistance in connection with C_0, the use of Eqs. (1) or (2) was not possible and the fitting results could give only a value of Y_0 which could not be used for the calculation of λ since its dimension is given in Ω^{-1} cm^{-2} s$^{\alpha}$.

It is interesting to note that for the same system, a $C_b{}^{-2}$ *vs.* E (M–S) dependence, shown in Fig. 7c, was also detected. Since the surface charge model predicts the existence of a thin continuous barrier-like layer of a wide band-gap semiconductor, it seems reasonable to obtain well defined M–S plots.

A simplification of the process occurring at semiconducting electrodes, assuming either a serial connection of C_{sc} and R_s or a parallel connection of C_{sc} and R_{sc}, is very often used in the literature.[24,51–56] At the same time, in most commercially available software for M–S plots, a serial connection is assumed, while in the case of EIS300 software of Gamry both situations can be used. In the case of serial connection of C_{sc} and R_s, the capacitance is calculated directly from the value of Z'', *i.e.*, $C_{sc} = 1/2\pi fZ''$ and plotted as $C_m{}^{-2}$ *vs.* E, while in the case of parallel connection of C_{sc} and R_{sc}, the capacitance is calculated directly from the value of Y'', *i.e.*, $C_{sc} = Y''/2\pi f$ and plotted as $C_m{}^{-2}$ *vs.* E. The results of such an approach for different frequencies (□ – 10 kHz; ○ – 1.0 kHz; △ – 100 Hz and ▽ – 10 Hz) are presented in Fig. 9 for the passive Nb_2O_5 film formed in 2.50 M NaOH for 1 h at 1.0 V and 3 h at 2.0 V. As can be seen, in both cases well-defined linear M–S plots were obtained with their slopes changing with the frequency. In case (a), the slope changed in the range of about 421–202 F^{-2} m^4 V^{-1}, with the corresponding N_{sc} values varying in the range 0.82×10^{20}–1.70×10^{20} cm^{-3} (accordingly E_{fb} changed from −0.47 to −0.73 V). Comparing these values with the one presented in Table I for this particular oxide film, it appears that in case (a) a low frequency of 10 Hz should be used in order to obtain agreement with the N_{sc} values determined by fitting the EIS spectra. In case (b), a positive slope was obtained for 10, 1.0 and 0.100 kHz, while for 10 Hz, the slope was negative.

The positive slope changed in the range 399–239 F^{-2} m^4 V^{-1}, with the corresponding N_{sc} values varying in the range 0.86×10^{20}–1.44×10^{20} cm^{-3} (accordingly E_{fb} changed from −0.44 to −0.72 V). Hence, in case (b), the M–S plot for 0.100 kHz should be used in order to obtain agreement with the N_{sc} values determined by fitting the EIS spectra. It is most likely that the change of the slope of the M–S plots is a consequence of the fact that the capacitance is not an exactly parallel plate condenser but is represented by the *CPE* and, although the values of α are close to unity (0.95–0.98), the values of C_{sc} are sensitive to such small deviations from unity. It is also important to note that in case (b), at a frequency of 10 Hz (▽), such an approach is not recommended, since the slope of the corresponding M–S plot changes, leading to the eventual conclusion that the investigated oxide film is a p-type semiconductor. Usually such an approach is used in the literature[24,51–56] at only one constant frequency (1.0 kHz in most cases), assuming that at such a particular frequency, the system could be described by the serial connection of the solution resistance and the oxide film capacitance (neglecting the contribution of the double layer capacitance). This is a correct assumption but, on the other hand, for impedance spectra of almost all systems this assumption (simplification) is valid. Hence, it seems reasonable to avoid direct M–S plots and obtain correct values of C_{sc} by fitting the EIS results and then plotting the corresponding M–S plots.

CONCLUSIONS

According to the results presented in this paper, homogeneous, nano-crystalline passive films of Nb_2O_5 could be formed onto an Nb electrode by a proper potentiostatic pulse procedure at potentials more negative than 3.0 V *vs.* SCE at concentrations of NaOH equal to, or lower than, 2.50 M. It was shown that such films are n-type semiconductors. Their semiconducting properties were found to be different depending on the conditions of the film formation (NaOH concentration and pulse regime). In 5.00 M NaOH, the properties of the passive film could be explained by the surface charge model, with the passive oxide film being heterogeneous.

ИЗВОД

ПОЛУПРОВОДНИЧКА СВОЈСТВА ОКСИДНИХ ФИЛМОВА ФОРМИРАНИХ НА Nb ЕЛЕКТРОДИ У РАСТВОРУ NaOH

ВЛАДИМИР Д. ЈОВИЋ И БОРКА М. ЈОВИЋ

Институт за мултидисциплинарна истраживања, п. пр. 33, 11030 Београд

У овом раду приказани су резултати потенциостатског формирања хомогених и хетерогених, нано-кристалних, пасивних филмова Nb_2O_5 на електроди од ниобијума у растворима NaOH различитих концентрација и на потенцијалима мањим од 3,0 V према ЗКЕ. Полупроводничка својства оваквих филмова испитивана су EIS методом. Након фитовања EIS резултата одговарајућим еквивалентним колом одређиване су вредности “space charge” капацитета (C_{sc}) и “space charge” отпора (R_{sc}). Густина носилаца наелектрисања (N_{sc}), “flat band”

потенцијал (E_{fb}) и дебљина "space charge" слоја (d_{sc}) ових оксидних филмова одређена су из одговарајућих Mott–Schottky зависности. Показано је да се у 5,00 M NaOH формира хетерогени оксидни филм са отвореним порама (пукотинама) на површини, док се при нижим концентрацијама NaOH формира компактан и хомоген оксидни филм. Mott–Schottky зависности са позитивним нагибом, регистроване за све добијене филмове, потврђују да су из свих раствора добијени полупроводнички филмови n–типа.

(Примљено 26. јуна, ревидирано 27. августа 2007)

REFERENCES

1. Y. Zhao, Z. Zhang, Y. Lin, *J. Phys. D: Appl. Phys.* **37** (2004) 3392
2. J. J. van Gladbeek, R. E. van De Leest, *Thin Solid Films* **201** (1991) 137
3. N. Ozer, M. D. Rubin, C. M. Lampert, *Sol. Energy Mater. Sol. Cells* **40** (1996) 285
4. C. G. Granquist, *Solid State Ion.* **53** (1992) 479
5. D. Rosenfeld, R. Sanjines, F. Levy, P. A. Buffat, V. Demame, A. Gisel, *J. Vac. Sci. Technol.* **A12** (1994) 135
6. http://www.lem.uni-karlsruhe.de/forschung/niobiumoxide/niobiumoxide.html
7. *Tech Topics…The Leading Edge*, Vol. 11, No. 1, KEMET Electronics Corp., Greenville, SC, USA, 2001
8. T. Zednicek, S. Zednicek, Z. Sita, *Technical Information*, AVX Czech Republic s.r.o., AVX Corporation, 2007: http://www.avxcorp.com
9. A. Zylbersztejn, N. F. Mott, *Phys. Rev.* **B11** (1975) 4383
10. M. Gupta, A. J. Freeman, D. E. Ellis, *Phys. Rev.* **B16** (1977) 3338
11. D. Paquet, P. Leroux-Hugon, *Phys. Rev.* **B20** (1980) 5284
12. L. Young, *Anodic Oxide Films*, Academic Press, London, 1961
13. D. A. Vermilyea, in *Advances in Electrochemistry and Electrochemical Engineering*, P. Delahay, Ed., Vol. 3, Interscience, New York, 1963, Ch. 4
14. W. S. Goruk, L. Young, F. G. R. Zobel, in *Modern Aspects of Electrochemistry*, J. O'M. Bockris, Ed., Vol. 4, Plenum Press, New York, 1966, Ch. 3
15. M. J. Dignam, in *Comprehensive Treatise of Electrochemistry*, J. O'M. Bockris, B. E. Conway, E. Yeager, R. E. White, Eds., Vol. 4, Plenum Press, New York, 1981, Ch. 5
16. J. A. Davies, B. Domeij, J. P. S. Pringle, F. Brown, *J. Electrochem. Soc.* **112** (1965) 675
17. A. J. Schrijner, A. Middelhock, *J. Electrochem. Soc.* **111** (1964) 1167
18. D. K. Murti, R. Kelly, *Thin Solid Films* **33** (1976) 149
19. W. Schmickler, J. W. Schultze, in *Modern Aspects of Electrochemistry*, J. O'M. Bockris, B. E. Conway, R. E. White, Eds., Vol. 17, Plenum Press, New York, 1986, Ch. 5
20. S. R. Morrison, *Electrochemistry at Semiconductor and Oxidized Metal Electrodes*, Plenum Press, New York, 1980
21. P. Clechet, J. Martin, R. Oliver, C. Vallony, *C. R. Acad. Sci. Ser.* **C282** (1976) 887
22. A. J. Nozik, *Ann. Rev. Phys. Chem.* **29** (1978) 189
23. T. Hurlen, H. Bentzen, S. Hornkjøl, *Electrochim. Acta* **32** (1987) 1613
24. W. A. Badawy, A. G. Gad-Allah, H. H. Rehan, *J. Appl. Electrochem.* **17** (1987) 559
25. A. G. Gad-Allah, *J. Appl. Electrochem.* **21** (1991) 346
26. A. Robin, *J. Appl. Electrochem.* **32** (2004) 623
27. G. E. Cavigliasso, M. J. Esplandiu, V. A. Macagno, *J. Appl. Electrochem.* **28** (1998) 1213
28. I. Lj. Arsova, A. R. Prusi, Lj. D. Arsov, *J. Solid State Electrochem.* **7** (2003) 217
29. I. Arsova, P. Abduraf, T. Grčev, Lj. Arsov, *J. Serb. Chem. Soc.* **71** (2006) 177.
30. I. Mickova, A. Prusi, T. Grcev, Lj. Arsov, *Croat. Chim. Acta* **79** (2006) 527

31. I. Sieber, H. Hildebrand, A. Friedrich, P. Schmuki, *Electrochem. Comm.* **7** (2005) 97
32. C. Baruffaldi, U. Casellato, S. Cattarin, M. Musiani, B. Tribollet, B. Vercelli, *Electrochim. Acta* **47** (2002) 2989
33. C. Baruffaldi, R. Bertoncello, S. Cattarin, P. Guerriero, M. Musiani, *J. Electroanal. Chem.* **545** (2003) 65
34. S. Cattarin, M. Musiani, *J. Electroanal. Chem.* **517** (2001) 101
35. J. Choi, J. H. Lim, J. Lee, K. J. Kim, *Nanotechnol.* **18** (2007) 055603
36. M. Bojinov, I. Betova, R. Raicheff, *J. Electroanal. Chem.* **411** (1996) 37
37. M. Bojinov, I. Kanazirski, A. Girginov, *Electrochim. Acta* **41** (1996) 2695
38. M. Bojinov, *Electrochim. Acta* **42** (1997) 3489
39. J. R. MacDonald, *Impedance Spectroscopy Emphasizing Solid Materials and Systems*, Wiley, New York, 1987
40. K. Sugimoto, G. Belanger, D. Piron, *J. Electrochem. Soc.* **126** (1979) 535
41. V. Lokshtanov, A. Rotinyan, *Elektrokhimiya* **5** (1969) 873
42. C. D. Alkaine, L. De Souza, F. Nart, *Corr. Sci.* **34** (1993) 109
43. J. van Muylder, N. De Zubov, M. Pourbaix, *Rapport Technique RT-53 of CEBELCOR*, 1957
44. http://www.gamry.com/App_Notes/PDF/jovic.pdf
45. C. H. Hsu, F. Mansfeld, *Corrosion* **57** (2001) 747
46. M. E. Orazem, P. Shukla, M. A. Membrino, *Electrochim. Acta* **47** (2002) 2027
47. V. D. Jović, M. W. Barsoum, B. M. Jović, A. Ganguly, T. El-Raghy, *J. Electrochem. Soc.* **153** (2006) B238
48. N. Ibris, J. C. Mirza Rosca, *J. Electroanal. Chem.* **526** (2002) 53
49. W. Wilhelmsen, *Electrochim. Acta* **33** (1988) 63
50. C. Y. Chao, L. F. Lin, D. D. MacDonald, *J. Electrochem. Soc.* **128** (1981) 1187
51. E. Sikora, D. D. MacDonald, *J. Electrochem. Soc.* **147** (2000) 4087
52. E.-J. Lee, S.-I. Pyun, *J. Appl. Electrochem.* **22** (1992) 156
53. S. Kudelka, J. W. Schultze, *Electrochim. Acta* **42** (1997) 2817
54. W. P. Gomes, D. Vanmaekelbergh, *Electrochim. Acta* **41** (1996) 967
55. J. Sikora, E. Sikora, D. D. MacDonald, *Electrochim. Acta* **45** (2000) 1875
56. E. Sikora, D. D. MacDonald, *Electrochim. Acta* **48** (2002) 69.

Journal of the Serbian Chemical Society
eVersion electronic
JSCS@tmf.bg.ac.yu • www.shd.org.yu/JSCS

J. Serb. Chem. Soc. 73 (3) 369–376 (2008) UDC 546.815'711'24:546.815'24'22:534:543.42–74
JSCS–3718 *Original scientific paper*

Plasmon – two phonon interaction in PbMnTe and PbTeS alloys

JELENA TRAJIĆ[1]*, NEBOJŠA ROMČEVIĆ[1], MAJA ROMČEVIĆ[1]
and VLADIMIR N. NIKIFOROV[2]

[1]Institute of Physics, Department for Solid State Physics and New Materials, P. O. Box 68,
11001 Belgrade, Serbia and [2]Department of Low-Temperature Physics,
Moscow State University, Moscow, Russia

(Received 18 December 2006)

Abstract: In this work far-infrared spectroscopy over a wide temperature range was used to investigate the vibration properties of $Pb_{1-x}Mn_xTe$ ($x \leq 0.12$) and $PbTe_{1-x}S_x$ ($x \leq 0.05$) single crystals. In the analysis of the experimental results, a dielectric function which in advance takes into account the existence of plasmon – two phonon interaction was employed. As a result of the best fit, the three frequencies of the coupled modes were obtained and then the values for the two LO modes and the plasma frequency (ω_P) were calculated. It was found that the phonons in $PbTe_{1-x}S_x$ and $Pb_{1-x}Mn_xTe$ showed two-mode behavior (each TO–LO mode pair for the end members degenerates to an impurity mode).

Keywords: semimagnetic semiconductors; far-infrared spectroscopy; vibration properties; phonon behavior.

INTRODUCTION

The lead telluride family of the IV–VI compounds are narrow-band gap semiconductors. Depending on the composition, their band gap can vary from almost zero to 0.30 eV.[1–5] Lead telluride and its solid solutions are used for active and passive devices. Namely, it is well known[3] that in lead chalcogenides electrically active native point defects (vacancies and interstitial atoms) produce energy states lying either above the bottom of the conduction band (donor defects) or below the top of the valence band (acceptors). This leads to high charge carrier concentrations in undoped crystals because of the deviation of the composition from stoichiometry. Furthermore, neither cooling nor a magnetic field has been observed to have a freeze-out effect on the charge carriers.

Solid solution $Pb_{1-x}Mn_xTe$ are semimagnetic semiconductors which have not been sufficiently studied.[6–9] Their crystal structure is cubic (NaCl-type), the lattice parameter changes linearly with the content of manganese concentration.

---

[*] Corrresponding author. E-mail: jelena@phy.bg.ac.yu

doi: 10.2298/JSC0803369T

If the manganese concentration is less than 20 at. %, Mn enters the PbTe lattice as Mn^{2+}, and is not an electroactive dopant. Doping of PbTe with Mn increases the band gap at the rate $\partial E_g/\partial x \cong 38–48$ meV/% MnTe[10] but does not provide for the appearance of local or quasi-local levels in the vicinity of the actual bands.[7]

$PbTe_{1-x}S_x$ is a narrow band gap semiconductor with a direct band gap in the infrared region.[4] Recent experimental studies[11,12] indicate that there is a second-order phase transition in the $PbTe_{1-x}S_x$ system. The phonon properties of $PbTe_{1-x}S_x$ have not yet been studied. Nevertheless, it is obvious that $PbTe_{1-x}S_x$ alloys cannot be treated by simply interpolating the phonon behavior between the two end-point materials. In addition, the subject of the former investigations was a mixed crystal with a relatively high concentration of sculpture.[12] Far-infrared spectroscopy is a powerful technique for investigation in this field.

In this paper, the results obtained using far infrared spectroscopy (FIR) to study the optical properties of $PbMn_{1-x}Te_x$ and $PbTe_{1-x}S_x$ mixed crystals are presented.

EXPERIMENTAL

The synthesis procedure for the preparation of single crystals of $Pb_{1-x}Mn_xTe$ has already been described in previous papers.[13-15] Briefly, single crystals of $Pb_{1-x}Mn_xTe$ were grown by a modified Bridgman method with a lowered rate of 1.0°mm h^{-1}. The sample was obtained from the elements of high purity. The chemical composition of the samples was checked by an electron microprobe, which revealed good chemical homogeneity of the material.

The chemical composition of $Pb_{1-x}Mn_xTe$ crystals were determined by the XRD technique.[13,14] All the samples were examined under the same conditions using a Philips PW 1729 X-ray generator, a Philips 1710 diffractometer and original APD software.

Single crystals of $PbTe_{1-x}S_x$ alloys were grown by the vapor–liquid–solid (VLS) technique, using metal and chalcogenide atoms of high purity as the source materials. The chemical composition of the sample was controlled by X-ray microprobe investigation. Far-infrared reflection spectra were measured between 10 K and 300 K on a BOMEM DA8 spectrometer.

Reflectivity analysis and fitting procedure

The theoretical model for the bulk dielectric function has been discussed by several authors.[16,17] It should be noticed briefly that the low-frequency dielectric properties of PbTe and related compounds have been described with not less than two classical oscillators ($l \geq 2$) corresponding to the TO-modes, superimposed by a Drude part, which takes into account the contribution of free carriers:[18]

$$\varepsilon_S(\omega) = \varepsilon_\infty + \sum_{k=1}^{l} \frac{\varepsilon_\infty\left(\omega_{LOk}^2 - \omega_{TOk}^2\right)}{\omega_{TOk}^2 - \omega^2 - i\gamma_{TOk}\omega} - \frac{\varepsilon_\infty \omega_P^2}{\omega(\omega + i\gamma_P)} \tag{1}$$

where ε_∞ is the bound charge contribution and is considered as a constant, ω_{LOk} and ω_{TOk} are the longitudinal and transverse optical-phonon frequencies, respectively, ω_P is the plasma frequency, γ_{TOk} and γ_P are the phonon and plasma damping, respectively. In the PbTe-based systems, the pure LO-modes ($\omega_{LO,PbTe}$) of the lattice are strongly influenced by the plasmon mode (ω_P) of free carriers. As a result, combined plasmon-LO phonon modes ($\omega_\pm$) were observed.[19]

Bearing this in mind, in the analysis of the reflectivity spectra of $Pb_{1-x}Mn_xTe$ and $PbTe_{1-x}S_x$, it was decided to use a dielectric function which takes into account the existence of plasmon-LO phonon interaction in advance:[20]

$$\varepsilon(\omega)=\varepsilon_{\infty}\frac{\prod_{j=1}^{m+n}\left(\omega^{2}+i\gamma_{lj}\omega-\omega_{lj}^{2}\right)}{\omega^{m}\prod_{i=1}^{m}\left(\omega+i\gamma_{\mathrm{P}i}\right)\prod_{i=1}^{n}\left(\omega^{2}+i\gamma_{ti}\omega-\omega_{ti}^{2}\right)}\prod_{k=1}^{s}\frac{\omega^{2}+i\gamma_{k\mathrm{LO}}-\omega_{k\mathrm{LO}}^{2}}{\omega^{2}+i\gamma_{k\mathrm{TO}}-\omega_{k\mathrm{TO}}^{2}} \tag{2}$$

The first term in Eq. (2) represents the coupling of *m* plasmons and *n* phonons, and the second term represents uncoupled modes of the crystal (*s*), also $l = n + s$. The ω_{lj} and γ_{lj} parameters of the first numerator are eigenfrequencies and damping coefficients of the longitudinal plasmon – *n* phonon waves. The parameters of the first denominator correspond to the corresponding characteristics of the transverse (TO) vibrations. In the second term ω_{LO} and ω_{TO} are the longitudinal and transverse frequencies, respectively, and γ_{LO} and γ_{TO} are damping. Therefore, the determinations of the LO-mode and plasma frequency are connected with a decoupled procedure.

A situation which considers the coupling of one plasmon and one phonon is explained in detail in the literature.[20] In this work, when the existence of this interaction in cases of $Pb_{0.98}Mn_{0.02}Te$ and $PbTe_{0.95}S_{0.05}$ alloys was taken into account and then the influence of free carrier eliminated, satisfactory results were not obtained. Considering this fact, it was decided to use a dielectric function which takes into account the existence of plasmon-two LO phonon interactions in the analysis of reflectivity spectra of $Pb_{0.98}Mn_{0.02}Te$ and $PbTe_{0.95}S_{0.05}$ alloys. This corresponds to $l = 2$ in dielectric function given by Eq. (1). The positions of the coupled modes are defined as the solutions of the real part of Eq. (1) ($\mathrm{Re}\{\varepsilon_{\mathrm{S}}\} = 0$). In this case, there are three coupled modes, which can be calculated by solving the Equations:

$$\omega^{6}-A\omega^{4}-B\omega^{2}-C=0 \tag{3}$$

$$A=\omega_{\mathrm{LO1}}^{2}+\omega_{\mathrm{LO2}}^{2}+\omega_{\mathrm{P}}^{2}\ ,\ \ B=\omega_{\mathrm{LO1}}^{2}\omega_{\mathrm{LO2}}^{2}+\omega_{\mathrm{P}}^{2}(\omega_{\mathrm{TO1}}^{2}+\omega_{\mathrm{TO2}}^{2})\ ,\ \ C=\omega_{\mathrm{TO1}}^{2}\omega_{\mathrm{TO2}}^{2}\omega_{\mathrm{P}}^{2} \tag{4}$$

If the dielectric function defined by Eq. (2) is used, the values of the initial ω_{LO1}, ω_{LO2} and ω_{P} modes can be determined by:

$$\omega_{P}=\frac{\omega_{l1}\omega_{l2}\omega_{l3}}{\omega_{t1}\omega_{t2}} \tag{5}$$

$$\begin{aligned}\omega_{\mathrm{LO1,2}}^{2}=&\frac{1}{2}\left(\omega_{l1}^{2}+\omega_{l2}^{2}+\omega_{l3}^{2}-\omega_{\mathrm{P}}^{2}\right)\pm\\&\pm\sqrt{\frac{1}{4}(\omega_{l1}^{2}+\omega_{l2}^{2}+\omega_{l3}^{2}-\omega_{\mathrm{P}}^{2})^{2}-\omega_{l1}^{2}\omega_{l2}^{2}-\omega_{l1}^{2}\omega_{l3}^{2}-\omega_{l2}^{2}\omega_{l3}^{2}+\omega_{P}^{2}(\omega_{t1}^{2}+\omega_{t2}^{2})}\end{aligned} \tag{6}$$

The parameters adjustment was performed automatically by means of the least-square fitting of the theoretical (*R*) and experimental (R_e) reflection coefficients at *k* points arbitrarily chosen:

$$\chi=\sqrt{\frac{1}{k}\sum_{j=1}^{k}(R_{ej}-R_{j})^{2}}\ ,\ \ R=\left|\frac{\sqrt{\varepsilon}-1}{\sqrt{\varepsilon}+1}\right|^{2} \tag{7}$$

where ε is given by Eq. (1) or (2). The value of χ was minimized until it become comparable with the usual experimental error. Practically, for all samples the determined errors of the eigenfrequencies and damping coefficients were about 3–6 % and 10–15 %, respectively.

RESULTS AND DISCUSSION

$Pb_{0.98}Mn_{0.02}Te$ *single crystal*

The far-infrared reflection spectra of the $Pb_{0.98}Mn_{0.02}Te$ single crystal sample are shown in Fig. 1. The experimental data are presented with circles. The solid lines in Fig. 1 were obtained using the dielectric function from Eq. (2). An oscillator of weak intensity, at about 70 cm^{-1} (denoted by * in Fig. 1), is a Brillouin zone edge mode because the phonon density of PbTe has a maximum at these frequencies.[21]

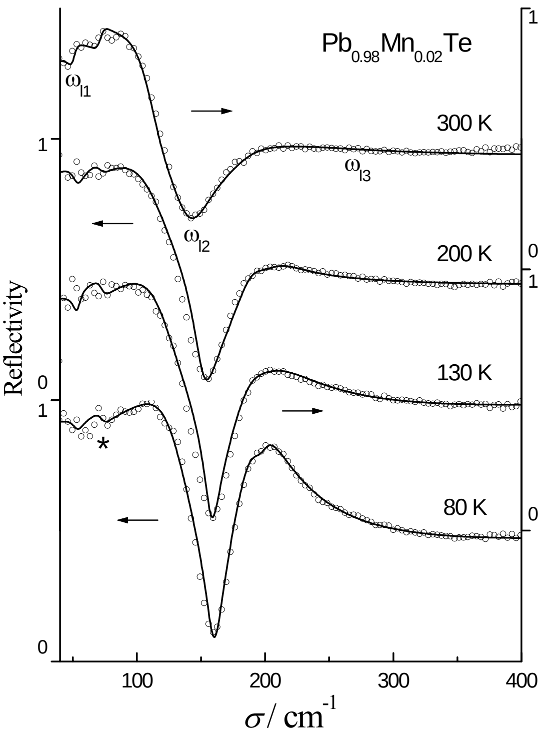

Fig.1. Far-infrared reflection spectra of $Pb_{0.98}Mn_{0.02}Te$ single crystal. Experimental spectra are presented by circles. The solid lines are calculated spectra obtained by a fitting procedure based on the model given by Eq. (2).

From the best fit, the frequencies of the coupled modes (ω_{l1}, ω_{l2} and ω_{l3}), marked in Fig. 1, and then the values for ω_{LO1}, ω_{LO2} and ω_P were calculated in the way described above. The characteristic parameters obtained in this way are shown in Fig. 2.

In Fig. 2, the solid circles (●) refer to the eigenfrequency spectra ω_{lj} obtained by Eq. (2). The solid lines in Fig. 2 were obtained by application of Eq. (3). The agreement of the plasmon – two LO phonon mode frequencies calculated in such a way with the experimentally determined values is very good. The open circles (○) in Fig. 2 represent the calculated values for ω_{LO1} and ω_{LO2} (Eq. (6)) and the experimentally determined values for ω_{TO1} and ω_{TO2} are denoted by stars (∗). The values determined in this way are in excellent agreement with calculated values based on the Genzel model,[22] mentioned above. The obtained results presented in Fig. 2 are the best demonstration of the fact that use of the dielectric function given by Eq. (2) is justifiable. Also, the results shown in Fig. 2 suggest that the optical phonons in $Pb_{1-x}Mn_xTe$ mixed crystals (Fig. 3) exhibit the well-known two-mode behavior (each TO–LO mode pair of the end members degenerates to an impurity mode), according to the notation of Genzel.[22] The behavior of the optical phonon modes is presented in Fig. 3. The solid lines were obtained employing the Genzel model. The experimental values are indicated by the same marks as used in Fig. 2.

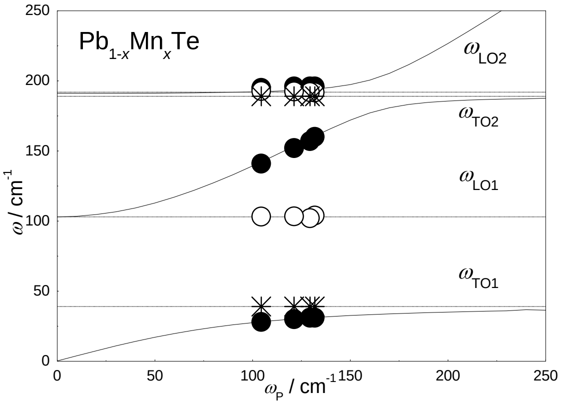

Fig. 2. The eigenfrequencies of the plasmon – two LO phonon modes (solid lines – Eq.(3)); ● – eigenfrequency spectra ω_{lj} obtained by Eq. (2); ○ – calculated values for ω_{LOi} (Eq. (6)) and ✳ - experimentally determined values for ω_{TOi}.

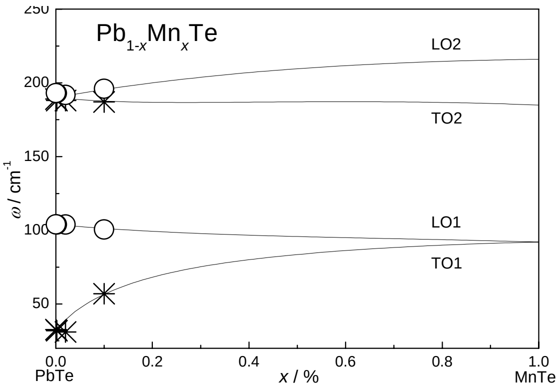

Fig. 3. Concentration dependence of the optical mode frequencies of $Pb_{1-x}Mn_xTe$ mixed crystal. ○ – calculated values for ω_{LO1} and ω_{LO2} (Eq. (6)); ✳ - ω_{TO}.

$PbTe_{0.95}S_{0.05}Te$ single crystal

The far-infrared reflection spectra of the $PbTe_{0.95}S_{0.05}$ single crystal sample are shown in Fig. 4, with the same notation as in the case of the $Pb_{0.98}Mn_{0.02}Te$ alloy described above.

The calculated values for ω_{LO1} and ω_{LO2} from Eq. (6) and the experimenttally determined values for ω_{TO1} and ω_{TO2} (Eq. (2)) for the $PbTe_{0.95}S_{0.05}$ single crystal are presented in Fig. 5. As can be seen, the agreement of the plasmon – two LO phonon mode frequencies calculated using Eq. (3) (solid line) with the experimentally determined values for ω_{l1}, ω_{l2} and ω_{l3} (Eq. 2) is very good.

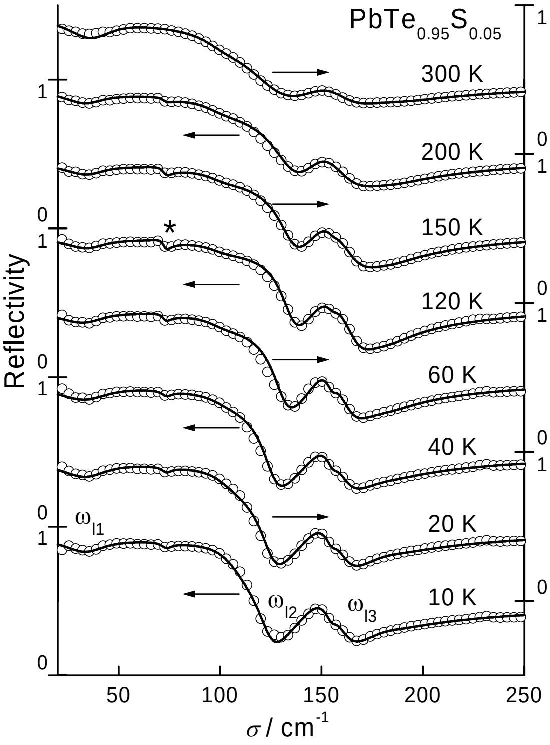

Fig.4. Far-infrared reflection spectra of a $PbTe_{0.95}S_{0.05}$ single crystal. Experimental spectra are presented by circles. The solid lines are calculated spectra obtained by a fitting procedure based on the model given by Eq. (2).

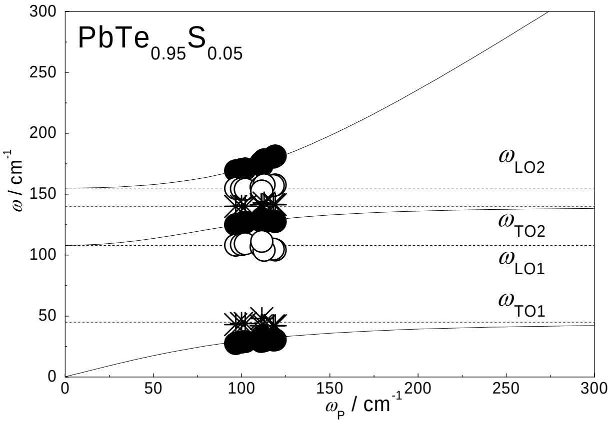

Fig.5. The eigenfrequencies of the plasmon – two LO phonon modes (solid lines – Eq. (3)); ● – eigenfrequency spectra ω_{lj} obtained using Eq. (2); ○ – calculated values for ω_{LOi} (Eq. (6)) and ✳ - experimentally determined values for ω_{TOi}.

The mode frequencies determined on this way suggest that the optical phonons in $PbTe_{1-x}S_x$ mixed crystals exhibit a two-mode behavior according to Genzel notation,[22] which is presented in Fig. 6.

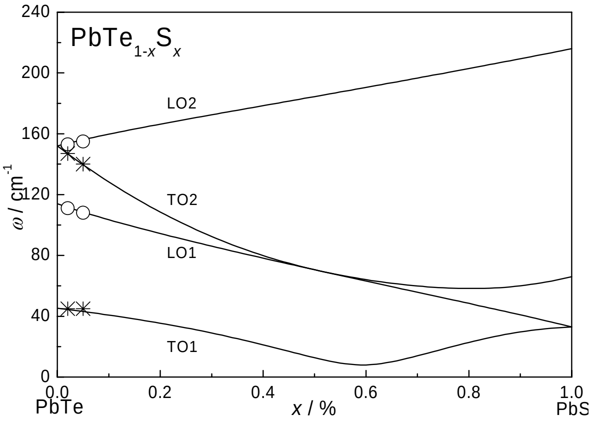

Fig.6. Concentration dependence of the optical mode frequencies of $PbTe_{1-x}S_x$ mixed crystals. ○ – calculated values for ω_{LO1} and ω_{LO2} (Eq. (6)); ✳ - ω_{TO}.

CONCLUSION

As a method for investigating the phonon properties of $Pb_{1-x}Mn_xTe$ and $PbTe_{1-x}S_x$ mixed crystals, far-infrared spectroscopy was employed. In spite of the strong plasmon – two LO phonon interaction, it was found that the long wavelength optical phonon modes of these mixed crystals exhibited a two-mode behavior.

Acknowledgements. This work was supported by Serbian Ministry of Science under Project 141028B.

ИЗВОД

ПЛАЗМОН – ДВО ФОНОН ИНТЕРАКЦИЈА КОД PbMnTe И PbTeS ЛЕГУРА

ЈЕЛЕНА ТРАЈИЋ[1], НЕБОЈША РОМЧЕВИЋ[1], МАЈА РОМЧЕВИЋ[1] и ВЛАДИМИР Н. НИКИФОРОВ[2]

[1]*Институт за физику, Центар за физику чврстог стања и нове материјале, п. пр. 68, 11001 Београд и*
[2]*Department of Low-Temperature Physics, Moscow State University, Moscow, Russia*

У овом раду су представљени резултати проучавања вибрационих својстава монокристала $Pb_{1-x}Mn_xTe$ ($x \leq 0{,}12$) и $PbTe_{1-x}S_x$ ($x \leq 0{,}05$) применом далеке инфрацрвене спектроскопије. Приликом анализе експерименталних резултата коришћена је диелектрична функција која унапред узима у обзир постојање плазмон – дво фонон интеракције. Као резултат најбољег фита, добијају се три учестаности спрегнутих модова и онда израчунавају вредности учестаности два LO мода и плазма учестаност (ω_P). Установили смо да оптички фонони у $PbTe_{1-x}S_x$ и $Pb_{1-x}Mn_xTe$ испољавају дво-модни тип понашања (сваки TO–LO пар модова се дегенерише у примесни мод).

(Примљено 18. децембра 2006)

REFERENCES

1. M. E. Lines, A. M. Glass, *Principles and Applications of Ferroelectrics and Related Materials, The Int. Series of Monographs on Physics*, Clarendon, Oxford, 1977
2. H. Kawamura, in *Narrow-Gap Semiconductors, Physics and Applications, Lecture Notes in Physics*, Vol. 33, W. Zawadski, Ed., Springer, Berlin, 1980

3. B. A. Volkov, L. I. Ryabova, D. R. Khokhlov, *Uspekhi Fizicheskih Nauk*, Russian Academy of Science **8** (2002) 875 [*Physics – Uspekhi* **8** (2002) 819]
4. T. Shimada, Kh. I. Kobayasi, Y. Katayama, K. F. Komatsubara, *Phys. Rev. Lett.* **39** (1977) 143
5. W. Jantsch, A. Lopez-Ortego, G. Bauer, *Infrared Phys.* **18** (1978) 877
6. D. G. Adrianov, C. A. Belokon, C. O. Klimonskii, V. M. Lakeenkov, *Fiz. Tekh. Poluprovodn.* **22** (1988) 670
7. J. Niewodniczanska-Zawadzka, G. Elsinger, L. Pametshofer, *Physica B&C* **C117** (1983) 458
8. A. V. Brodovoi, G. V. Lashkarev, M. B. Radchenko, E. I. Sl’inko, K. D. Tovstuk, *Fiz. Tekh. Poluprovodn.* **18** (1984) 1547 [*Sov. Phys. Semicond.* **18** (1984) 970]
9. J. Nuerwirth, W. Jantsch, L. Palmetchhofer, W. Zulehner, *J. Phys. C* **19** (1986) 2475
10. Z. Korczak, M. Subotowicz, *Phys. Stat. Sol. (a)* **77** (1983) 497
11. Kh. A. Abdulin, A. I. Lebedev, A. M. Gas'kov, V. N. Demin, V. P. Zlomanov, *Pi'ma Zh. Eksp. Teor. Fiz.* **40** 229 (1984) [*JETP Lett.* **40** (1984) 998]
12. Z. Vang, B. A. Bunker, *Phys. Rev. B* **46** (1992) 11277
13. A. Golubović, S. Nikolić, J. Trajić, S. Đurić, N. Romčević, M. Romčević, A. J. Nadolny, B. Taliashvili, V. Domukhovski, V. N. Nikiforov, *Mat. Sci. Forum* **453** (2004) 99
14. N. Romčević, A. Golubović, M. Romčević, J. Trajić, S. Nikolić, S. Đurić, V. N. Nikiforov, *J. Alloys Comp.* **402** (2005) 36
15. J. Trajić, M. Romčević, N. Romčević, S. Nikolić, A. Golubović, S. Đurić, V. N. Nikiforov, *J. Alloys Comp.* **365** (2004) 89
16. E. Burstein, A. Pinczuk, R. F. Wallis, in *The Physics of Semimetals and Narrow-Gap Semiconductors*, D. L. Carter, R. T. Bate, Eds., Pergamon, New York, 1971, p. 251.
17. M. A. Kinch, D. D. Buss, *Solid State Commun.* **11** (1972) 319
18. V. Gopal, *Infrared Phys.* **18** (1978) 121
19. S. Takaoka, T. Hamaguchi, S. Shimomura, K. Murase, *Solid State Commun.* **54** (1985) 99
20. A. A. Kuharskii, *Solid State Commun.* **8** (1970) 1275
21. W. Cochran, R. A. Cowley, G. Dolling, M. M. Elcombe, *Proc. Royal. Soc.* **A293** (1966) 433
22. L. Genzel, T. P. Martin, C. H. Perry, *Phys. Status Solidi (b)* **62** (1974) 83.

JSCS@tmf.bg.ac.yu • www.shd.org.yu/JSCS

J. Serb. Chem. Soc. *73* (3) 377–384 (2008) UDC 546.682'86'815:544.344+544.015.3:536.7
JSCS–3719 *Original scientific paper*

Prediction of phase equilibria in the In–Sb–Pb system

DUŠKO MINIĆ[1]*, DRAGAN MANASIJEVIĆ[2#], DRAGANA ŽIVKOVIĆ[2#],
NADA ŠTRBAC[2] and ZVONIMIR STANKOVIĆ[2]

[1]*University of Priština, Mining and Metallurgy Faculty, 38220 Kosovska Mitrovica and*
[2]*University of Belgrade, Technical Faculty, VJ 12, 19210 Bor, Serbia*

(Received 30 June 2007)

Abstract: Binary thermodynamic data, successfully used for phase diagram calculations of the binary systems In–Sb, Pb–Sb and In–Pb, were used for the prediction of the phase equilibria in the ternary In–Sb–Pb system. The predicted equilibrium phase diagram of the vertical Pb–InSb section was compared with the results of differential thermal analysis (DTA) and optical microscopy. The calculated phase diagram of the isothermal section at 300 °C was compared with the experimentally (SEM, EDX) determined composition of phases in the chosen alloys after annealing. Very good agreement between the binary-based thermodynamic prediction and the experimental data was found in all cases. The calculated liquidus projection of the ternary In–Sb–Pb system is also presented.

Keywords: In–Sb–Pb system; phase diagram; thermodynamics.

INTRODUCTION

Knowledge of phase equilibria in ternary systems of the corresponding metals with elements of III–V compound semiconductors is an important step towards a better understanding of contact formation and presents a basis for the development of new and improved contact materials.

In previous studies related to phase equilibria in ternary systems with III–V compounds, the phase equilibria in Ga–Sb–Pb and In–Sb–Bi ternary systems were investigated,[1,2] using experimental techniques (SEM–EDX and DTA) and the analytical CALPHAD approach. However, thermodynamic modeling of the ternary In–Sb–Pb system still has not been presented in the literature.

The aim of this study was to calculate phase equilibria of the In–Sb–Pb system according to the CALPHAD method[3–5] and to compare the obtained results with experimentally based results from this work and the literature.

---

* Corresponding author. E-mail: dminic65@ptt.yu

[#] Serbian Chemical Society member.

doi: 10.2298/JSC0803377M

THERMODYNAMIC MODELING

Pure elements

The pure solid elements at 298.15 K and 1.0 bar in their stable form were chosen as the reference state for the systems (SER). Version 4.4 of the SGTE unary database (scientific group thermodata Europe) of the phase stabilities for stable and metastable states of the pure elements was used.[6]

Binary systems

The thermodynamic descriptions of the binary alloys, *i.e.*, the In–Sb system,[7] the Pb–Sb system[8] and the In–Pb system,[9] were taken from the literature.

Liquid and solid solution phases

The molar Gibbs energies of liquid and solid solution phases, referred to the enthalpies of the pure elements in their stable state at 298.15 K, ${}^{0}H_{i}^{\mathrm{SER}}(298.15\ \mathrm{K})$, are described by the sub-regular solution model with the Redlich–Kister polynomial as follows:

$$\begin{aligned}G_{m}^{\varphi} - \sum_{i=\mathrm{A,B,C}} x_{i}^{\varphi}\,{}^{0}H_{i}^{\mathrm{SER}} &= \\ &= \sum_{i=\mathrm{A,B,C}} x_{i}^{\varphi}\left({}^{0}G_{i}^{\varphi} - {}^{0}H_{i}^{\mathrm{SER}}\right) + RT \sum_{i=\mathrm{A,B,C}} x_{i}^{\varphi}\ln\left(x_{i}^{\varphi}\right) + G^{\varphi,\mathrm{xs}}\end{aligned} \tag{1}$$

where $G^{\varphi,\mathrm{xs}}$ represents the excess Gibbs energy of a ternary solution expressed by the Redlich–Kister–Muggianu expression:

$$\begin{aligned}G^{\varphi,\mathrm{xs}} &= x_{\mathrm{A}}^{\varphi}x_{\mathrm{B}}^{\varphi}\sum_{\nu=1}^{n}{}^{\nu}L_{\mathrm{A,B}}^{\varphi}\left(x_{\mathrm{A}}^{\varphi} - x_{\mathrm{B}}^{\varphi}\right)^{\nu} + \\ &+ x_{\mathrm{B}}^{\varphi}x_{\mathrm{C}}^{\varphi}\sum_{\nu=1}^{n}{}^{\nu}L_{\mathrm{B,C}}^{\varphi}\left(x_{\mathrm{B}}^{\varphi} - x_{\mathrm{C}}^{\varphi}\right)^{\nu} + x_{\mathrm{C}}^{\varphi}x_{\mathrm{A}}^{\varphi}\sum_{\nu=1}^{n}{}^{\nu}L_{\mathrm{C,A}}^{\varphi}\left(x_{\mathrm{C}}^{\varphi} - x_{\mathrm{A}}^{\varphi}\right)^{\nu} + x_{\mathrm{A}}^{\varphi}x_{\mathrm{B}}^{\varphi}x_{\mathrm{C}}^{\varphi}L_{\mathrm{A,B,C}}^{\varphi}\end{aligned} \tag{2}$$

where ${}^{\nu}L_{\mathrm{A,B}}^{\varphi}$ is the temperature-dependent binary parameter optimized on the basis of the available thermodynamic and phase diagram data, and *i*, *j* are the elements of the system.

The term ${}^{\nu}L_{\mathrm{A,B,C}}^{\varphi}$ is a ternary interaction parameter, which is expressed as:

$$x_{\mathrm{A}}^{\varphi}x_{\mathrm{B}}^{\varphi}x_{\mathrm{C}}^{\varphi}L_{\mathrm{A,B,C}}^{\varphi} = x_{\mathrm{A}}^{\varphi}x_{\mathrm{B}}^{\varphi}x_{\mathrm{C}}^{\varphi}(x_{\mathrm{A}}^{\varphi}\,{}^{0}L_{\mathrm{A,B,C}}^{\varphi} + x_{\mathrm{B}}^{\varphi,1}L_{\mathrm{A,B,C}}^{\varphi} + x_{C}^{\varphi,2}L_{\mathrm{A,B,C}}^{\varphi}) \tag{3}$$

The terms $L_{i,j}^{\varphi}$, which can be temperature-dependent, are expressed by:

$${}^{\nu}L_{i,j}^{\varphi} = {}^{\nu}A_{i,j}^{\varphi} + {}^{\nu}B_{i,j}^{\varphi}T + \ldots \tag{4}$$

InSb stoichiometric compound

The InSb phase is a stoichiometric compound. The Gibbs energy of the compound, *i.e.*, $\mathrm{X}_{m}\mathrm{Y}_{n}$, is generally described as:

$$G_m^{X_mY_n} = \frac{m}{m+n}G_X + \frac{n}{m+n}G_Y + \Delta G_{X_mY_n}^{f} \tag{5}$$

where $\Delta G_{X_mY_n}^{f}$ represents the Gibbs energy of formation per mole of atoms of the X_mY_n compound and is expressed by the following equation:

$$\Delta G_{X_mY_n}^{f} = A + BT \tag{6}$$

The Pb–In–Sb ternary system

There are only three references concerning the thermodynamic properties and phase equilibria of alloys of the Pb–In–Sb ternary system.

Predel and Gerdes[10] determined the enthalpy changes of mixing molten InSb with liquid lead at 883 K using a high temperature calorimeter. The results were discussed with the aid of the regular solution model and also under the assumption of the existence of InSb associates in the ternary melt.

Geis and Peretti[11] experimentally investigated lead-rich and antimony-rich regions of the Pb–In–Sb ternary system and gave a partial liquidus projection for the concentration range InSb–Pb–Sb. Minić *et al.*[12] researched the thermodynamic properties of some alloys in the Pb–In–Sb ternary system using an Oelsen calorimetry and general solution model calculations.

EXPERIMENTAL

Alloys of the In–Sb–Pb system were prepared from the pure metals (99.99 %) by melting weighed amounts of indium, antimony and lead under an argon atmosphere.

After melting, alloys were subjected to a homogenizing annealing in evacuated glass capsules. The samples were annealed at 300 °C for 100 h. After annealing, the samples to be used for DTA measurements were cooled inside the furnace to the room temperature, while the samples for SEM–EDX investigation were quenched into ice water from 300 °C.

DTA Measurements were performed with a Derivatograph 1500 (MOM Budapest) apparatus under the following conditions: air atmosphere, heating rate 10 °C min^{-1}. The total mass of each sample was approximately 2 g. The precision of the measurement in the investigated temperature interval was ±2 °C.

The equilibrium compositions in the quenched samples were determined using a JEOL scanning electron microscope with an accelerating voltage of 20 kV and an EDX analyzer.

Optical microscopy was performed using a Reichert MeF2 microscope.

RESULTS AND DISCUSSION

The values of the integral molar Gibbs excess energies, G_{ij}^{E}, for the constitutive binary systems In–Sb, Pb–Sb and In–Pb, taken from Ansara *et al.*[7], Ohtani and Ishida[8] and Bolcavage *et al.*,[9] respectively, were used as the starting binary thermodynamic data for the calculation. All these data, given in Table I, are included in the COST 531 binary database.[13]

Gibbs energy of the intermediate InSb phase was optimized by Ansara *et al.*[7] as:

G(ZINCBLENDE_B3,IN:SB;0)= 0.5*GHSERIN+0.5*GHSERSB –15849.3 +
+ .293139*T + 1.293581*T*LN(T) (298.14< T < 3000.00)

Calculation of the characteristic phase diagrams of the In–Sb–Pb system was performed using Thermo-Calc software (TC4A version).

TABLE I. The Redlich–Kister parameters for the constitutive binary systems

Phase	Parameter	In-Pb[9]	In-Sb[7]	Pb-Sb[8]
FCC_A1	$^{0}L_{\mathrm{A,B}}$	4846.2–2.56363*T	–20000+15*T	11400–22.66*T
	$^{1}L_{\mathrm{A,B}}$	305.1	-	-
LIQUID	$^{0}L_{\mathrm{A,B}}$	3771.4–0.96292*T	25631.2+102.9324*T– –13.45816*T*LN(T)	110–2.5*T
	$^{1}L_{\mathrm{A,B}}$	207.7	–2115.4–1.31907*T	–420+1.05*T
	$^{2}L_{\mathrm{A,B}}$	–	2908.9	0.36*T
TETRAGONAL_A6	$^{0}L_{\mathrm{A,B}}$	–3118.2	–	–
	$^{1}L_{\mathrm{A,B}}$	3741.1	–	–
TET_ALPHA1	$^{0}L_{\mathrm{A,B}}$	3207.99–2.1104311*T	–	–
	$^{1}L_{\mathrm{A,B}}$	–2075.44+7.9804712*T	–	–
RHOMBOHEDRAL_A7	$^{0}L_{\mathrm{A,B}}$	6000	15*T	21360–5.66*T

In order to experimentally verify the calculated phase diagram of the InSb–Pb section, alloys with 20, 40, 60, 80 and 90 at. % of lead were studied in this work by means of DTA and optical microscopy.

The results of the DTA measurements are given in Table II, together with the interpretation of the various thermal effects. To test the reproducibility of the results, every measurement was repeated one more time. No significant temperature deviation was found between the first series and the repeated series of DTA measurements.

TABLE II. DTA Results for the quasi-binary InSb–Pb alloys

Composition, at. % Pb	t / °C	
	Eutectic reaction	Liquidus (heating)
20	297	480
40	297	442
60	297	399
80	297	347
90	298	–

The phase diagram calculated from the DTA results obtained in this study is shown in Fig. 1.

The differential thermal analysis curves well confirmed the predicted lines of the investigated polythermal InSb–Pb section.

The predicted and experimentally determined eutectic temperatures are in excellent agreement (both at 297 °C) and with a very close eutectic concentration: 89 at.% Pb (calculated) and 90 at.% Pb (experimentally obtained). The liquidus temperatures obtained by DTA are little underestimated in comparison with the thermodynamic predicted ones.

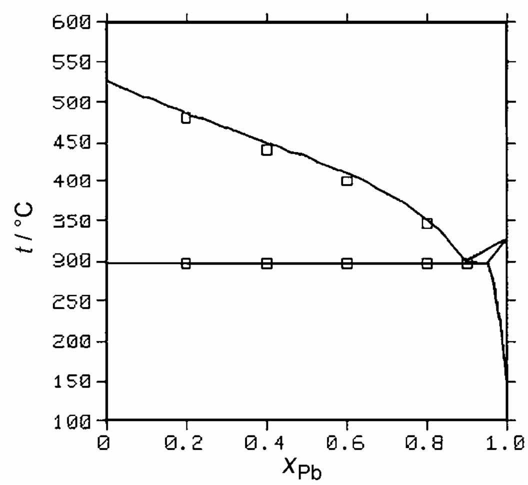

Fig. 1. Calculated Pb–InSb quasi-binary section and DTA results from this work.

The results from this work are in accordance with the experimental results of Geis and Peretti[11] (299 °C and 89.2 at. % Pb).

A characteristic microphotograph recorded by optical microscopy for the samples with 40 at. % Pb is given in Fig. 2.

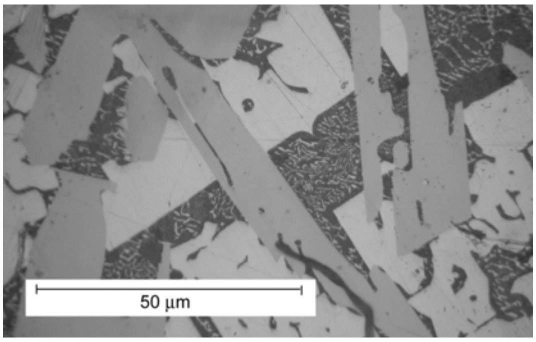

Fig. 2. Characteristic optical microphotograph (magnification 300×) for the $In_{30}Sb_{30}Pb_{40}$ alloy (light regions: primary solidified InSb crystals; dark regions: quasi-binary eutectic InSb + Pb).

The results of SEM analysis are given in Table III and in Fig. 3a. The agreement between the predicted phases and the experimentally determined ones of samples 1 and 2 is perfect.

The calculated phase diagrams of the isothermal sections at 300 and 350 °C are shown in Fig. 3.

The predicted isothermal section of the In–Sb–Pb ternary system at 350 °C includes one three-phase region (InSb + rhombo + liquid), three two-phase regions (InSb + rhombo, InSb + liquid and rhombo + liquid) and one single-phase region (liquid). At 300 °C, the In–Sb–Pb phase diagram includes three three-phase regions (one InSb + rhombo + liquid region and two InSb + FCC + liquid regions), seven two-phase regions (two InSb + liquid regions, two liquid + FCC regions, one InSb + FCC region, one rhombo + liquid region and one InSb + rhombo region) and three single-phase regions (two liquid regions and one FCC region).

TABLE III. Results of the SEM–EDX analysis

Sample	Overall experimental composition, at. %	Theoretically predicted phases	Experimentally determined phases	Exp. compositions of phases, at.%		
				In	Sb	Pb
1	(61.1±1.2) In	InSb	InSb	50.6±0.4	49.4±0.3	–
	(19.6±1.6) Sb	Liquid	Liquid	66.5±1.1	4.2±0.8	29.3±1.5
	(19.3±1.2) Pb					
2	(19.6±1.1) In	Rhombo	Rhombo	–	97.6±1.1	2.4±0.5
	(61.2±1.5) Sb	InSb	InSb	50.5±0.5	49.5±0.3	–
	(19.2±0.9) Pb	Liquid	Liquid	1.4±0.3	25.3±0.4	73.3±1.3

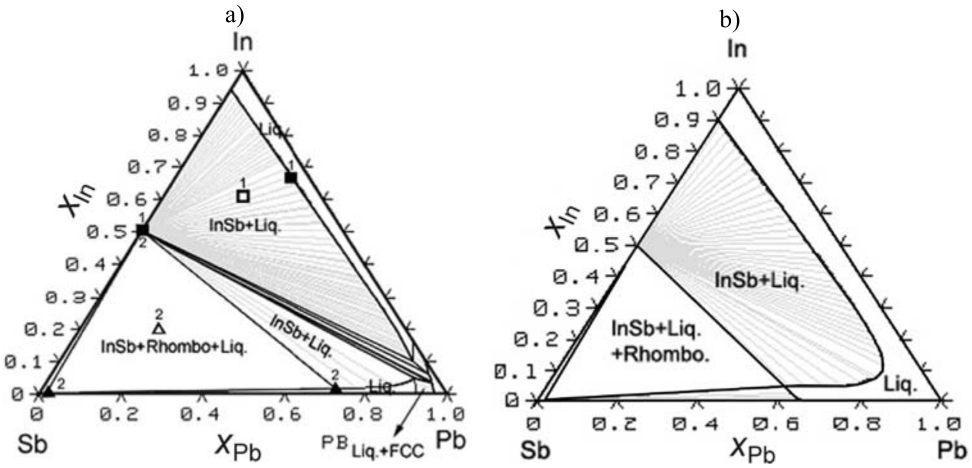

Fig. 3. Predicted phase diagrams of isothermal sections in the ternary In–Sb–Pb system. a) at 300 °C with EDX results: empty symbols – overall composition, full symbols – – compositions of the phases (see Table III) b) at 350 °C.

The liquidus projection of the investigated In–Sb–Pb ternary system was constructed based on the results of thermodynamic prediction. The obtained diagram is shown in Fig. 4.

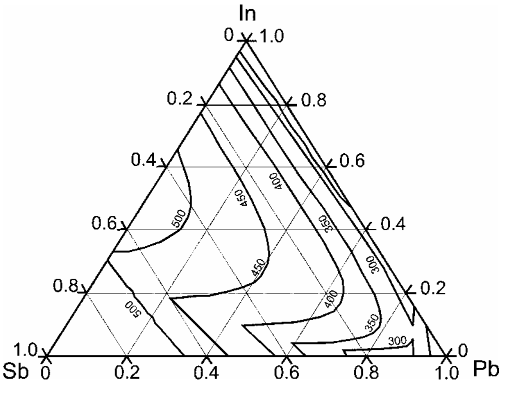

Fig. 4. Liquidus projection in the In–Sb–Pb system.

CONCLUSION

The binary-based thermodynamic prediction of the characteristic phase diagrams in the In–Sb–Pb system was successfully performed using optimized thermodynamic parameters for the constitutive binary systems from the literature. The estimated phase diagram of the Pb–InSb vertical section shows very good agreement with the experimental results from this work and the literature data of Geis and Peretti.[11] The predicted phase diagram of isothermal section at 300 °C is in excellent agreement with the results of SEM–EDX analysis from this work. The calculated phase diagrams of isothermal sections at different temperatures were used for the construction of a liquidus projection of the investigated In–Sb–Pb ternary system. According to the results presented in this study, it could be concluded that the thermodynamic ternary parameters have a negligible influence on the equilibria of this ternary system.

Acknowledgments. The authors are grateful to the Ministry of Science of the Republic of Serbia (Project No. 142043) for financial support and to Prof. Jan Vrestal, Masaryk University, Brno (Czech Republic).

ИЗВОД

ПРЕДВИЂАЊЕ ФАЗНИХ РАВНОТЕЖА У In–Sb–Pb СИСТЕМУ

ДУШКО МИНИЋ[1], ДРАГАН МАНАСИЈЕВИЋ[2], ДРАГАНА ЖИВКОВИЋ[2],
НАДА ШТРБАЦ[2] и ЗВОНИМИР СТАНКОВИЋ[2]

[1]*Факултет техничких наука, Универзитет у Приштини, Књаза Милоша 9,Косовска Митровица и*
[2]*Технички факултет, Униврзитет у Београду, ВЈ 12, 19210 Бор*

Оптимизирани термодинамички подаци, успешно употребљени за прорачун равнотежних фазних дијаграма саставних бинарних система: In–Sb, Pb–Sb и In–Pb, су искоришћени за предвиђање равнотежних фазних дијаграма у In–Sb–Pb систему. Предвиђени фазни дијаграм вертикалног Pb–InSb пресека је упоређен са DTA резултатима и резултатима оптичке микроскопије. Прорачунати фазни дијаграм изотермалног пресека на 300 °C је упоређен са експериментално одређеним (SEM–EDX) саставима фаза у испитиваним узорцима после жарења. У свим случајевима је уочено веома добро међусобно слагање између резултата термодинамичког предвиђања и експерименталних резултата. Ликвидус пројекција In–Sb–Pb система је, такође, представљена.

(Примљено 30. јуна 2007)

REFERENCES

1. D. Manasijević, D. Živković, M. Cocić, D. Janjić, Ž. Živković, *Thermochim. Acta* **419** (2004) 295
2. D. Minić, D. Manasijević, D. Živković, Ž. Živković, J. Serb. Chem. Soc. **71** (2006) 843
3. www.calphad.org
4. M. Hillert, *Phase equilibria, Phase Diagrams and Phase Transformations: Their Thermodynamic Basis*, University Press, Cambridge, 1998
5. N. Saunders, A. P. Miodownik, *CALPHAD (calculation of phase diagrams): A comprehensive guide*, Pergamon, New York, 1998

6. Version 4.4 of the SGTE Unary Database
7. I. Ansara, C. Chatillon, H. L. Lukas, T. Nishizawa, H. Ohtani, K. Ishida, M. Hillert, B. Sundman, B. B. Argent, A. Watson, T. G. Chart, T. Anderson, *CALPHAD* **18** (1994) 177
8. H. Ohtani, K. Ishida, *J. Phase Equilibria* **16** (1995) 416
9. A. Bolcavage, C. R. Kao, S. L. Chen, Y. A. Chang, in *Proceedings of the Symposium on Application of Thermodynamics in the Synthesis and Processing of Materials*, P. Nash, B. Sundman, Eds., TMS, Warrendale, PA, 1995, p. 171
10. B. Predel, F. Gerdes, *J. Less-Comm. Met.* **59** (1978) 153
11. D. R. Geis, E. A. Peretti, *J. Less-Comm. Met.* **4** (1962) 523
12. D. Minić, D. Živković, Ž. Živković, *Thermochim. Acta* **400** (2003) 143
13. Version 1.1 of the COST 531 Database for Lead Free Solders.